

TRYPTOPHAN INDOLE-LYASE INHIBITORS: A SYNTHETIC AND KINETIC STUDY

&

*S*-METHYL-*D*-CYSTEINE: A CONTROL FOR THE VASOCONSTRICTION AGONIST *S*-  
METHYL-*L*-CYSTEINE

by

Austin Patrick Harris

Under the Direction of Robert S. Phillips

#### ABSTRACT

Benzimidazole analogs of L-tryptophan were hypothesized to be inhibitors of the enzyme tryptophan indole-lyase (trpase).  $\beta$ -(Benzimidazol-1-yl)-L-alanine, 2-amino-4-(benzimidazol-1-yl)butyric acid, and 2-amino-5-(benzimidazol-1-yl)pentanoic acid were synthesized and tested enzymatically in a tryptophan indole-lyase assay. It was determined from the conducted enzymatic studies that  $\beta$ -(benzimidazol-1-yl)-L-alanine functioned as a substrate of trpase while 2-amino-4-(benzimidazol-1-yl)butyric acid, a homologue of  $\beta$ -(benzimidazol-1-yl)-L-alanine, behaved as a potent inhibitor of trpase, having a  $K_i$  of 16  $\mu$ M. Contrastingly, 2-amino-5-(benzimidazol-1-yl)pentanoic acid was found to be trpase inactive at a concentration of 600  $\mu$ M. Because 2-amino-4-(benzimidazol-1-yl)butyric acid was found to function as an inhibitor of

trpase, we then hypothesized that homologues of trpase substrates would likely function as inhibitors of trpase. Pursuant to the former hypothesis, 2-amino-4-(benzimidazol-1-yl)butyric acid and S-benzyl-L-homocysteine, homologues of trpase substrates, were synthesized and it was discovered that both functioned as inhibitors of trpase. The  $K_i$  values for 2-amino-4-(benzimidazol-1-yl)butyric acid, and S-benzyl-L-homocysteine were calculated as 15  $\mu$ M and 14  $\mu$ M correspondingly.

Previous works demonstrated that inhibitors of trpase would also likely serve as inhibitors of the enzyme tryptophan synthase.  $\beta$ -(Benzimidazol-1-yl)-L-alanine, 2-amino-4-(benzimidazol-1-yl)butyric acid, 2-amino-4-(benzimidazol-1-yl)butyric acid, and S-benzyl-L-homocysteine were thus hypothesized as inhibitors of tryptophan synthase. Preliminary studies showed that both  $\beta$ -(benzimidazol-1-yl)-L-alanine and 2-amino-4-(benzimidazol-1-yl)butyric acid were tryptophan synthase active; however, the  $K_i$  for these compounds was not determined. At the time of the documentation of this work, 2-amino-4-(benzimidazol-1-yl)butyric acid, and S-benzyl-L-homocysteine had not yet been tested in the tryptophan synthase assay.

S-Methyl-D-cysteine was synthesized in an effort to determine if the vasoconstriction which was observed in laboratory mice when said mice consumed S-methyl-L-cysteine, was stereospecific. Following the synthesis of S-methyl-D-cysteine our collaborators began testing S-methyl-D-cysteine in the vasoconstriction assay. The data from the vasoconstriction assay is still being collected.

INDEXED WORDS: Tryptophan indole-lyase, Tryptophan, Benzimidazole, Substrate,

Inhibition constant, Steady-state, Pre-steady-state, Kinetics, Vasodilation.

TRYPTOPHAN INDOLE-LYASE INHIBITORS: A SYNTHETIC AND KINETIC STUDY

&

*S*-METHYL-*D*-CYSTEINE: A CONTROL FOR THE VASOCONSTRICTION AGONIST *S*-  
METHYL-*L*-CYSTEINE

by

Austin Patrick Harris

B.S., The University of Georgia, 2003

A Dissertation Submitted to the Graduate Faculty of The University of Georgia in Partial  
Fulfillment of the Requirements for the Degree

Doctor of Philosophy

ATHENS GEORGIA,

2009

© 2009

Austin Patrick Harris

All Rights Reserved

TRYPTOPHAN INDOLE-LYASE INHIBITORS: A SYNTHETIC AND KINETIC STUDY

&

*S*-METHYL-*D*-CYSTEINE: A CONTROL FOR THE VASOCONSTRICTION AGONIST *S*-  
METHYL-*L*-CYSTEINE

by

AUSTIN PATRICK HARRIS

Major Professor: Robert S. Phillips  
Committee: George Majetich  
Vladimir Popik

Electronic Version Approved:  
Maureen Grasso  
Dean of Graduate School  
The University of Georgia  
August 2009

## **DEDICATION**

This dissertation is dedicated to my parents Kenneth Ray Harris and Karen Patrice Harris and my sister JoAnn Marie Holmes. Without the love and support of each of you, I would not have been able to complete this work. I love you all very much.

## ACKNOWLEDGMENTS

I would first like to acknowledge Dr. Robert S. Phillips for his support throughout this process. Dr. Phillips, you have been amazingly kind and understanding over the past 9 years of my time at the University of Georgia and I hope that we will have the opportunity to work together on a professional level in the future. I would also like to acknowledge Phanneth Som. Phanneth, thank you for your friendship and support, I have learned a lot about Chemistry and friendship from you over the years and our time as friends has made me a better person. Thank you for always having my back. I would like to acknowledge Vijay Gwandi, Andrew Osborne, and Michael Cash, thank you all for helping me through my years as an undergraduate and beginning graduate researcher. Finally, I would like to acknowledge Musa Musa, Chandan Matrini, and Sunil Kumar. Thank you all for being there and supporting me through my graduate studies. I would further like to thank you all for saving my eye sight the day my eyes were burned with ammonia. If you guys hadn't been there and quickly taken control of the situation, I would likely be blind today.

**TABLE OF CONTENTS**

LIST OF TABLES .....	x
LIST OF FIGURES .....	xi
LIST OF ABBREVIATIONS .....	xiii
CHAPTER 1: INTRODUCTION.....	1
BACTERIAL BIOFILM .....	1
THE ROLE OF INDOLE IN TRPTOPHAN INDOLE-LYASE ACTIVE BACTERIA.....	3
A CORRELATION: BACTERIAL BIOFILM AND TRYPTOPHAN INDOLE-LYASE ...	6
BIOFILM FORMATION AND INHIBITORS OF TRYPTOPHAN INDOLE-LYASE .....	9
TRYPTOPHAN INDOLE-LYASE ACTIVITY AND <i>E. COLI</i> PATHOGENICITY .....	12
CONCLUSION.....	14
CHAPTER 2: BENZIMIDAZOLE ANALOGS AS INHIBITORS OF TRYPTOPHAN INDOLE-LYASE .....	1
INTRODUCTION.....	1
SYNTHESIS OF BENZIMIDAZOLE ANALOGS OF L-TRYPTOPHAN.....	4
KINETICS TESTING OF BENZIMIDAZOLE ANALOGS OF L-TRYPTOPHAN.....	12
RESULTS.....	14

DISCUSSION .....	16
CONCLUSION.....	22
CHAPTER 3: HOMOLOGUES OF AROMATIC AMINO ACIDS AS INHIBITORS OF TRYPTOPHAN INDOLE-LYASE .....	24
INTRODUCTION.....	24
SYNTHESIS OF HOMOLOGUES OF AROMATIC AMINO ACIDS .....	26
KINETICS TESTING OF HOMOLOGUES OF AROMATIC AMINO ACIDS.....	30
RESULTS.....	30
DISCUSSION .....	33
CONCLUSION.....	37
CHAPTER 4: INHIBITORS OF TRYPTOPHAN INDOLE-LYASE CAN ALSO INHIBIT TRYPTOPHAN SYNTHASE .....	38
INTRODUCTION.....	38
STEADY-STATE KINETICS STUDIES OF TRYPTOPHAN SYNTHASE .....	39
RESULTS.....	39
DISCUSSION .....	40
CONCLUSION.....	40
CHAPTER 5: THE SYNTHESIS OF S-METHYL-D-CYSTEINE.....	42
INTRODUCTION.....	42
SYNTHESIS AND RESOLUTION OF S-METHYL-D-CYSTEINE.....	43

RESULTS.....	46
REFERENCES .....	47
APPENDICES.....	50
Appendix 1: Electrospray Mass Spectrum of Benzimidazolyl-L-Alanine .....	50
Appendix 2: Benzimidazolyl-L-Alanine <sup>1</sup> H-NMR.....	51
Appendix 3: Electrospray Mass Spectrum, 2-amino-4-(benzimidazol-1-yl)butanoic acid. .	52
Appendix 4: 2-amino-4-(benzimidazol-1-yl)butanoic acid <sup>1</sup> H-NMR.....	53
Appendix 5: 2-amino-5-(benzimidazol-1-yl)pentanoic acid <sup>1</sup> H-NMR.....	54
Appendix 6: Benzimidazol-1-yl-L-alanine 16 mM stopped-flow spectrum.....	55
Appendix 7: 2-amino-4-(benzimidazol-1-yl)butyric acid 2 mM stopped-flow spectrum. ...	56
Appendix 8: Absorbance versus time decay of the 2-amino-4-(benzimidazol-1-yl)butyric acid <i>gem</i> -diamine at 340 nm.....	57
Appendix 9: Absorbance versus time plot for the formation of the 2-amino-4- (benzimidazol-1-yl)butyric acid quinonoid at 340 nm.....	58
Appendix 10: Mass Spectrum for 2-amino-4-(benzimidazol-1-yl)butyric acid.....	59
Appendix 11: 2-amino-4-(benzimidazol-1-yl)butyric acid <sup>1</sup> H-NMR.....	60
Appendix 12 <sup>1</sup> H-NMR S-benzyl-L-homocysteine.....	61
Appendix 13: 2-amino-4-(benzimidazol-1-yl)butyric acid stopped flow spectrum.....	62
Appendix 14: Absorbance versus time plot for the decay of the 2-amino-4- (benzimidazol-1-yl)butyric acid <i>gem</i> -diamine at 340 nm.....	63

Appendix 15: Absorbance versus time plot for the formation of the 2-amino-4-(benzimidazol-1-yl)butyric acid quinonoid at 340 nm.....	64
Appendix 16: Rate versus concentration of 2-amino-(benzimidazol-1-yl)-butyric acid.....	65
Appendix 17: S-Benzyl-L-homocysteine stopped-flow spectrum.....	66
Appendix 18: Absorbance versus time plot for the decay of the S-benzyl-L-homocysteine acid <i>gem</i> -diamine at 340 nm.....	67
Appendix 19: Absorbance versus time plot for the formation of the S-benzyl-L-homocysteine quinonoid at 340 nm.....	68
Appendix 20: <sup>1</sup> H-NMR spectrum for S-methyl-L-cysteine.....	69
Appendix 21: <sup>1</sup> H-NMR spectrum of N-acetyl-S-methyl-DL-cysteine.....	70
Appendix 22: Steady-state inhibition kinetics data for β-(benzimidazol-1-yl)alanine.....	71
Appendix 23: Steady-state inhibition kinetics data for 2-amino-4-(benzimidazol-1-yl)butyric acid.....	72
Appendix 24: Steady-state inhibition kinetics data for 2-amino-4-(benzimidazol-1-yl)butyric acid.....	73
Appendix 25: Steady-state inhibition kinetics data for S-benzyl-L-homocysteine.....	74
Appendix 26: β-(benzimidazol-1-yl)alanine substrate data.....	75

## LIST OF TABLES

Table 1: Activation of Gene Expression by Conditioned Medium.....	6
Table 2: Properties of the <i>Escherichia coli</i> S17-1 parental strain and derived insertional mutants defective in adherence of biofilm formation.....	7
Table 3: Properties of the S17-1 strain and Tn5 inserted derivatives 3715 and 3720.....	9
Table 4: Effects of oxindolyl-L-alanine and exogenous indole on <i>E. coli</i> biofilm formation and growth yield.....	10
Table 5: Steady-state kinetic parameters for the reaction of benzimidazolyl analogs of tryptophan with <i>E. coli</i> Tryptophan Indole-lyase.....	16
Table 6: Comparison of the tryptophan indole-lyase inhibition constants of homologous aromatic amino acids.....	33

## LIST OF FIGURES

Figure 1: Degradation of L-tryptophan to indole and ammonium pyruvate.....	4
Figure 2: Effects of Indole on Expression .....	5
Figure 3: <i>tna</i> operon.....	8
Figure 4: Effects of 0.5 mg/mL of oxindolyl-L-alanine (Ox) on biofilm formation and bacterial growth of different indole-producing clinical strains in Luria–Bertani (LB) medium , A, and in synthetic urine, C).....	12
Figure 5: Paralysis and killing of <i>C. elegans</i> by rol-6 by pathogenic <i>E. coli</i> . .....	13
Figure 6: The EPEC tryptophan indole-lyase gene is required for paralysis and killing of <i>C. elegans</i> . .....	14
Figure 7: Degradation of L-tryptophan to indole and ammonium pyruvate.....	1
Figure 8: L-tryptophan, tryptophan indole-lyase mechanism.....	2
Figure 9: Benzimidazole analogs of L-tryptophan. ....	3
Figure 10: The general scheme for the synthesis of I(a), I(b), and I(c). ....	4
Figure 11: The scheme for the synthesis of IV(c).....	5
Figure 12: Proposed mechanism for benzimidazolyl-L-alanine reaction .....	19
Figure 13: Proposed mechanism for benzimidazolyl-L-alanine reaction .....	20
Figure 14: Proposed kinetic mechanism for the 2-amino-4-(benzimidazol-1-yl)butanoic acid/tryptophan indole-lyase reaction .....	20

Figure 15: Homologous aromatic amino acids.....	25
Figure 16: Synthetic scheme for 2-amino-4-(benzimidazol-1-yl)butyric acid.....	26
Figure 17: Methionine, S-benzylcysteine reaction scheme.....	29
Figure 18: L-Tryptophan, tryptophan indole-lyase mechanism.....	36
Figure 19: Mechanistic analysis for why this 2-amino-4-(benzimidazol-1-yl)butyric acid has a longer reaction time.....	36
Figure 20: Tryptophan synthase catalyzed synthesis of L-tryptophan.....	38
Figure 21: Synthetic scheme for the S-methyl-D-cysteine.....	43

**LIST OF ABBREVIATIONS**

PLP: PYRIDOXAL-5-PHOSPHATE

TRPASE: TRYPTOPHAN-INDOLE-LYASE

*E. coli*: ESCHERCHIA COLI

S17-1: Wild-type *E. coli*

NOM: Nematode Growth Medium Agar

## CHAPTER 1: INTRODUCTION

### BACTERIAL BIOFILM

Bacterial infection is the most commonly treated medical condition in the world. Since 1674 when the first bacterium was observed by Anton van Leeuwenhoek, much effort has been made on the part of scientists to fully understand and combat bacterial infection. (Porter, 1976) Of the many advances made in understanding bacteria, classifying bacteria via their Gram-stain has been of the most notable. The Gram-stain of a bacterium corresponds to whether or not a particular bacterium will retain crystal violet dye subsequent to the Gram staining process. Based on Gram staining, bacteria can be divided into two distinct classes, Gram-negative and Gram-positive bacteria. Gram positive bacteria are classified as those bacteria which retain crystal violet dye, subsequent to the Gram staining process while Gram-negative do not. (Beveridge, 1999)

Of the two classifications of bacteria mentioned above, Gram-negative bacteria tend to be more virulent to humans in bacterial infection and less susceptible, than Gram positive bacteria, to antimicrobial agents, when treated medically. With the ever increasing ineffectiveness of current microbial prophylactic measures, new and more robust therapeutics will be a prerequisite for human survival in the decades ahead. (Flournoy, Reinert, Bell-Dixon, & Gentry, 2000) When considering new ways to combat bacterial infection, on the molecular level, the mechanisms through which bacteria infect a host should be considered. The mechanisms through which different species of bacteria infect their hosts are highly varied biological processes. However, the common denominator between each of these varied processes is that

bacterial colonization of a host must occur before infection can be initiated. (Costerton, Stewart, & Greenberg, 1994)

Planktonic bacteria begin the colonial process by first attaching themselves to some biotic or abiotic surface. Initial bacterial attachment to surfaces can occur via several physical mechanisms including the use of bacterial surface organelles such as pili, curli, flagella and Van der Waals interactions. (Pratt & Kolter, 1998) Once a planktonic bacterium has attached to a surface, it can anchor itself permanently to the surface via cell adhesion. Cell adhesion generally involves secretion, by the bacterium, of a sticky matrix composed of various polymeric substances. (Costerton, Stewart, & Greenberg, 1994) Once bound to a surface, the bacterium divides, forming a complex community of bacterial cells known as biofilm. Biofilm communities have been shown to exhibit varying patterns of gene expression, likening said communities to small factories, with each portion of the biofilm community assigned to carry out a specific biological function. Biofilm communities are often highly organized, containing various channels where nutrients and waste can circulate in and out of the biofilm structure. (Costerton, Stewart, & Greenberg, 1994) The primary function of biofilm is to serve as a protective armor for bacterial communities, shielding the overall community from harsh environmental condition, promoting growth and efficiency within the community.

The formation of biofilm communities are important medically because they have been shown to mark the beginning of the infection process. Once formed, biofilm communities release antigens, which stimulate autoimmune responses in host-bodies. Antibodies released by the autoimmune system of a host-body in order to fight a bacterial infection often face difficulties penetrating biofilm communities, due to the properties of the biofilm polymeric matrix. As a result, host-bodies may experience difficulty fighting bacterial infections through

typical autoimmune response mechanisms. (Costerton, Stewart, & Greenberg, 1994) Because of the difficulty host-bodies face autonomously combating bacterial infections, the need to produce potent antimicrobial agents became apparent at the time bacteria were first discovered to cause disease. (Flournoy, Reinert, Bell-Dixon, & Gentry, 2000)

To date, many antimicrobial agents such as  $\beta$ -lactams, aminoglycosides, macrolides, and sulfonamides have been synthesized to aid host-bodies in combating bacterial infection. Each of the fore-mentioned antimicrobial agents participates in a specific mechanism of action which slows the proliferation of bacterial infection, ultimately eliminating it. (Walsh & Wright, 2005) Though there are diverse ranges of antimicrobial agents which may be utilized when treating bacterial infections, there is an imminent concern that bacteria will continue to become resistant to said antimicrobial agents. In order to continue to provide adequate treatment for bacterial infection, potent new antimicrobial agents will need to be realized. (Walsh & Wright, 2005) Due to the correlation between biofilm formation, and the infection process, research into the mechanisms of biofilm formation has become an interest of scientists.

## **THE ROLE OF INDOLE IN TRPTOPHAN INDOLE-LYASE ACTIVE BACTERIA**

Indole-positive gram-negative bacteria such as *Escherichia coli*, *Klebsiella oxytoca*, *Providencia stuartii*, *Citrobacter koseri*, *Morganella morganii*, and *Haemophilus influenza* have long been known to compromise the integrity of public health. Indole-positive microbes are characterized by their ability to degrade L-tryptophan into indole and ammonium pyruvate, using the enzyme tryptophan indole-lyase (trpase). (Wang, Ding, & Rather, 2001) See Figure 1. Until recently, the role that trpase has played in indole-positive microbes has been the subject of much



discovered that increasing concentrations of indole in a conditioned medium containing *E. coli* cells resulted in an increase in the expression of the *tnaB* (MT113), *atsD* (MT48), and *gapT* (MT114) fused genes. The expression of the *cysK::lacZ* (MT9) was not affected by changes in concentration of indole (Figure 2).

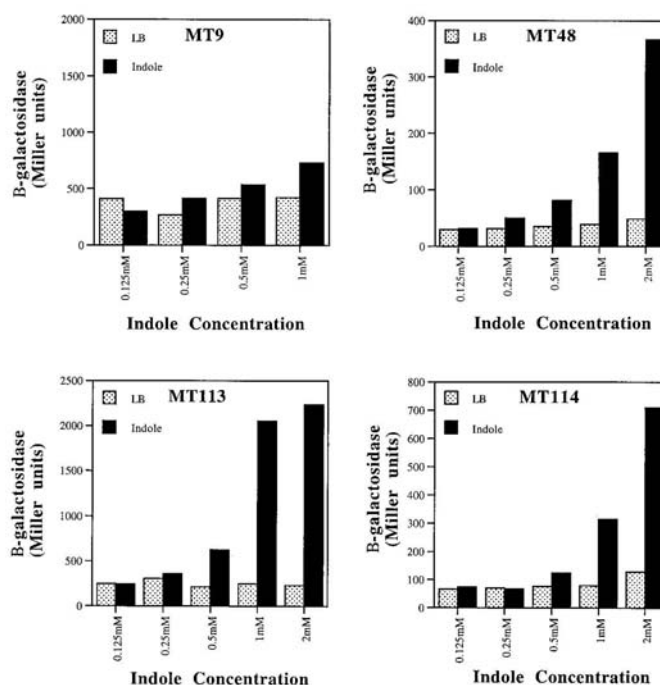


**Figure 2: Effects of Indole on Expression**

In the same study, Wang *et al.* also compared the expression of the *cysK* (MT9), *atsD* (MT48), *tnaB* (MT113), and *gapT* (MT114) genes in wild type *E. coli* with the expression of the same genes in a trpase inactive mutant *E. coli*. This comparison revealed that when trpase was inactivated, the expression of the *cysK* (MT9), *atsD* (MT48), *tnaB* (MT113), and *gapT* (MT114) genes were reduced relative to the trpase active wild type *E. coli* cells, as seen in Table 1.

**Table 1: Activation of Gene Expression by Conditioned Medium**

Strain	Growth condition <sup>a</sup>	Mean b-galactosidase activity (+/-) SD (Miller units) <sup>b</sup>
MT9	LB	262 ± 3
	CM (wild type)	3,466 ± 66 (13.2)
	CM ( <i>tnaA</i> :: <i>Cm</i> <sup>r</sup> )	2,526 ± 61 (9.6)
MT48	LB	39 ± 3
	CM (wild type)	341 ± 16 (9.0)
	CM ( <i>tnaA</i> :: <i>Cm</i> <sup>r</sup> )	200 ± 6 (5.3)
MT113	LB	177 ± 15
	CM (wild type)	1,500 ± 46 (8.5)
	CM ( <i>tnaA</i> :: <i>Cm</i> <sup>r</sup> )	464 ± 5 (2.6)
MT114	LB	39 ± 3
	CM (wild type)	405 ± 21 (10.4)
	CM ( <i>tnaA</i> :: <i>Cm</i> <sup>r</sup> )	302 ± 8 (7.7)

<sup>a</sup> CM, conditioned medium

<sup>b</sup> Values in parentheses are fold induction relative to growth in

Because indole concentration, and trpase activity were found to have a significant effect on the expression of the *astD*, *tnaB*, and *gapT* genes, it was hypothesized that indole, produced through the degradation of L-tryptophan via trpase is likely involved in extracellular regulatory signaling in *E. coli*. (Wang, Ding, & Rather, 2001)

### **A CORRELATION: BACTERIAL BIOFILM AND TRYPTOPHAN INDOLE-LYASE**

In a 2002 study designed to better understand the mechanisms associated with bacterial biofilm formation, Di Martino *et al.* isolated 97 random insertion mutants of *Escherichia coli* (*E. coli*) strain S17-1 using a Tn5 transposon. (DiMartino, Merieau, Phillips, Orange, & Hulen, 2002) Di Martino classified each mutant as a function of their adherence to A549 epithelia cells,

fibronectin, and their ability to form biofilm on polystyrene. Of the 97 mutants generated by Di Martino, 80 showed a decrease in biofilm formation on polystyrene, 8 showed a decrease adherence to A549 epithelia cells, and 7 of the mutants demonstrated a decrease in their adherence to fibronectin. The mutants which demonstrated the most dramatic reductions in cell adherence and biofilm formation are shown in the Table 2 below:

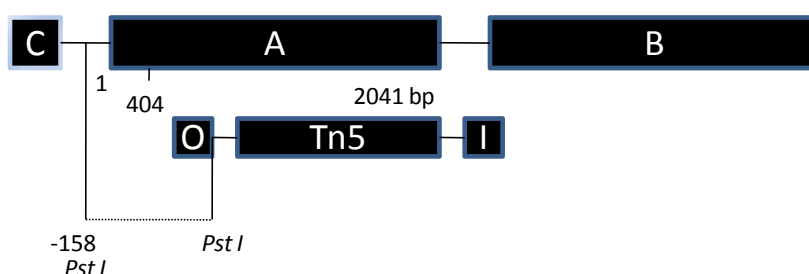
**Table 2: Properties of the *Escherichia coli* S17-1 parental strain and derived insertional mutants defective in adherence of biofilm formation.**

Bacterial Strain	Adherence index to A549 cells (bacteria/cell)	Adherence index to fibronectin (10 <sup>4</sup> CFU/well)	Biofilm formation (OD <sub>595</sub> )
S17-1	8.23±1.09	2.7±0.5	0.37±0.06
3701	7.53±0.67	0.10±0.01	0.09±0.02
3702	7.97±0.94	0.10±0.02	0.09±0.01
3703	10.06±2.43	1.0±0.1	0.09±0.01
3704	2.25±0.34	1.2±0.2	0.09±0.01
3705	7.63±1.03	1.6±0.1	0.10±0.02
3706	6.88±0.19	1.6±0.1	0.10±0.01
3707	9.31±1.86	1.4±0.1	0.08±0.01
3708	0.50±0.19	2.8±0.2	0.09±0.01
3709	1.28±0.09	3.2±0.4	0.10±0.02
3710	2.50±0.46	2.8±0.1	0.08±0.02
3711	4.25±0.75	2.3±0.1	0.08±0.01
3712	2.84±0.22	3.4±0.9	0.09±0.01
3713	0.94±0.04	3.6±0.9	0.09±0.01
<u>3714</u>	2.11±0.37	2.5±0.2	0.10±0.01
3715	7.03±0.95	2.8±0.7	0.10±0.01

Note: adapted from (DiMartino, Merieau, Phillips, Orange, & Hulen, 2002)

To understand how insertion of the Tn5 transposon into the S17-1 mutant's genome resulted in a reduction of each mutant's cell adherence and biofilm formation, a DNA genomic extraction

followed by a Southern blot was carried out on each mutant genome shown, in Table 2. The information derived from the Southern blot and clone sequence analysis of the 3714 mutant was the most telling because it revealed that the Tn5 transposon had truncated the *tna* operon, see Figure 3.



Note: Adapted from (DiMartino, Merieau, Phillips, Orange, & Hulen, 2002)

**Figure 3: *tna* operon**

As can be seen in Figure 3, the *tna* operon consists of regulatory sequences of three genes: *tnaC*, *tnaB*, and *tnaA*. *tnaC* encodes a 24 residue leader peptide while *tnaB* encodes a low affinity tryptophan permease, and *tnaA* encodes the structural information for the enzyme tryptophan indole-lyase (trpase). The Tn5 transposon is designated in Figure 3 and its point of insertion into the *tna* operon is indicated as being between the *tnaC* and *tnaA* genes. The insertion of the transposon at this position effectively inactivated the transcription of trpase in the 3714 mutant. From the indicated data, Di Martino hypothesized that trpase activity plays a role in the formation of biofilm in *E. coli*.

Di Martino tested the former hypothesis by inserting the pMD6 plasmid containing the complete *tnaA* gene into the 3714 mutant. Following the insertion of the *tnaA* gene into 3714 mutant, biofilm formation and A549 cell adherence was restored, as seen in Table 3. In Table 3, the S17-1 (wild-type *E. coli*) strain is compared with both the 3714 trpase inactive mutant and

the 3714 pMD6 plasmid insert which restored trpase activity in the 3714 mutant. As indicated by Table 3, when the 3714 mutant was allowed to proliferate in the absence of trpase activity, the bacterial growth of the 3714 mutant remained similar to that of the S17-1 *E. coli* strain; however, biofilm formation was reduced by about one-third. In contrast, when the pMD6 plasmid was inserted into the 3714 mutant restoring trpase activity, biofilm formation in the 3714 mutant was restored to levels similar to those of the trpase active S17-1 strain. The above data suggests that trpase activity plays an integral role in the formation of biofilm in *E. coli*.

**Table 3: Properties of the S17-1 strain and Tn5 inserted derivatives 3715 and 3720.**

Bacterial strain <sup>a</sup>	Indole production <sup>b</sup>	Biofilm formation				A549 cells adherence			
		OD <sub>595</sub>	pH		Bacterial growth at T <sub>20</sub> <sup>c</sup>	Adherence index	pH		Bacterial growth at T <sub>3</sub> <sup>c</sup>
			T <sub>0</sub>	T <sub>20</sub>					
S17-1	+	0.37±0.06	7.0	7.30±0.24	0.33±0.03	8.23±1.09	7.5	6.80±0.10	0.52±0.04
3714	-	0.10±0.01	7.0	6.25±0.45	0.35±0.01	2.11±0.37	7.5	6.05±0.15	0.50±0.06
3714 pMD6	+	0.50±0.06	7.0	6.95±0.05	0.32±0.07	7.90±1.11	7.5	7.15±0.25	0.67±0.01
3720	+	0.44±0.08	7.0	7.33±0.21	0.36±0.02	9.65±2.17	7.5	6.97±0.20	0.48±0.01
3720 pMD6	+	0.40±0.05	7.0	6.95±0.05	0.31±0.03	8.44±1.65	7.5	7.35±0.25	0.71±0.03

Note: +, indole production; -, no indole production; T, incubation time in hours. All the values presented in this table are means of three separate experiments. <sup>a</sup>The 3720 clone had a transposon insertion that did not affect A549 cells adherence and biofilm formation. 3714 pMD6 and 3720 pMD6: 3714 and 3720 mutants transformed with the pMD6 plasmid harboring wild-type *Escherichia coli* tnaA gene and regulatory sequences. <sup>b</sup>Bacteria were tested for indole production with the RapIDone identification system and the spot indole reagent (IDS, Atlanta, Ga., U.S.A.). <sup>c</sup>Bacterial growth was measured by optical density OD<sub>620</sub>. The bacterial inoculum was initially adjusted at OD<sub>620</sub> = 0.05 and 0.2 for biofilm and A549 cells adherence experiments, respectively.

## BIOFILM FORMATION AND INHIBITORS OF TRYPTOPHAN INDOLE-LYASE

In 2003 Di Martino *et al.* conducted further studies on wild type *E. coli* (S17-1) and the above mentioned tryptophan indole-lyase inactive mutant, 3714, to determine what effect inhibitors of trpase would have on biofilm formation. (DiMartino, Fursy, Bret, Sundararaju, &

Phillips, 2003) In order to determine the former, a biofilm assay conducted in LB medium, supplemented with varying quantities of the trpase inhibitor oxindolyl-L-alanine, was run on S17-1. The assay revealed that a dose-response relationship existed between biofilm formation and varying oxindolylalanine concentration, as seen in Table 4. These results suggest that trpase activity plays a role in biofilm formation in *E. coli*.

**Table 4: Effects of oxindolyl-L-alanine and exogenous indole on *E. coli* biofilm formation and growth yield.**

<i>E. coli</i> strain	Growth Medium Supplementation	Biofilm Formation <sup>b</sup>	Bacterial Growth (%) <sup>c</sup>
S17-1	—	0.37±0.06	100±2.2
	Ox (0.5 mg/mL)	0.16±0.06	106.4±5.7
	Ox (0.25 mg/mL)	0.27±0.03	106.9±8.9
	Ox (0.125 mg/mL)	0.34±0.06	108.6±6.3
	Ox (0.5 mg/mL) + indole (312.5 µM)	0.29±0.005	97.0±0.6
	Indole (312.5 µM)	0.35±0.03	115.2±1.8
3714	—	0.10±0.01	100±2.9
	Indole (1250 µM)	0.20±0.01	20±1.4
	Indole (625 µM)	0.31±0.01	51.4±0.6
	Indole (312.5 µM)	0.17±0.003	91.4±0.6
	Indole (156.25 µM)	0.12±0.004	100±1.1
	Indole (78.125 µM)	0.10±0.003	102.9±0.6
	Indole (39 µM)	0.085±0.003	102.9±0.6

<sup>a</sup> All experiments were done in Luria-Bertani (LB) medium supplemented with oxindolyl-L-alanine (Ox) or indole.

—, control no supplementation

<sup>b</sup> Crystal violet staining quantification (OD<sub>595</sub>)

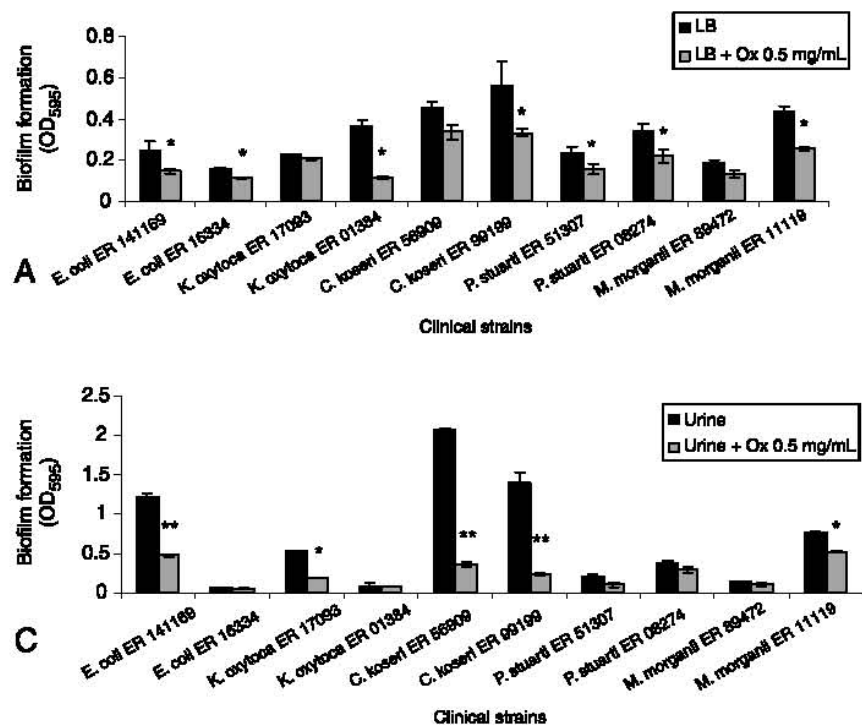
<sup>c</sup> Bacterial growth was measured by optical density at 620 nm. It is expressed as the percentage of bacterial growth of the corresponding strain in LB medium

Note: Adapted from (DiMartino, Fursy, Bret, Sundararaju, & Phillips, 2003)

To determine if the decreased presence of indole was responsible for the decrease in biofilm activity that was observed when oxindolylalanine was supplemented into the LB medium of the previous experiments, a second experiment was conducted. In the second experiment, Di Martino et. al. examined the effect varying concentrations of indole would have on biofilm formation in the trpase inactive mutant 3714. The results of this experiment revealed that when the trpase inactive mutant 3714 was supplemented with indole, biofilm formation increased in a

dose-response manner, as seen in Table 4. The restoration of biofilm formation in the trpase inactive 3714 mutant suggested that the presence of indole is biologically linked to biofilm formation. To determine whether the same effect on biofilm formation could be observed in other trpase active bacteria, a final experiment was conducted.

In a final experiment, the effect oxindolylalanine had on biofilm formation in several clinical strains of indole producing bacteria, was examined. The results from the final experiment revealed that the each of the following clinical strains: *E. coli*, *K. oxytoca*, *C. koseri*, *P. stuartii*, and *M. morgani*, demonstrated a decrease in biofilm formation when they were grown on both LB medium and in synthetic urine, in the presence of the trpase inhibitor oxindolylalanine, as seen in Figure 4. The results from this experiment implicate trpase activity in the process through which indole-positive microbes form biofilm. Because biofilm formation is an essential step in bacterial infection, potent inhibitors of trpase could potentially serve as a new class of antimicrobial agents.



Note: Adapted from (DiMartino, Fursy, Bret, Sundararaju, & Phillips, 2003)

**Figure 4: Effects of 0.5 mg/mL of oxindolyl-L-alanine (Ox) on biofilm formation and bacterial growth of different indole-producing clinical strains in Luria-Bertani (LB) medium, A, and in synthetic urine, C).**

### TRYPTOPHAN INDOLE-LYASE ACTIVITY AND *E. COLI* PATHOGENICITY

In 2005 Anyanful et al. discovered a correlation between trypase activity and the pathogenicity of enteropathogenic (EPEC), enterohaemorrhagic (EHEC), enteroinvasive (EIEC), and enterotoxigenic (ETEC) strains of *E. coli*. (Anyanful, et al., 2005) The correlation was discovered through indirectly exposing the nematode, *Caenorhabditis elegans* (*C. elegans*), to various strains of *E. coli*. Initial tests revealed that when *C. elegans* was placed in a nematode growth medium agar (NOM) with various strains of *E. coli* (EPEC, EHEC, EIEC, and ETEC),

the nematode was rendered paralyzed within 30 minutes and subsequently died. In contrast, when the nematode was placed in the NOM with non-enteropathogenic *E. coli*, K-12 and OP50, (the typical food source of the worms) paralysis and death did not occur (Figure 5).

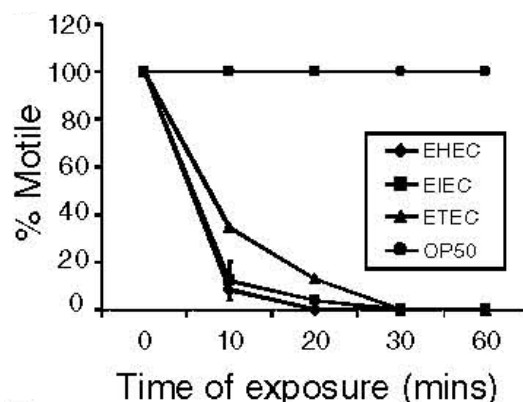


**Figure 5: Paralysis and killing of *C. elegans* by rol-6 by pathogenic *E. coli*.**

Further experiments conducted determined that the presence of L-tryptophan in the NOM agar was necessary to produce paralysis and death of *C. elegans* to occur, in the presence of EPEC *E. coli*. The former led to the hypothesis that tryptophan indole-lyase (trpase) activity may be linked to the biological mechanism which renders *C. elegans* paralyzed, when the nematodes are exposed to certain strains virulent strains of *E. coli*.

In testing the former hypothesis, Anyanful *et al.* developed a trpase inactive mutant of EPEC (EPEC $\Delta$ trpase) and measured the EPEC $\Delta$ trpase mutant's ability to paralyze *C. elegans* against a trpase active strain, EPEC $\Delta$ trpase+trpase, in a tryptophan supplemented medium. The testing revealed that the trpase inactive strain, EPEC $\Delta$ trpase failed to paralyze *C. elegans*, while the trpase active strain EPEC $\Delta$ trpase+trpase and EPEC paralyzed and killed *C. elegans*, as seen in Figure 6.

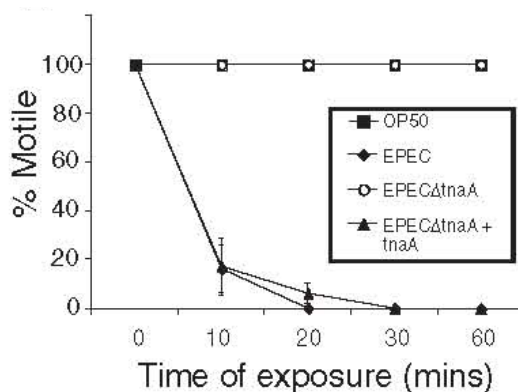


**Figure 6: The EPEC tryptophan indole-lyase gene is required for paralysis and killing of *C. elegans*.**

In this final study, Anyanful demonstrated that exposure of the nematode *C. elegans* to EPEC *E. coli*, result in paralysis of the nematode within 30 minutes of said exposure. In contrast, when *C. elegans* is exposed to a trpase inactive mutant of EPEC, paralysis does not ensue. The former suggests that there is a correlation between the activity of tryptophan indole-lyase and the ability of EPEC *E. coli* to paralyze the nematode *C. elegans*.

## CONCLUSION

Formation of biofilm is generally the first step in bacterial infection pathway. Due to the direct correlation between trpase and the ability for indole-positive bacteria to generate biofilm, trpase should be considered as a therapeutic target for the creation of new antimicrobial agents. Further, the correlation which exists between trpase activity and the virulence of enterohaemorrhagic *E. coli* substantiates the theory that inhibitors of trpase could serve as a new

class of antimicrobial agents. In determining which compounds would serve best as inhibitors of trpase, derivatives of intermediates in the trpase mechanism of action be considered.

## CHAPTER 2: BENZIMIDAZOLE ANALOGS AS INHIBITORS OF TRYPTOPHAN

### INDOLE-LYASE

#### INTRODUCTION

The importance of tryptophan indole-lyase (trpase) activity in the *E. coli* biofilm formation mechanism has been extensively studied. (DiMartino, Merieau, Phillips, Orange, & Hulen, 2002), (DiMartino, Fursy, Bret, Sundararaju, & Phillips, 2003), (Anyanful, et al., 2005) Because bacterial adherence to biotic and abiotic surfaces marks one of the first steps in the bacterial infection pathway, trpase should be considered as a target for creating new antibacterial agents. Tryptophan indole-lyase (trpase) is a pyridoxal-5- phosphate (PLP) dependent enzyme that catalyzes the hydrolytic cleavage of L-tryptophan to indole and ammonium pyruvate. (Figure 7).

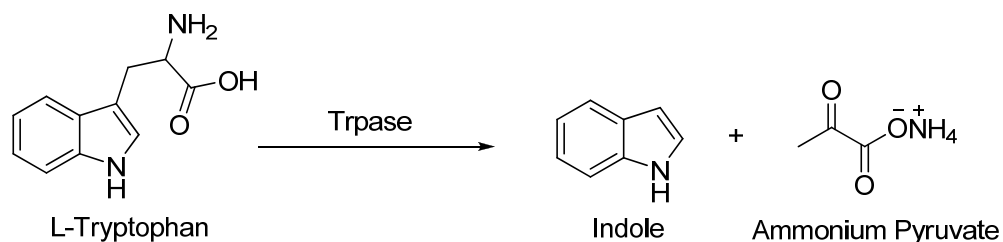


**Figure 7: Degradation of L-tryptophan to indole and ammonium pyruvate**

The mechanism for the enzymatic degradation of L-tryptophan via tryptophan indole-lyase (trpase) was initially proposed by Davis & Metzler and suggests that L-tryptophan undergoes

cleavage of the C3-indole carbon-carbon bond by way of tautomerization of the indole ring of L-tryptophan to a derivatized indolenine intermediate, shown in Figure 8 (Davis & Metzler, 1972).

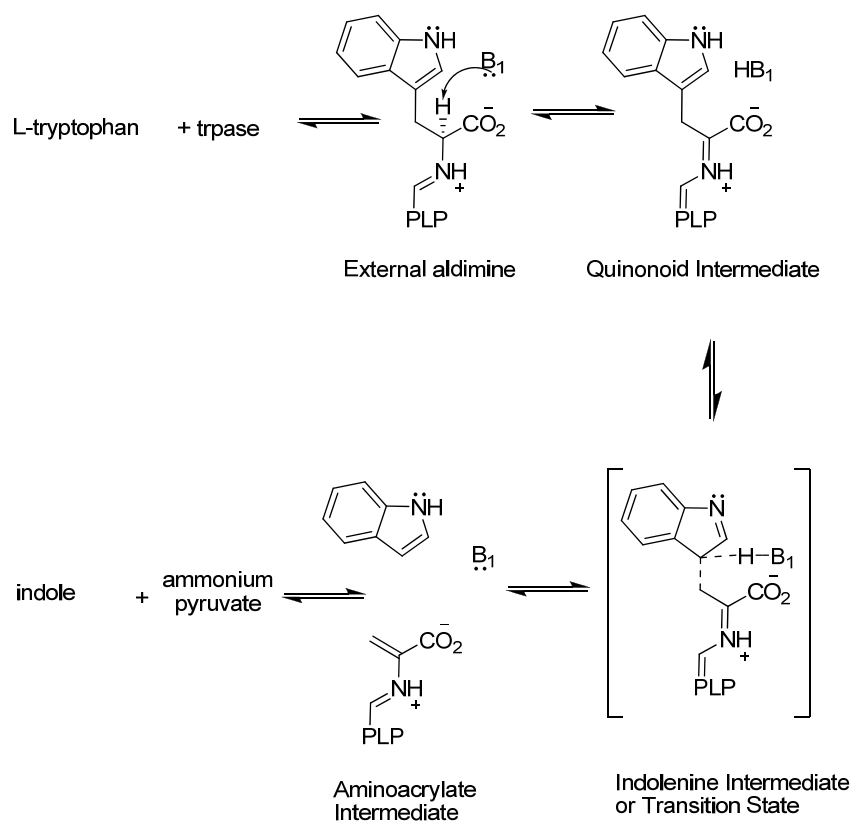


**Figure 8: L-tryptophan, tryptophan indole-lyase mechanism.**

Due to the correlation between trpase activity and biofilm formation in *E. coli*, and other indole-positive bacteria, the development of effective inhibitors of trpase could lead to the development of a new class of antimicrobial agents.

Phillips *et al.* demonstrated that analogues of the indolenine transition-state, 2,3-dihydrotryptophan and oxindolylalanine are potent competitive inhibitors of trpase. (Phillips, Miles, & Cohen, 1984) Benzimidazole, a compound which is also structurally similar to the indolenine transition-state, observed in the trpase/L-tryptophan mechanism, also functions as a competitive inhibitor to trpase. Due to the structural similarities between benzimidazole and the

proposed indolenine intermediate described in Figure 8, we hypothesized that benzimidazole analogs of tryptophan may function as inhibitors of trpase. This work embodies the synthesis of  $\beta$ -(benzimidazol-1-yl)-L-alanine, **I(a)**, 4-(benzimidazol-1-yl)-2-aminopropionic acid, **I(b)**, and 5-(benzimidazol-1-yl)-2-amino-pentanoic acid **I(c)**. See Figure 9.

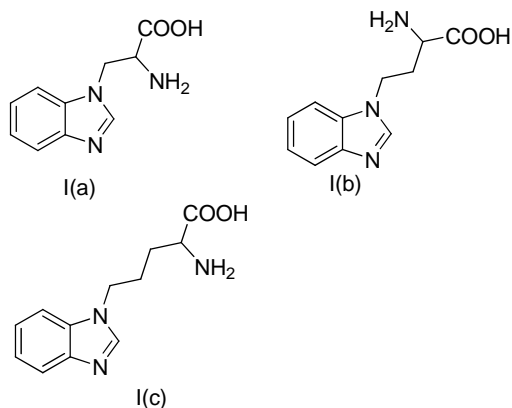


**Figure 9: Benzimidazole analogs of L-tryptophan.**

In order to gain an understanding of the role the structural features of each compound in Figure 9 plays in the rates and mechanisms of interaction **I(a)**, **I(b)**, and **I(c)** have with trpase; **I(a)**, **I(b)**, and **I(c)** were synthesized and analyzed via steady-state and pre-steady-state kinetic methods.

## SYNTHESIS OF BENZIMIDAZOLE ANALOGS OF L-TRYPTOPHAN

Figure 10, below, depicts a general reaction scheme for the synthesis of compounds **I(a)**, **I(b)** and **I(c)**. Note, the synthesis of **I(c)**, begins with the starting material **IV(c)** derived from the scheme shown below, in Figure 11.

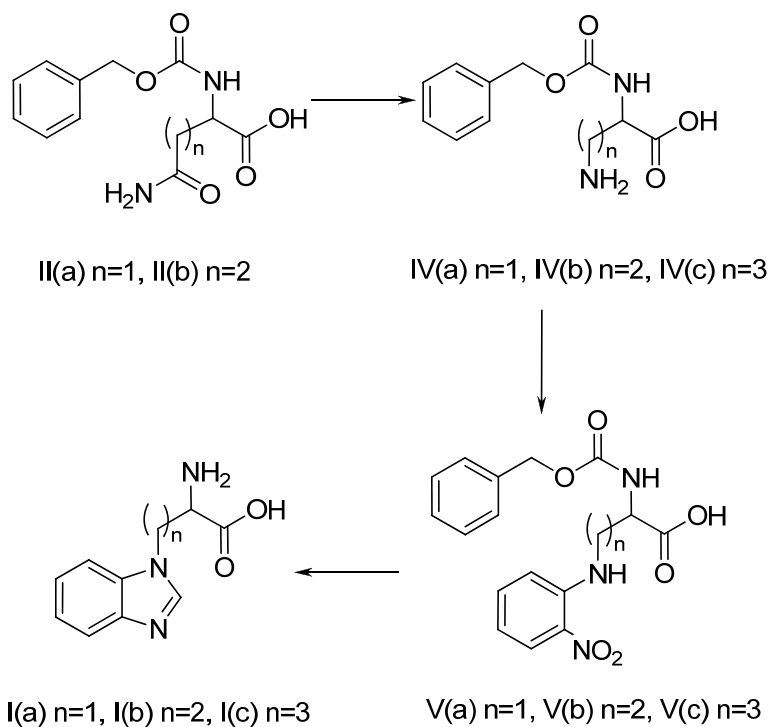


**Figure 10:** The general scheme for the synthesis of **I(a)**, **I(b)**, and **I(c)**.

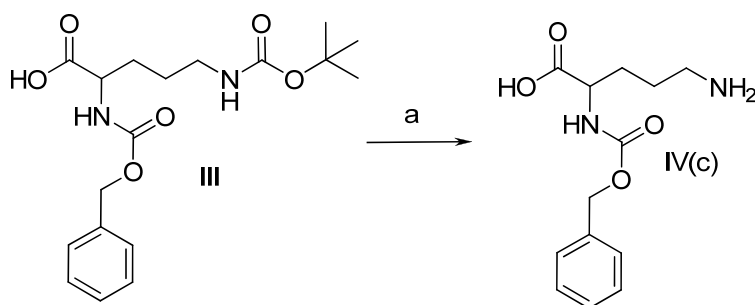


**Figure 11: The scheme for the synthesis of IV(c).**

## SYNTHESIS OF BENZIMIDAZOLYL-L-ALANINE

***β-amino-L-alanine, IV(a).*** N<sup>α</sup>-Benzyloxycarbonyl-L-asparagine, **II(a)**, (USB Corporation). (1 g, 3.75 mmol) and 50 ml of THF were combined in a 100ml round bottom flask. While stirring, the solution was cooled to 10 °C using an ice bath. Iodobenzene diacetate (Acros) 1.6 g (4.88 mmol) was added to the THF solution, and the reaction was allowed to stir at room temperature for 8 hrs, yielding a white precipitate. The precipitate was filtered and the precipitate was washed twice with THF, yielding 0.625 g (70%) of Compound **IV(a)**. (Zhang, Kauffman, Pesti, & Yin, 1997) The presence of **IV(a)** was confirmed qualitatively via TLC and ninhydrin staining.

***2-amino-3-(2-nitrophenylamino)propanoic acid.*** Compound **IV(a)** (0.625 g, 2.63 mmol) and 25ml of DMF were combined in a 50 ml round bottom flask along with 0.797 g (7.89 mmol) of triethylamine. While stirring, 0.371g (2.63 mmol) of 2-fluoronitrobenzene, (Acros), was added drop-wise to the reaction mixture. The reaction mixture was stirred at 100°C for 48

hrs. The reaction mixture was cooled to room temperature and 100 ml of water was added to the solution. The pH of the solution was adjusted to 2.0 with 1 N HCl and the reaction mixture was extracted 3 times with 15 ml portions of ethyl acetate. The ethyl acetate extractions were then combined and dried under sodium sulfate. The ethyl acetate was next removed, under reduced pressure, at 60°C yielding an orange oil, **V(a)**, 0.360 g (1.60 mmol) 60.8%.

**Benzimidazol-1-yl-L-alanine.** Without further purification, **V(a)** (0.360 g, 1.60 mmol) was dissolved in 30 ml of formic acid. Zinc dust, 1 g, was added to the solution and the solution was allowed to reflux for 24 hrs. The reaction mixture was then cooled and filtered. The filtrate containing the formic acid was then collected and the formic acid was removed at 80 °C, under reduced pressure, yielding a clear oil. The oil was then dissolved in 6 N HCl and allowed to reflux at 100 °C for 12 hrs. Following reflux, the acid was removed at 80°C, under reduced pressure, producing **I(a)** a white crystalline solid 0.308 g (1.5 mmol) 94%. **I(a)** was characterized by <sup>1</sup>H-NMR and mass spectrometry.

**Spectral Analysis of β-(Benzimidazol-1-yl)-L-alanine.** β-(Benzimidazol-1-yl)-L-alanine was characterized by electrospray mass spectrometry and <sup>1</sup>H-NMR. Appendix 1 shows the electrospray mass spectrum of benzimidazolyl-L-alanine. It can be seen from Appendix 1 that there is a base peak at 206 amu. The base peak at 206 amu corresponds to the molecular mass of the protonated benzimidazolyl-L-alanine species, C<sub>10</sub>H<sub>12</sub>N<sub>3</sub>O<sub>2</sub><sup>+</sup>. The mass spectrum of the sample confirms the presence of **I(a)** insofar as the mass of the compound. <sup>1</sup>H-NMR was utilized to deduce the structure of **I(a)**.

The <sup>1</sup>H-NMR shown in Appendix 2 was collected on a 400 Mhz Varian Mercury Plus instrument, in D<sub>2</sub>O. The spectrum in Appendix 2 shows five peaks which are significant to the structure of **I(a)**. The triplet peak at δ 4.376 which integrates to 1.0 corresponds to the proton at

the alpha position to the carboxylic acid, labeled (**H<sub>a</sub>**). The chemical shift of (**H<sub>a</sub>**) is consistent with that of a proton located at the alpha position of a carboxylic acid. The multiplet peak at  $\delta$  4.936 which integrates to 2.36 corresponds to the protons (**H<sub>b</sub>**) and (**H<sub>b'</sub>**). The complex splitting that is observed in the peak at  $\delta$  4.936 can be attributed to the diastereomeric relationship which exists between protons (**H<sub>b</sub>**) and (**H<sub>b'</sub>**). The multiplet peak at  $\delta$  7.540 integrates to 2.08 and corresponds to the protons (**H<sub>d</sub>**) and (**H<sub>e</sub>**) in the benzimidazole ring. The complex splitting that is observed at  $\delta$  7.540 can be attributed to the overlap of the peaks corresponding to the protons (**H<sub>d</sub>**) and (**H<sub>e</sub>**). The multiplet peak at  $\delta$  7.765 which integrates to 2.01 corresponds to the protons (**H<sub>c</sub>**) and (**H<sub>f</sub>**) in the benzimidazole ring. Protons at (**H<sub>d</sub>**) and (**H<sub>e</sub>**) are shifted up-field relative to the protons (**H<sub>c</sub>**) and (**H<sub>f</sub>**) because the protons on carbons (**H<sub>d</sub>**) and (**H<sub>e</sub>**) are positioned further away from the electronegative nitrogen atoms composing the benzimidazole ring. Finally, the singlet at  $\delta$  9.174 which integrates to 0.81 corresponds to proton (**H<sub>g</sub>**). Proton (**H<sub>g</sub>**) is shifted furthest down-field because it is an aromatic methine hydrogen. Based on the foregoing analysis, the structure of benzimidazolyl-L-alanine can properly be confirmed.

## **SYNTHESIS OF 2-AMINO-4-BENZIMIDAZOLYL BUTANOIC ACID**

*2-(benzyloxycarbonylamino)-4-aminobutanoic acid IV(b)*. N <sup>$\alpha$</sup> - benzyloxycarbonyl-L-glutamine (Sigma) (2 g, 7.14 mmol) and 50ml of THF were combined in a 100 ml round bottom flask. While stirring, the solution was cooled to 10°C using an ice bath. Iodobenzene diacetate (3.05 g, 9.29 mmol) was then added to the THF solution, and the reaction was allowed to stir at room temperature for 8 hrs. The THF was removed from the system at 80 °C, under reduced

pressure. The resulting clear oil was then dissolved in water and extracted three times with chloroform. The chloroform was discarded and the water from the aqueous layer was then removed at 80 °C, under reduced pressure, yielding 1.5 g of a light brown solid **IV(b)**. (Rodinov, Rodionova, Baidakova, Romashko, Balashova, & Federation, 2002) The presence of **IV(b)** was confirmed using a reversed phase TLC plate which was eluted in 20% aqueous ethanol. A single spot present on the eluted plate was visible under UV light and stained produced a ninhydrin stain confirming the presence of **IV(b)**.

*2-(benzyloxycarbonylamino)-4-(2-nitrophenylamino)butanoic acid, V(b)*. **IV(b)** (1.5 g, 5.95 mmol) and 25 ml of DMF were combined in a 50 ml round bottom flask along with triethylamine (1.8 g, 17.85 mmol). While stirring, 2-fluoronitrobenzene, (0.839 g, 5.95 mmol), was added drop-wise to the reaction mixture. The reaction mixture was stirred at 100 °C for 48 hrs. The reaction mixture was then allowed to cool to room temperature and 100 ml of water was added to the solution. The pH of the solution was adjusted to 2.0 with 1 N HCl and the reaction mixture was extracted 3 times with 15 ml portions of ethyl acetate. The ethyl acetate layer was separated from the water layer and dried with sodium sulfate. The ethyl acetate was then removed under reduced pressure yielding **V(b)**, (.954 g, 2.56 mmol, 43%), an orange oil. The presence of **V(b)** was confirmed using TLC eluted in a 70/30 ethyl acetate/hexanes solution.

*2-amino-4-(benzimidazol-1-yl)butanoic acid, I(b)*. Without further purification, **V(b)** (.954 g, 2.56 mmol) was dissolved in 30 ml of formic acid. Zinc dust (1 g) was added to the flask, and the solution was allowed to reflux for 24 hrs. Following reflux, the reaction mixture was cooled and filtered. The filtrate containing the formic acid was then collected and the formic acid was removed at 80 °C, under reduced pressure, yielding a clear oil. The oil was then dissolved in 6 N HCl and refluxed at 100 °C for 12 hrs. Following reflux, the formic acid was

removed at 80 °C, under reduced pressure, yielding **I(b)** (0.510 g, 2.32 mmol, 91%), a white crystalline solid. The structure of **I(b)** was confirmed via <sup>1</sup>H-NMR and mass spectrometry.

*Spectral analysis of 2-amino-4-(benzimidazol-1-yl)butanoic acid.* 2-Amino-4-(benzimidazol-1-yl)butanoic acid was characterized by electrospray mass spectrometry, see Appendix 3. Appendix 3 shows a base peak at 220 amu. The base peak at 220 amu corresponds to the molecular mass of protonated 2-amino-4-(benzimidazol-1-yl)butyric acid, C<sub>11</sub>H<sub>14</sub>N<sub>3</sub>O<sub>2</sub><sup>+</sup>. The mass spectrum of the sample confirms the presence of **I(b)** insofar as the mass of the compound. <sup>1</sup>H-NMR was utilized to deduce the structure of the **I(b)**.

The <sup>1</sup>H-NMR spectrum in Appendix 4 depicts six peaks which are significant to the structure of **I(b)**. The triplet peak at δ 2.200 which integrates to 1.83 and corresponds to the two diastereotopic protons (**H<sub>b</sub>**) and (**H<sub>b</sub>'**). The complex splitting that is observed in the peak at δ 2.200 can be attributed to the diastereomeric nature of the protons (**H<sub>b</sub>**) and (**H<sub>b</sub>'**). The triplet peak at δ 3.772 which integrates to 0.93 corresponds to the proton (**H<sub>a</sub>**). The chemical shift of the proton at carbon (**H<sub>a</sub>**) is consistent with the fact that proton (**H<sub>a</sub>**) is positioned alpha to the carboxylic acid. The triplet peak located at δ 4.380, which integrates to 2.08, corresponds to protons (**H<sub>c</sub>**). The chemical shift of protons (**H<sub>c</sub>**) is consistent with the fact that protons (**H<sub>c</sub>**) are affixed to a carbon which is directly attached to an aromatic nitrogen. The multiplet peak at δ 7.227 integrates to 2.18 and corresponds to the aromatic protons (**H<sub>d</sub>**) and (**H<sub>g</sub>**). The complex splitting that is observed at δ 7.227 can be attributed to the overlap of the peaks corresponding to the protons (**H<sub>d</sub>**) and (**H<sub>g</sub>**). The multiplet peak at δ 7.468 integrates to 2.21 and corresponds to the protons (**H<sub>e</sub>**) and (**H<sub>f</sub>**) in the benzimidazole ring. Protons (**H<sub>d</sub>**) and (**H<sub>g</sub>**) are shifted up-field relative to the protons (**H<sub>e</sub>**) and (**H<sub>f</sub>**) because the protons (**H<sub>d</sub>**) and (**H<sub>g</sub>**) are positioned further away from the electronegative aromatic nitrogen atoms composing the benzimidazole ring.

Finally, the singlet at  $\delta$  8.871 integrates to 1.00 and corresponds to proton (**H<sub>h</sub>**). The proton (**H<sub>h</sub>**) is shifted furthest down-field because it is an aromatic methine proton. Based on the foregoing analysis, the structure of 2-amino-4-benzimidazolylbutyric acid can properly be confirmed.

### SYNTHESIS OF 2-AMINO-5-(BENZIMIDAZOL-1-YL)PENTANOIC ACID

*N*-CBZ-*L*-Ornithine **IV(c)**. *N* <sup>$\alpha$</sup> -Benzyloxycarbonyl-*N* <sup>$\delta$</sup> -tert-butoxycarbonyl-*L*-ornithine, **III**, was synthesized according to Rzeszotarska. (Wiejak, Masiukiewicz, & Rzeszotarska, 2001) *N* <sup>$\alpha$</sup> -Benzyloxycarbonyl-*L*-ornithine, **IV(c)**, was synthesized pursuant to the reaction scheme in Figure 11. **III** (11.3 g, 8.57 mmol) was dissolved in a flask containing 50 ml of methylene chloride and 10 ml of trifluoroacetic acid. The solution was allowed to stir for 30 min and the solvent was removed at 50 °C, under reduced pressure. The resulting clear oil was then dissolved in 50 ml of H<sub>2</sub>O and purified using a DOW-50 EX cation exchange column, yielding **IV(c)** (1.98 g, 7.92 mmol, 92%).

*N* <sup>$\alpha$</sup> -CBZ-5-(2-nitrophenylamino)-*L*-Ornithine, **V(c)**. **IV(c)** (1 g, 4.00 mmol) and 25 ml of DMF were combined in a 50 ml round bottom flask along with 1.21 g (12.00 mmol) of triethylamine. While stirring, 2-fluoronitrobenzene (0.564 g, 4.00 mmol) was added drop-wise to the reaction mixture. The reaction mixture was stirred at 100 °C for 48 hrs. The reaction mixture was then allowed to cool to room temperature and 100 ml of water was added to the solution. The pH of the solution was adjusted to 2.0 with 1 N HCl, and the reaction mixture was extracted 3 times with 15 ml portions of ethyl acetate. The ethyl acetate extractions were

combined and dried with sodium sulfate. The ethyl acetate was next removed at 60°C, under reduced pressure, yielding **V(c)** (0.804 g, 2.08 mmol, 52%) as an orange oil.

**2-amino-5-(benzimidazol-1-yl)pentanoic acid, I(c)**. Without further purification, **V(c)** (0.804 g, 2.08 mmol) was dissolved in 30 ml of formic acid and combined with zinc dust, 1 g. The reaction mixture was heated to reflux for 24 hrs. Following reflux, the reaction mixture was cooled and filtered. The filtrate containing the formic acid was then collected and the formic acid was removed at 80 °C, under reduced pressure, yielding a brown oil. The crude oil was then dissolved in 6 N HCl and allowed to reflux at 100 °C for 12 hrs. Following reflux, the formic acid was removed at 80°C, under reduced pressure, producing a black solid, **I(c)**. The black solid was next purified on a C-18 reversed phase column using a 20 % aqueous methanol mobile phase. Upon removal of the mobile phase, **I(c)** was isolated (0.001g, .004 mmol, 0.206%). The structure of **I(c)** was confirmed using <sup>1</sup>H-NMR.

**Spectral analysis of 2-amino-5-(benzimidazol-1-yl)pentanoic acid.** The <sup>1</sup>H-NMR of 2-amino-5-(benzimidazol-1-yl)pentanoic acid is shown in Appendix 5. The triplet peak at  $\delta$  1.353 which integrates to 1.90 and corresponds to the two diastereotopic protons (**H<sub>b</sub>**) and (**H<sub>b</sub>'**). The complex splitting that is observed in the peak at  $\delta$  1.353 can be attributed to the diastereomeric nature of the protons (**H<sub>b</sub>**) and (**H<sub>b</sub>'**). The quintet peak at  $\delta$  1.725 which integrates to 2.13 corresponds to the two protons affixed to carbon (**H<sub>c</sub>**). The triplet peak located at  $\delta$  3.021 which integrates to 0.97 corresponds to the proton (**H<sub>a</sub>**). The chemical shift of proton (**H<sub>a</sub>**) is consistent with the fact that proton (**H<sub>a</sub>**) is positioned alpha to the carboxylic acid side chain, causing the chemical shift of proton (**H<sub>a</sub>**) to be shifted down field. The triplet peak located at  $\delta$  4.095 which integrates to 2.21 corresponds to protons (**H<sub>d</sub>**). The chemical shift of protons (**H<sub>d</sub>**) is consistent with the fact that protons (**H<sub>d</sub>**) are affixed to a carbon directly attached to an

aromatic nitrogen. The multiplet peak at  $\delta$  7.194 integrates to 2.09 and corresponds to the protons (**H<sub>f</sub>**) and (**H<sub>g</sub>**) attached to the benzimidazole ring. The complex splitting that is observed at  $\delta$  7.194 can be attributed to the overlap of the peaks corresponding to the protons (**H<sub>f</sub>**) and (**H<sub>g</sub>**). The protons (**H<sub>f</sub>**) and (**H<sub>g</sub>**) are shifted down-field relative to the protons at carbons (**H<sub>e</sub>**) and (**H<sub>h</sub>**) because the protons on carbons (**H<sub>f</sub>**) and (**H<sub>g</sub>**) are positioned further away from the electronegative aromatic nitrogen atoms composing the benzimidazole ring. The doublet peak at  $\delta$  7.440 integrates to 1.08 and corresponds to the proton (**H<sub>e</sub>**). The chemical shift of the proton (**H<sub>e</sub>**) is positioned further up-field than proton (**H<sub>h</sub>**) because carbon (**H<sub>e</sub>**) is positioned closer to the electron-donating carbons composing the amino acid side chain. The doublet peak at  $\delta$  7.549 integrates to 0.94 and corresponds to the proton affixed to carbon (**H<sub>h</sub>**). Finally, the singlet at  $\delta$  7.999 integrates to 1.00 and corresponds to proton (**H<sub>i</sub>**). Proton (**H<sub>i</sub>**) is shifted furthest down-field affixed to an aromatic carbon which is situated between two electronegative aromatic nitrogen atoms. Based on the foregoing analysis, the structure of 2-amino-4-(benzimidazol-1-yl)pentanoic acid can properly be confirmed.

## KINETICS TESTING OF BENZIMIDAZOLE ANALOGS OF L-TRYPTOPHAN

**Materials.** Benzimidazolyl-L-alanine, 2-amino-4-(benzimidazol-1-yl)butyric acid, and 2-amino-5-(benzimidazol-1-yl)pentanoic acid were synthesized pursuant to the synthetic procedures indicated in above. Lactate dehydrogenase (from rabbit muscle lyophilized) and NADH, disodium salt were obtained from U.S. Biochemical Corp. S-(o-nitrophenyl)-L-cysteine

(SOPC) for enzyme assays was prepared from L-cysteine and 2-fluoronitorbenzene as previously described by Phillips. (Phillips, 1989)

**Enzyme Assays.** Tryptophan indole-lyase was purified from cells of the *E. coli tnaA* JM101 containing plasmid pMD6, with the *E. coli tnaA* gene under natural regulation, as described except that the Sepharose treatment was performed in a column rather than batchwise. (Phillips & Gollnick, 1989) Inhibition activity assays were performed with SOPC in 0.1 M potassium phosphate, pH 8.0, at 25°C, following the absorbance decrease at 370 nm ( $\Delta\epsilon=-1860 \text{ M}^{-1}\text{cm}^{-1}$ ). (Suelter, Wang, & Snell, 1976) The activities of substrates were measured with the lactate dehydrogenase coupled assay, following the decrease in absorbance at 340 nm ( $\Delta\epsilon=-6220 \text{ M}^{-1}\text{cm}^{-1}$ ) in 0.1 M potassium phosphate, pH 8.0, at 25°C. (Morino & Snell, 1970) Enzyme concentrations were estimated from the absorbance of the holoenzyme at 278 nm ( $A_{1\%} = 9.19$ ) (Phillips & Gollnick, 1989) using a subunit molar mass of 52 kDa. (Kagamiyama & Snell, 1972)

**Steady-state kinetic measurements.** Steady-state kinetic measurements were performed at 25°C as described previously (Kiick & Phillips, 1988) using a Cary 1 UV/Vis spectrophotometer equipped with a thermoelectric cell block. Steady-state kinetic data were analyzed by using the FORTRAN program of Cleland (1979) to fit the data to eq 1 and eq 2.

$$v_{obs} = \frac{k_{cat}[S]}{K_m + [S]}$$

Equation 1

$$v_{obs} = \frac{k_{cat}[S]}{K_m \left( 1 + \frac{[I]}{K_i} \right) + [S]}$$

Equation 2

***Pre-Steady-State Kinetic Measurements.*** Rapid scanning stopped-flow kinetic experiments were performed using an RSM-1000 spectrophotometer and a stopped-flow compartment with a 10-mm pathlength observation cell from Olis Inc. Rapid scanning measurements were performed at 1 kHz. Prior to the rapid kinetics experiments, the stock enzyme was separated from excess PLP on a short desalting column (PD-10, Pharmacia) equilibrated with 0.020 M Potassium phosphate, pH 8.0 and 0.16 M KCl, and reactions were performed in the same buffer. The stopped-flow kinetic measurements were performed at room temperature. Generally, the enzyme solutions were mixed with the solutions of the corresponding tryptophan analogue in the same buffer. The data obtained from the scans was fit with Olis Globalworks software.

## RESULTS

***β-(Benzimidazol-1-yl)alanine.*** The concentrations of SOPC and β-(benzimidazol-1-yl)alanine were varied as indicated in Appendix 22. The rates for each reaction mixture were recorded and the data were fit to Equation 2. The fit revealed the  $K_i$  of benzimidazolyl-L-alanine to be  $300 \pm 5 \mu\text{M}$ . A substrate test was next conducted on β-(benzimidazol-1-yl)alanine. The concentration of the β-(benzimidazol-1-yl)alanine was varied as indicated in Appendix 26 and

the data was fit to Equation 1. The fit revealed the  $K_m$  of the benzimidazolyl-L-Alanine to be  $507 \pm 6 \mu\text{M}$ . The pre-steady-state kinetic measurements taken of  $\beta$ -(benzimidazol-1-yl)alanine revealed the reaction was too fast to monitor at 1000 scans per second. At first scan, the reaction had reached steady-state. This can be seen in Appendix 6. The data shown in Appendix 6 corresponds to  $\beta$ -(benzimidazol-1-yl)alanine/trpase reaction monitored over a period of 14 seconds. As can be seen from the graph, there is no substantial change in the graph over the monitored period. At 0 seconds, the reaction absorbance at all pertinent wavelengths is essentially the same as the absorbance at 14 seconds.

**2-amino-4-(benzimidazol-1-yl)butanoic acid.** The concentrations of SOPC and 2-amino-4-(benzimidazol-1-yl)butanoic acid were varied as indicated in the Appendix 23. The rates for each reaction mixture were recorded and the data was fit to Equation 2. The fit revealed the  $K_i$  of 2-amino-4-(benzimidazol-1-yl)butanoic acid to be  $16 \pm 2 \mu\text{M}$ . A substrate test was next conducted on 2-amino-4-(benzimidazol-1-yl)butanoic acid and no activity was observed.

The pre-steady-state kinetics shown in Appendix 7 revealed that upon mixing 2 mM 2-amino-4-(benzimidazol-1-yl)butanoic acid with 2 mg/ml trpase, 2-amino-4-(benzimidazol-1-yl)butanoic acid initially formed a decaying *gem*-diamine peak at 340 nm. (Kallen, et al., 1985) A time versus absorbance plot at 340 nm documented in Appendix 8 shows that during the stopped-flow dead-time, the *gem*-diamine peak had already formed and over the lifetime of the reaction the absorbance at 340 nm, corresponding to the *gem*-diamine peak, decays.

In Appendix 7, it can further be observed that as the *gem*-diamine peak at 340 nm decays, a peak at 497 nm corresponding to a quinonoid intermediate forms. The time versus absorbance plot at 497 nm shown in Appendix 9 indicates that at time zero, the concentration of the quinonoid species in the reaction mixture was negligible. However, as the reaction moves to

completion, the absorbance at 497 nm, corresponding to the quinonoid peak increases. The isosbestic point between the peaks at 340 nm and 497 nm, shown in Figure 18, suggest that the *gem*-diamine reacts to form the quinonoid.

A global fit of the pre-steady-state kinetics data revealed the reaction to be triphasic and composed of four species whose corresponding rate constants are  $4.5 \pm 0.2 \times 10^{-1} \text{ s}^{-1}$ ,  $7.6 \pm 0.3 \times 10^{-2} \text{ s}^{-1}$ , and  $4.3 \pm 0.2 \times 10^{-2} \text{ s}^{-1}$ . The rate constants for the reaction were found not to be concentration dependent, indicating that the apparent reaction is first order.

**2-amino-5-(benzimidazol-1-yl)pentanoic acid.** The steady-state kinetics tests revealed that 2-amino-5-(benzimidazol-1-yl)pentanoic acid was inactive as a substrate or as an inhibitor for tryptophan indole-lyase at a concentration of 600 mM. Pre-steady-state kinetics experiments were not conducted on this compound.

## DISCUSSION

**Table 5: Steady-state kinetic parameters for the reaction of benzimidazolyl analogs of tryptophan with *E. coli* Tryptophan Indole-lyase.**

Substrate	$K_i$ (mM)	$k_{cat}$ ( $\text{s}^{-1}$ )	$K_m$ (mM)	$k_{cat}/K_m$ ( $\text{mM}^{-1} \text{ s}^{-1}$ )
L-tryptophan <sup>a</sup>	-	4	0.15	27
$\beta$ -Indazolyl-L-alanine <sup>b</sup>	-	0.54	0.2	2.7
Benzimidazolyl-L-alanine <b>I(a)</b>	0.298	5.63	0.507	11.11
2-amino-4-benzimidazolyl-butyric acid <b>I(b)</b>	0.016	-	-	-
2-amino-5-benzimidazolyl-pentanoic acid <b>I(c)</b>	-	-	-	-

<sup>a</sup> Data from Lee and Phillips (1995).  
<sup>b</sup> Data from Sloan and Phillips (1996)

***β-(benzimidazol-1-yl)alanine***. The reaction rates calculated for β-(benzimidazol-1-yl)alanine are shown in Table 5. The  $K_i$  of β-(benzimidazol-1-yl)alanine was found to be 0.298 mM while the  $K_m$  was found to be 0.507 mM. These values differ by a factor of approximately one and a half and this difference is not kinetically significant.

When comparing the steady-state kinetics of L-tryptophan with β-(benzimidazol-1-yl)alanine, it can be seen that the  $K_m$  values of each compound are on the same order of magnitude, 0.150 mM for L-tryptophan and 0.507 mM for β-(benzimidazol-1-yl)alanine. Although the  $K_m$  of L-tryptophan is approximately three times greater than β-(benzimidazol-1-yl)alanine (see Table 5) this difference is not kinetically significant. The enzyme efficiency for the two substrates also differ slightly, the  $k_{cat}/K_m$  for L-tryptophan was determined to be 27  $\text{mM}^{-1}\text{s}^{-1}$  while the  $k_{cat}/K_m$  for β-(benzimidazol-1-yl)alanine was determined to be 11  $\text{mM}^{-1}\text{s}^{-1}$  (See Table 5). The  $k_{cat}/K_m$  for L-tryptophan is about two times greater than the  $k_{cat}/K_m$  for β-(benzimidazol-1-yl)alanine and this difference is also kinetically insignificant. The small differences that exist between the steady state kinetics of L-tryptophan and β-(benzimidazol-1-yl)alanine can be attributed to their structural similarities.

We now compare β-indazolyl-alanine to β-(benzimidazol-1-yl)alanine because like β-indazolyl-alanine, β-(benzimidazol-1-yl)alanine functions as a substrate of trpase and both substrates possess an amino acid side chain that is attached to a nitrogen atom in their respective heterocyclic rings. The  $K_m$  of β-indazolyl-alanine was calculated as 0.200 mM, while the  $K_m$  of β-(benzimidazol-1-yl)alanine was calculated as 0.507 mM. The difference between these two  $K_m$  values are not kinetically significant; however, when the  $k_{cat}/K_m$  values for the two compounds are compared, it was noted that the  $k_{cat}/K_m$  for β-(benzimidazol-1-yl)alanine (11.11  $\text{mM}^{-1}\text{s}^{-1}$ ) was nearly six times greater than that of β-indazolyl-alanine (2.7  $\text{mM}^{-1}\text{s}^{-1}$ ). We

attribute the difference between the efficiency of trpase with  $\beta$ -indazolyl-alanine and  $\beta$ -(benzimidazol-1-yl)alanine to the fact that the resonance stabilization that takes place in the proposed mechanism for the degradation of  $\beta$ -(benzimidazol-1-yl)alanine (see Figure 13) makes the benzimidazole ring in  $\beta$ -(benzimidazol-1-yl)alanine a better leaving group than the indazole ring present in  $\beta$ -indazolyl-alanine. The fact that indazole is a poor leaving group can account for reduced catalytic turn-over of  $\beta$ -indazolyl-alanine as compared to  $\beta$ -(benzimidazol-1-yl)alanine.

Based on the similarities between  $\beta$ -(benzimidazol-1-yl)alanine and L-tryptophan, two mechanisms were hypothesized for the benzimidazolyl-L-alanine/trpase reaction. Figure 12 proposes that  $\beta$ -(benzimidazol-1-yl)alanine first reacts with trpase to form an external aldimine. The aldimine is then deprotonated, leading to a quinonoid intermediate. The quinonoid intermediate is then protonated at the proximal nitrogen, forming the indicated transition state. The indolenine intermediate then collapses to form benzimidazole and the aminoacrylate.

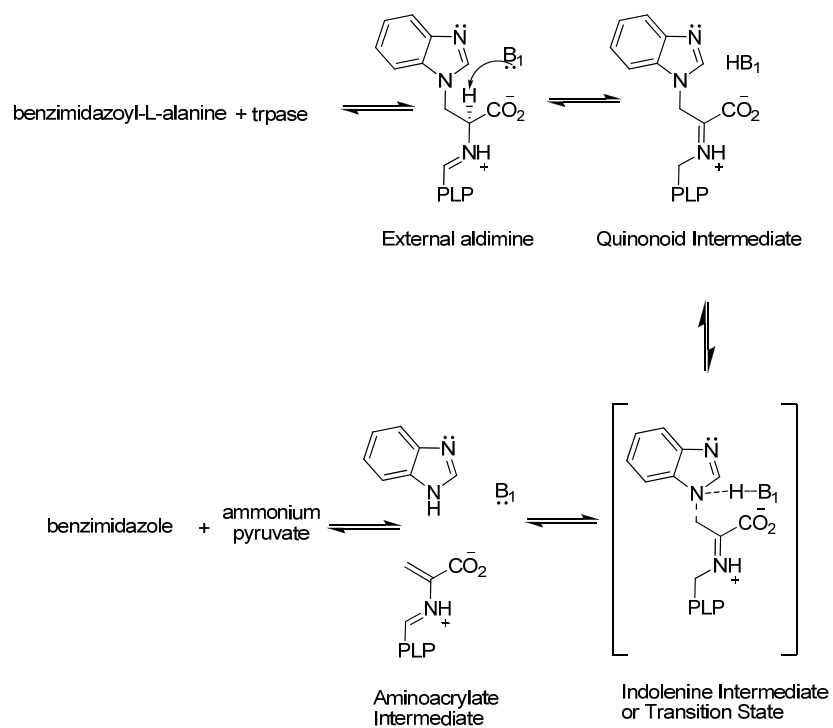


**Figure 12: Proposed mechanism for benzimidazolyl-L-alanine reaction**

Figure 13, proposes an alternative mechanism for the benzimidazolyl-L-alanine/trpase reaction. The first step in the mechanism is the formation of an external aldimine. The aldimine is then deprotonated to form a quinonoid. After the quinonoid is formed, beta elimination occurs in one concerted step whereby the distal nitrogen of the benzimidazole ring is protonated.

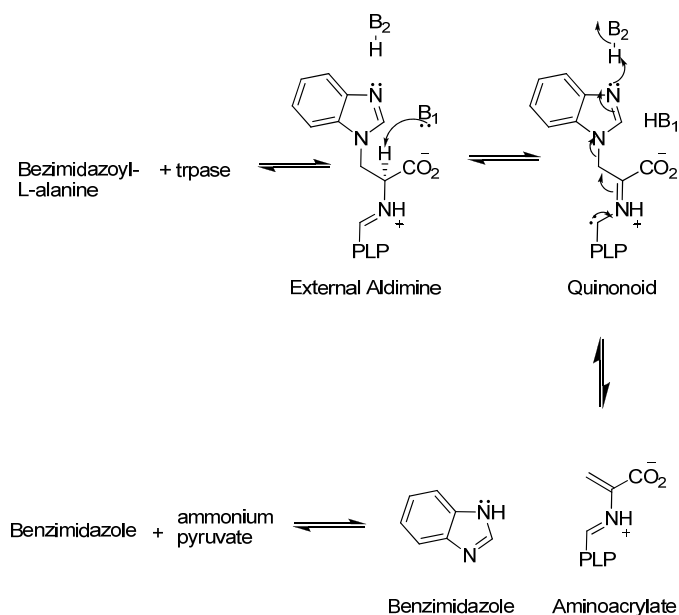
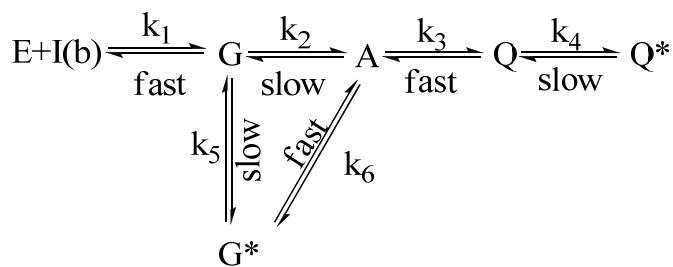


**Figure 13: Proposed mechanism for benzimidazolyl-L-alanine reaction**



Note: E: enzyme (trpase); G: *gem*-diamine; G\*: conformationally different *gem*-diamine; A: external aldimine; Q: quinonoid; Q\* conformationally different quinonoid.

**Figure 14: Proposed kinetic mechanism for the 2-amino-4-(benzimidazol-1-yl)butanoic acid/tryptophan indole-lyase reaction**

***Pre-steady-state kinetic data: 2-amino-4-(benzimidazol-1-yl)butanoic acid.***

A global fit of the time course of decay of the *gem*-diamine at 340 nm and the formation of the quinonoid species at 496 nm revealed that the reaction had three observable steps. Based on the L-tryptophan/trpase mechanism and the pre-steady state data, we propose that the **I(b)**/trpase reaction consists of seven steps, as shown in Figure 14. The first step in the reaction involves the unobserved process of **I(b)** reacting with trpase (**E** + **I(b)**) to form the *gem*-diamine (**G**). The rate for this step,  $k_1$ , we characterize as fast because formation of the *gem*-diamine was complete within the first observed scan (1 msec). Next, **G** inter-converts to an external aldimine (**A**). Because neither the formation nor the decay of **A** is observable in the UV/Vis spectrum, we conclude that there is no significant accumulation of **A** and characterize the rate constant,  $k_3$ , for this step, as slow. Subsequently, (**A**) inter-converts to a quinonoid species (**Q**) at a rate,  $k_3$ , which we characterize as fast as compared to  $k_2$ . In characterizing  $k_2$  as slow and  $k_3$  as fast, we account for the fact that **A**, which is a necessary intermediate in the formation of **Q**, has no significant life-time, while the formation of **Q** is observed. These rate constants suggest that  $k_2$  is the rate-limiting step between the conversion of the *gem*-diamine to the quinonoid and thus is the only rate observed in the interconversion process. We propose that the steps composed of **G**→**A**→**Q** were observed as one step by the global fit and correspond to the rate constant  $4.5 \times 10^{-1} \text{ s}^{-1}$ . We next propose that **G** can interconvert to a conformational isomer, (**G\***), we characterize the rate constant of this step,  $k_5$ , as fast. We hypothesize the existence of the conformational isomer **G\*** based on the known intermediates in the L-tryptophan/trpase mechanism. Subsequent to its formation, we propose that **G\*** interconverts to **A** and we characterize the rate constant for this step,  $k_6$ , as slow corresponding to the rate constant  $7.6 \times 10^{-1}$

<sup>2</sup> s<sup>-1</sup>. Because **G** and **G\*** are in fast equilibrium, we hypothesize that the rate constant **k<sub>5</sub>** is the faster of both rate constants **k<sub>2</sub>** and **k<sub>6</sub>**. In characterizing **k<sub>5</sub>** as fast and **k<sub>6</sub>** as slow, we note that **k<sub>6</sub>** is the rate determining step in the **G** → **G\*** → **A** reaction. Finally, after **Q** forms, the **Q** interconverts more slowly to a structurally different quinonoid (**Q\***) at a rate, **k<sub>4</sub>**, 4.3 x 10<sup>-2</sup> s<sup>-1</sup>. We reason that this is a structurally different quinonoid because after the *gem*-diamine has finished decaying, the absorbance at 497 nm continues to increase.

## CONCLUSION

This study was conducted in order to determine whether benzimidazole analogs of tryptophan could serve as inhibitors of tryptophan indole-lyase. Benzimidazolyl-L-alanine was synthesized first due to its structural similarities to L-tryptophan. Steady-state kinetic testing revealed benzimidazolyl-L-alanine to be a substrate of tryptophan indole-lyase having a  $K_m$  of 0.507 mM. Pre-steady-state kinetic testing of benzimidazolyl-L-alanine revealed that the reaction proceeded too fast to observe at 1000 scans per second. We next hypothesized that by increasing the amino acid side chain of benzimidazolyl-L-alanine by one methylene group we would be able to make a benzimidazole analog of tryptophan which functioned as a more potent inhibitor of tryptophan indole-lyase than  $\beta$ -(benzimidazol-1-yl)alanine. After synthesizing 2-amino-4-benzimidazolylbutyric acid, we tested its steady state kinetics in the tryptophan indole-lyase reaction. The steady-state kinetic data revealed that 2-amino-4-(benzimidazol-1-yl)butyric acid functioned as an inhibitor of tryptophan indole-lyase, having a  $K_i$  of 16  $\mu$ M. Pre-steady-state kinetics of 2-amino-4-(benzimidazol-1-yl)butyric acid revealed that the reaction rapidly forms a *gem*-diamine which interconverts to a quinonoid intermediate and because elimination of

the benzimidazole ring cannot take place, the quinonoid intermediate accumulates. In a final effort to produce a more potent inhibitor of tryptophan indole-lyase, we next increased the amino acid side chain of 2-amino-4-(benzimidazol-1-yl)butyric acid by a methylene group, generating 2-amino-5-(benzimidazol-1-yl)pentanoic acid. Steady-state kinetics of 2-amino-5-(benzimidazol-1-yl)pentanoic acid revealed that this compound was not an inhibitor of tryptophan indole-lyase at 600  $\mu\text{M}$ .

## CHAPTER 3: HOMOLOGUES OF AROMATIC AMINO ACIDS AS INHIBITORS OF TRYPTOPHAN INDOLE-LYASE

### INTRODUCTION

In the previous chapter we synthesized three benzimidazole analogs of L-tryptophan. The first,  $\beta$ -(benzimidazol-1-yl)-L-alanine, like L-tryptophan, has a three carbon amino acid side chain. Steady-state kinetics revealed  $\beta$ -(benzimidazol-1-yl)-L-alanine to be a substrate of tryptophan indole-lyase (trpase) exhibiting a  $K_m$  of 500  $\mu$ M. In an attempt to create a more potent inhibitor of trpase, we elongated the amino acid side chain by one methylene group, producing 2-amino-4-(benzimidazol-1-yl)butyric acid as a product. Steady-state kinetics revealed 2-amino-4-(benzimidazol-1-yl)butyric acid to be an inhibitor of trpase with an inhibition constant of 16  $\mu$ M. By extending the amino acid side chain by one methylene, we observed nearly a 50 fold increase in binding. In an effort to make even more potent inhibitor of trpase, we extended the amino acid side chain of 2-amino-4-(benzimidazol-1-yl)butyric acid by one methylene group producing, 2-amino-5-(benzimidazol-1-yl)pentanoic acid as a product. Steady-state kinetics revealed 2-amino-5-(benzimidazol-1-yl)pentanoic acid is trpase inactive at a concentration of 600  $\mu$ M. Because optimization of inhibition was achieved with 2-amino-4-(benzimidazol-1-yl)butyric acid, a homologous amino acid, this study seeks to synthesize two additional aromatic amino acids which are composed of 4 carbon amino acid side chains. 2-Amino-4-(benzimidazol-1-yl)butyric acid, **I(d)**, was hypothesized to be an inhibitor of tryptophan indole-lyase because it is simply an analog of the known trpase inhibitor, 2-amino-4-

(benzimidazol-1-yl)butyric acid. S-benzyl-homocysteine, **VIII**, was hypothesized to be an inhibitor of trpase because it is a homolog of the trpase substrate S-benzyl-cysteine. This work embodies the synthesis of **I(d)** and **VIII**, as shown in Figure 15. Once synthesized, steady-state and pre-steady state kinetics will be conducted on **I(d)** and **VIII** to determine if each are active as inhibitors of tryptophan indole-lyase. Further, a comparative analysis of 2-amino-4-(benzimidazol-1-yl)butyric acid, **I(d)**, 2-amino-4-(benzimidazol-1-yl)butyric acid, **I(b)**, S-benzyl-homocysteine, **VIII**, and homophenylalanine will be conducted to better understand how homologues of aromatic amino acids react with tryptophan indole-lyase.

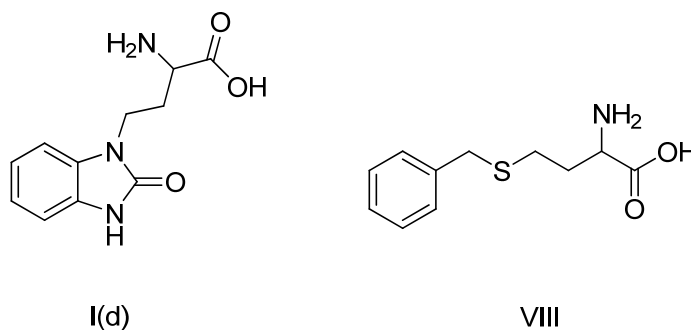


**Figure 15: Homologous aromatic amino acids.**

## SYNTHESIS OF HOMOLOGUES OF AROMATIC AMINO ACIDS

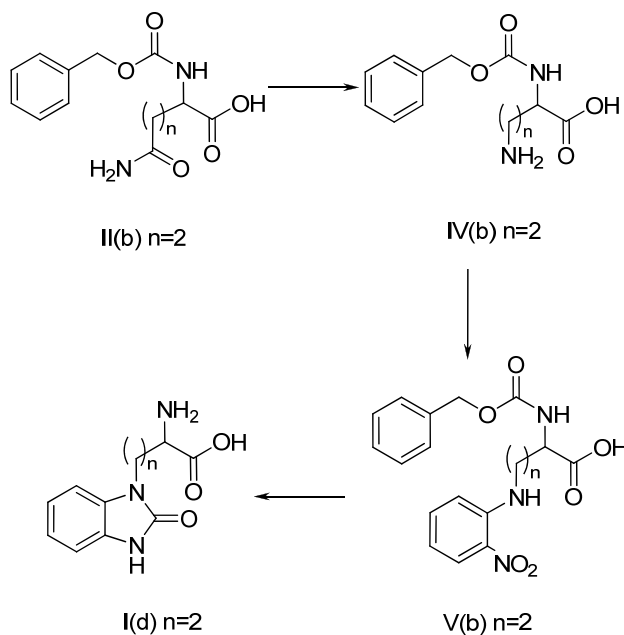


Figure 16: Synthetic scheme for 2-amino-4-(benzimidazol-1-yl)butyric acid.

## SYNTHESIS OF 2-AMINO-4-(BENZIMIDAZOLON-1-YL)BUTYRIC ACID

The synthesis of 2-amino-4-(benzimidazol-1-yl)butyric acids was carried out pursuant to the scheme shown in Figure 16.

*N<sup>α</sup>-CBZ-γ-aminobutyric acid IV(b)*. N<sup>α</sup>- benzyloxycarbonyl-L-glutamine **II(b)**, (2 g, 7.14 mmol) (Sigma), and 50 ml of THF were combined in a 100 ml round bottom flask. While stirring, the solution was cooled to 10 °C using an ice bath. Iodobenzene diacetate (3.05 g, 9.29 mmol) was then added to the THF solution, and the reaction was allowed to stir at room temperature for 8 hrs. The THF was removed from the system at 80 °C, under reduced pressure. The resulting clear oil was then dissolved in water and extracted three times with chloroform.

The chloroform was discarded and the water from the aqueous layer was then removed at 80 °C, under reduced pressure, yielding **IV(b)** (1.5 g, 5.95 mmol 83%), a light brown solid. (Rodinov, Rodionova, Baidakova, Romashko, Balashova, & Federation, 2002) The product was qualitatively characterized by TLC and ninhydrin staining.

*N<sup>α</sup>-CBZ-4-(2-nitrophenylamino)glutamine, V(b)*. **IV(b)** (1.5g, 5.95 mmol), and 25 ml of DMF were combined in a 50 ml round bottom flask along with triethylamine (1.8 g, 17.85 mmol). While stirring, 2-fluoronitrobenzene (Sigma) (0.839g, 5.95 mmol), was added dropwise to the reaction mixture. The reaction mixture was stirred at 100 °C for 48 hrs. The reaction mixture was then allowed to cool to room temperature and 100 ml of water was added to the solution. The pH of the solution was adjusted to 2.0 with 1 N HCl. The reaction mixture was then extracted 3 times with 15 ml portions of ethyl acetate and dried with sodium sulfate. The ethyl acetate was then removed under reduced pressure yielding **V(b)**, an orange oil (1.11 g, 2.96 mmol 51%). The product was qualitatively characterized by TLC.

*2-amino-4-(benzimidazol-1-yl)butyric acid I(d)*. **V(b)** (1.11 g, 2.96 mmol) was combined with urea, 3 g, and K<sub>2</sub>CO<sub>3</sub>, 500 mg, and dissolved in *N,N*-dimethyl acetamide, 20 ml. The reaction mixture was heated to 200 °C and stirred for 24 hrs. Next, concentrated hydrochloric acid, 40 ml, was added to the reaction mixture, and the reaction refluxed for 12 hrs. The solvent was removed at 70 °C, under reduced pressure, producing brown crystals. The brown crystals were a mixture of **I(d)** and dimethyl ammonium chloride and were purified on a cation exchange column eluting **I(d)** with aqueous ammonium hydroxide. The aqueous ammonium hydroxide was removed at 60°C under reduced pressure. The purity of the resulting brown crystals was checked by reversed phase TLC in 20% aqueous ethanol. The TLC showed the crystals to be impure and **I(d)** was further purified on a C-18 reverse phase column in 20%

aqueous ethanol yielding **I(d)** (0.301 g, 1.27 mmol 43%). The structure of **I(d)** was verified using electrospray mass spectrometry and H-NMR.

*Spectral analysis of 2-amino-4-(benzimidazol-1-yl)butanoic acid.* 2-amino-4-(benzimidazol-1-yl)butanoic acid was characterized by electrospray mass spectrometry. Appendix 10 shows a base peak at 236 amu. The base peak at 236 amu corresponds to the molecular mass of a protonated 2-amino-4-(benzimidazol-1-yl)butyric acid,  $C_{11}H_{14}N_3O_3^+$ . The mass spectrum of the sample confirms the presence of **I(d)** insofar as the mass of the compound.  $^1H$ -NMR was utilized to deduce the structure of the **I(d)**.

The  $^1H$ -NMR shown in Appendix 11 was collected on a 400 Mhz Varian Mercury Plus instrument, in  $D_2O$ . The spectrum in Appendix 11 depicts four peaks which are significant to the structure of **I(d)**. The complex peak at  $\delta$  2.004 which integrates to 2.05 corresponds to the two diastereotopic protons (**H<sub>b</sub>**) and (**H<sub>b'</sub>**). The complex splitting that is observed in the peak at  $\delta$  2.004 can be attributed to the diastereomeric nature of the protons (**H<sub>b</sub>**) and (**H<sub>b'</sub>**). The poorly resolved peak at  $\delta$  3.493 which integrates to 1.25 corresponds to the proton (**H<sub>a</sub>**). The chemical shift of the proton (**H<sub>a</sub>**) is consistent with the fact that (**H<sub>a</sub>**) is located alpha to the carboxylic acid. The peak located at  $\delta$  3.737 which integrates to 2.10 corresponds to protons (**H<sub>c</sub>**). The chemical shift of protons (**H<sub>c</sub>**) is consistent with the fact that protons (**H<sub>c</sub>**) are affixed to a carbon which is directly attached to an aromatic nitrogen. The complex peak at  $\delta$  6.925 integrates to 4.00 and corresponds to the aromatic protons (**H<sub>d</sub>**), (**H<sub>3</sub>**), (**H<sub>f</sub>**) and (**H<sub>g</sub>**). Based on the foregoing analysis, the structure of 2-amino-4-(benzimidazol-1-yl)butyric acid can properly be confirmed.

## SYNTHESIS OF S-BENZYLHOMOCYSTEINE

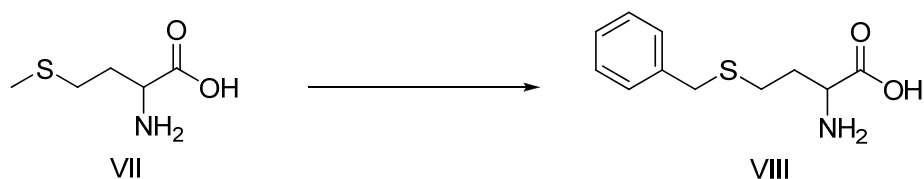


**Figure 17: Methionine, S-benzylcysteine reaction scheme.**

***S-benzyl-L-homocysteine.*** S-Benzyl-L-homocysteine was synthesized pursuant to Dekker. (Dekker & Fruton, 1947) L-methionine (5 g, 33.9 mmol) was dissolved in concentrated hydrochloric acid, 50 ml. Benzyl bromide (5.73 g, 33.5 mmol) was added to the reaction mixture and the reaction was refluxed for 6 hrs. After reflux, the hydrochloric acid was removed at 80 °C under reduced pressure. Water, 50 ml was added to the reaction flask, and the pH of the reaction mixture was adjusted to 7.0, generating crystals. The crystals were isolated using suction filtration yielding **VIII** (6.86 g, 30.4 mmol 91%). **VIII** was characterized by <sup>1</sup>H-NMR.

***Spectral analysis of S-benzyl-homocysteine.*** The H-NMR shown in Appendix 12 was collected on a 400 Mhz Varian Mercury Plus instrument, in D<sub>2</sub>O/NaOD. The spectrum in Appendix 12 depicts five peaks which are significant to the structure of **VIII**. The complex peak at  $\delta$  1.384 which integrates to 1.62 corresponds to the two diastereotopic protons (**H<sub>b</sub>**) and (**H<sub>b</sub>'**). The complex splitting that is observed in the peak at  $\delta$  1.384 can be attributed to the diastereomeric nature of the protons (**H<sub>b</sub>**) and (**H<sub>b</sub>'**). The triplet at  $\delta$  2.096 which integrates to 2.29 corresponds to protons (**H<sub>c</sub>**). The peak located at  $\delta$  2.888 which integrates to 1.00 corresponds to proton (**H<sub>a</sub>**). The chemical shift of proton (**H<sub>a</sub>**) is consistent with the fact that

(**H<sub>a</sub>**) is positioned alpha to the carboxylic acid. The singlet located at  $\delta$  3.396 corresponds to the benzylic protons (**H<sub>d</sub>**). The complex peak at  $\delta$  7.008 which integrates to 5.52 corresponds to the aromatic protons (**H<sub>e</sub>**), (**H<sub>f</sub>**), (**H<sub>g</sub>**) and (**H<sub>h</sub>**). Based on the foregoing analysis, the structure of S-benzylhomocysteine can properly be confirmed.

## KINETICS TESTING OF HOMOLOGUES OF AROMATIC AMINO ACIDS

*Materials and Methods.* See pgs. 12-14.

## RESULTS

*2-Amino-4-(benzimidazol-1-yl)butyric acid.* The concentrations of SOPC and 2-amino-4-(benzimidazol-1-yl)butyric acid were varied as indicated in Appendix 24. The rates for each reaction mixture were recorded and the data was fit to Equation 2. The fit revealed the  $K_i$  of 2-amino-4-(benzimidazol-1-yl)butyric acid to be  $15 \pm 2 \mu\text{M}$ . A substrate assay was conducted on 2-amino-4-(benzimidazol-1-yl)butyric acid and no activity was observed.

The pre-steady-state kinetics shown in Appendix 13 revealed that upon mixing 2 mM 2-amino-4-(benzimidazol-1-yl)butyric acid with 2 mg/ml trypsin, 2-amino-4-(benzimidazol-1-yl)butyric acid initially formed a decaying *gem*-diamine peak at 340 nm. A time versus absorbance plot at 340 nm documented in Appendix 14 shows that during the stopped flow dead-time, the *gem*-diamine peak had already formed and over the lifetime of the reaction, the absorbance decreased at 340 nm, corresponding to the *gem*-diamine decay.

In Appendix 13, it can further be observed that as the *gem*-diamine peak at 340 nm decays, a peak at 497 nm corresponding to a quinonoid intermediate forms. The time versus absorbance plot at 497 nm shown in Appendix 15 indicates that at time zero the concentration of the quinonoid in the reaction mixture was negligible. However, as the reaction moves to completion, the absorbance at 497 nm, corresponding to the quinonoid peak, increases. The isobestic point between the peaks at 340 nm and 497 nm, shown in Appendix 13, suggests that the *gem*-diamine reacts to form the quinonoid.

A global fit of the pre-steady-state kinetic data revealed the reaction to be triphasic and composed of four steps. The rate constant for the first observable step was concentration dependent, increasing linearly with the concentration of the inhibitor, and is second order, as seen in Appendix 16. A linear regression fit to the rate constants revealed the second order rate constants for the first step of the 2-amino-4-(benzimidazol-1-yl)butyric/trypase reaction were determined to be  $k_f = 0.0949 \text{ mM}^{-1} \text{ s}^{-1}$  and  $k_r = 0.843 \text{ s}^{-1}$ . The rate constants for the second and third steps were  $5.74 \pm 0.2 \times 10^{-1} \text{ s}^{-1}$  and  $8.5 \pm 0.3 \times 10^{-2} \text{ s}^{-1}$  correspondingly. Because the rate constants for the second and third observable steps were not dependent upon the concentration of the inhibitor, these steps are considered first order.

***S*-benzyl-L-homocysteine.** The concentrations of SOPC and *S*-benzyl-L-homocysteine were varied as indicated in Appendix 25. The rates for each reaction mixture were recorded and the data was fit to Equation 2. The fit revealed the  $K_i$  of *S*-benzyl-L-homocysteine to be  $14 \pm 4 \text{ } \mu\text{M}$ . A substrate assay was conducted on *S*-benzyl-L-homocysteine and no activity was observed.

The pre-steady-state kinetics shown in Appendix 17 revealed that upon mixing 2 mM *S*-benzyl-L-homocysteine with 2 mg/ml trypase, *S*-benzyl-L-homocysteine initially formed a

decaying *gem*-diamine peak at 340 nm. A time versus absorbance plot at 340 nm documented in Appendix 18 shows that during the stopped-flow dead-time, the *gem*-diamine peak had already formed and over the lifetime of the reaction the absorbance at 340 nm, corresponding to the *gem*-diamine, decays.

In Appendix 17, it can further be observed that as the *gem*-diamine peak at 340 nm decays, a peak at 497 nm corresponding to a quinonoid intermediate forms. The time versus absorbance plot at 497 nm shown in Appendix 19 indicates that at time zero the concentration of the quinonoid had formed in moderate quantities; however, as the reaction moves to completion, the absorbance at 497 nm, corresponding to the quinonoid peak, increases. The isosbestic point between the peaks at 340 nm and 497 nm, shown in Appendix 17, suggests that the *gem*-diamine reacts to form the quinonoid. We also note that in the spectrum shown in Appendix 17, a small peak at 389 nm slowly forms as the *gem*-diamine decays. The peak at 389 nm corresponds to the formation of the external-aldimine, which exists in equilibrium with the quinonoid peak.

Initial global fitting of the pre-steady-state kinetics data revealed the reaction to be triphasic and composed of four species. The rate constants derived from the global fit were not concentration dependent. Thus the reaction of S-benzylhomocysteine with trpase is a first order process. The rates for steps 1, 2, and 3 were determined to be  $6.6 \pm 0.3 \times 10^{-1}$ ,  $1.25 \pm 0.5 \times 10^{-1}$ , and  $1.06 \pm 0.7 \times 10^{-2}$ , correspondingly.

## DISCUSSION

**Table 6: Comparison of the tryptophan indole-lyase inhibition constants of homologous aromatic amino acids.**

Tryptophan Indole-Lyase Inhibitor	K <sub>i</sub> ( $\mu$ M)	Reaction Completion Time (s)
2-amino-4-(benzimidazol-1-yl)butyric acid <b>I(b)</b>	16	60
2-amino-4-(benzimidazol-1-yl)butyric acid <b>I(d)</b>	15	10
S-benzylhomocysteine <b>VIII</b>	14	15
Homophenylalanine <sup>a</sup>	110	5

<sup>a</sup> adapted from (Phillips, Bender, Brzovic, & Dunn, 1990)

As can be seen from the Table 6 that each of the inhibition constants for the homologous inhibitors are similar. When the pre-steady-state kinetics were observed for 2-amino-4-(benzimidazol-1-yl)butyric acid, 2-amino-4-(benzimidazol-1-yl)butyric acid, and S-benzylhomocysteine, it was clearly demonstrated that each inhibitor rapidly forms a *gem*-diamine at 320 nm, during the dead time of the stopped-flow. Subsequently, each *gem*-diamine decays forming a quinonoid species at 497 nm. The global fit of the pre-steady-state kinetic data revealed that 2-amino-4-(benzimidazol-1-yl)butyric acid, 2-amino-4-(benzimidazol-1-yl)butyric acid, and S-benzylhomocysteine/trpase reactions are observed as three step processes and are triphasic. 2-amino-4-(benzimidazol-1-yl)butyric acid, 2-amino-4-(benzimidazol-1-yl)butyric acid, and S-benzylhomocysteine each behave mechanistically as described on pages 20-22 herein. In contrast, the pre-steady-state kinetic data for homophenylalanine shows an initial peak at 420 nm corresponding to the free enzyme and as the homophenylalanine/trpase

reaction proceeds, the enzyme peak at 420 nm decreases and a *gem*-diamine peak at 320 nm appears transiently, decaying to form the quinonoid peak at 425 nm. (Phillips, Bender, Brzovic, & Dunn, 1990). The fact that the formation of the *gem*-diamine is observed in the homophenylalanine/trpase reaction but not in the 2-amino-4-(benzimidazol-1-yl)butyric acid, 2-amino-4-(benzimidazol-1-yl)butyric acid, and S-benzyl-L-homocysteine/trpase reactions suggests that 2-amino-4-(benzimidazol-1-yl)butyric acid, 2-amino-4-(benzimidazol-1-yl)butyric acid, and S-benzylhomocysteine react faster with the trpase to form the *gem*-diamine than homophenylalanine.

The first observed step in the 2-amino-4-(benzimidazol-1-yl)butyric acid/trpase and homophenylalanine/trpase reactions were shown to be second order processes. The observed concentration dependence for the first observed step for each of these reactions suggests that at concentrations as high as 16 mM of 2-amino-4-(benzimidazol-1-yl)butyric acid, 1.2 mM homophenylalanine and 2 mg/ml trpase, the trpase active site is not completely saturated with 2-amino-4-(benzimidazol-1-yl)butyric acid, and homophenylalanine respectively for the step of the reaction in which the *gem*-diamine forms. In contrast, the rates for each of the steps corresponding to the global fit for the data obtained for the 2-amino-4-(benzimidazol-1-yl)butyric acid/trpase and S-benzyl-L-homocysteine/trpase reactions were not concentration dependent and were categorized as first order. The independence of the rate on concentration for these reactions suggests that at a concentration as low as 2 mM of 2-amino-4-(benzimidazol-1-yl)butyric acid, and 2 mg/ml trpase; and at a concentration as low as 2 mM S-benzyl-L-homocysteine and 2 mg/ml trpase, the trpase active site is completely saturated for the step of the reaction in which the *gem*-diamine forms.

The time in which it took the 2-amino-4-(benzimidazol-1-yl)butyric acid, S-benzylhomocysteine and homophenylalanine/trpase reactions to go to completion were 10 s, 15 s, and 5 s correspondingly. The differences between these reaction times are insignificant; however, the time in which it took the 2-amino-4-(benzimidazol-1-yl)butyric/trpase reaction to proceed to completion was 60 s. We now attempt to account for the longer reaction time observed for the 2-amino-4-(benzimidazol-1-yl)butyric and trpase reaction mechanistically. According to the L-tryptophan/trpase mechanism, a base is required to remove a proton from the indole ring of L-tryptophan, as seen in Figure 18. Because there is no hydrogen attached to the nucleophilic nitrogen of the benzimidazole ring in 2-amino-4-(benzimidazol-1-yl)butyric acid, the basic residue in the active-site which is normally used to deprotonate the indole ring in L-tryptophan repels the basic nitrogen in the benzimidazole ring as seen in Figure 19. Thus, in order for the benzimidazole ring to be adequately stabilized in the active site of the enzyme, the repulsion of these two bases needs to be diminished. The former can be accomplished by allowing a proton to diffuse into the active site of the enzyme as seen in Figure 19. The concentration of the protonated species shown in Figure 19 is low extending the 2-amino-4-(benzimidazol-1-yl)butyric acid/trpase reaction time to 60 s.

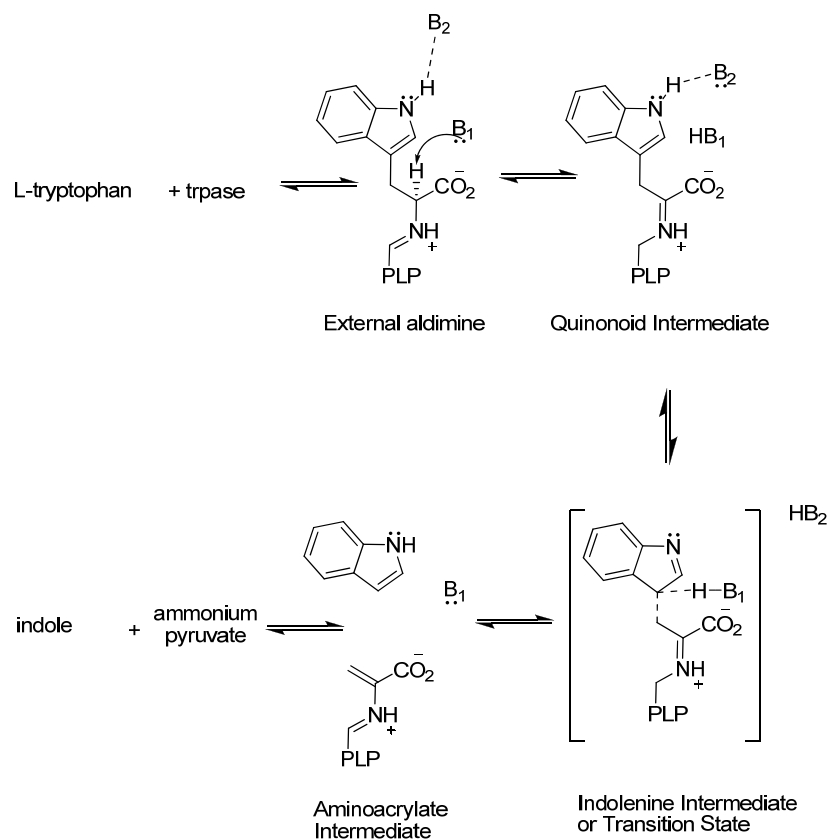


**Figure 18: L-Tryptophan, tryptophan indole-lyase mechanism.**

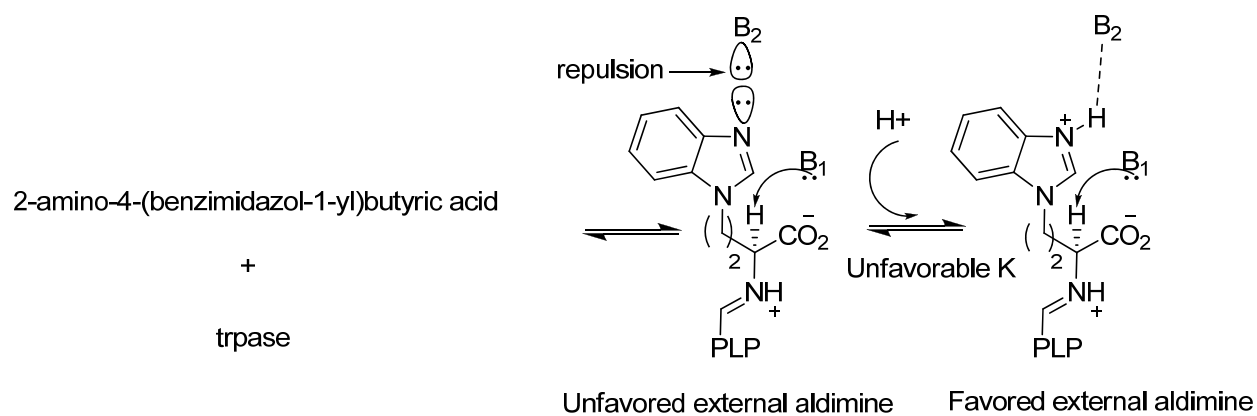


**Figure 19: Mechanistic analysis for why this 2-amino-4-(benzimidazol-1-yl)butyric acid has a longer reaction time.**

## CONCLUSION

In the experiments conducted in this section, we synthesized four homologous aromatic amino acids; subsequently testing their steady-state and pre-steady-state kinetics. The steady state kinetics affirmed our hypothesis that aromatic homologous amino acids will behave as inhibitors of tryptophan indole-lyase. The pre-steady-state kinetics revealed that each aromatic homologous amino acid that we synthesized would be best fit to a three step mechanism in which one step consisted of a *gem*-diamine decaying to form a stable quinonoid species.

## CHAPTER 4: INHIBITORS OF TRYPTOPHAN INDOLE-LYASE CAN ALSO INHIBIT TRYPTOPHAN SYNTHASE

### INTRODUCTION

Tryptophan Synthase is an  $\alpha_2\beta_2$  multi-enzyme complex which catalyzes synthesis of L-tryptophan from indole-3-glycerol phosphate and L-serine. The  $\alpha$ -subunit catalyzes the cleavage of indole-3-glycerol phosphate to indole, while the  $\beta$ -subunit catalyzes the synthesis of L-tryptophan from indole and L-serine, as seen in Figure 20. The activity of tryptophan synthase has been linked

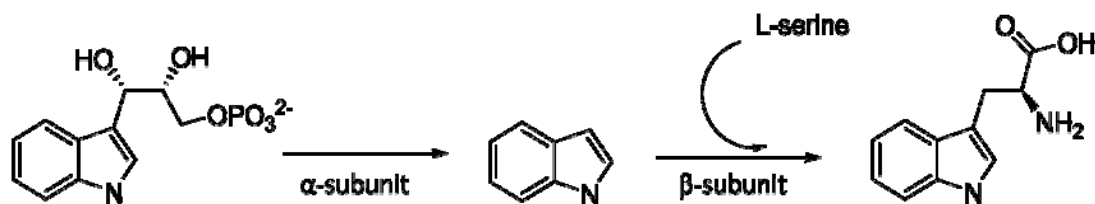


**Figure 20: Tryptophan synthase catalyzed synthesis of L-tryptophan.**

to the pathogenicity of *Chlamydia trachomatis*, and various other virulent strains of gram negative bacteria, which effect both humans and plants. (Caldwell, et al., 2003) In a 1985 study, Phillips et al. discovered that 2,3-dihydro-L-tryptophan, a known competitive inhibitor of tryptophan indole-lyase also functioned as an inhibitor of tryptophan synthase. (Phillips, Miles, & Cohen, 1985) Because it has been shown that inhibitors of tryptophan indole-lyase can also

function as inhibitors of tryptophan synthase, we seek to determine if the inhibitors of trpase, discussed previously will also function as inhibitors of tryptophan synthase.

### STEADY-STATE KINETICS STUDIES OF TRYPTOPHAN SYNTHASE

**Materials.** Pyridoxal-5-phosphate (Sigma).

**Enzymes and Assays.** The  $\alpha_2\beta_2$  complex of tryptophan synthase was prepared from *E. coli* strain W3110 *trpR cysB*  $\Delta$  *trp* LD102 *trpB*<sup>+</sup> *trpA*<sup>+/F'</sup> *colVB cysB*<sup>+</sup> *trpA*<sup>+</sup> as described by Higgins et al. (Higgins, Fairwell, & Miles, 1979) Assays were carried out as previously described by Phillips. (Phillips, Miles, & Cohen, 1984)

### RESULTS

Initial inhibition kinetics revealed  $\beta$ -(benzimidazol-1-yl)alanine to inhibit tryptophan synthase at a concentration of 0.500 mM. The inhibition assay was also run on 2-amino-4-(benzimidazol-1-yl)alanine and inhibition of tryptophan synthase was observed at a concentration of 0.250 mM. Due to time constraints, further kinetic analysis could not be included in this work; however, the  $K_i$  values for  $\beta$ -(benzimidazol-1-yl)alanine, 2-amino-4-(benzimidazol-1-yl)butyric acid, 2-amino-4-(benzimidazol-1-yl)butyric acid, and homophenylalanine will be determined in an attempt to demonstrate that aromatic homologues of amino acids will serve as inhibitors of tryptophan synthase.

## DISCUSSION

***β-(benzimidazol-1-yl)alanine***. Initial steady-state inhibition studies of β-(benzimidazol-1-yl)alanine revealed that β-(benzimidazol-1-yl)alanine was tryptophan synthase active at a concentration of 0.500 mM. The initial kinetic studies suggest that due to the similar structure of β-(benzimidazol-1-yl)alanine and L-tryptophan ( $K_i = 170 \mu\text{M}$ ), β-(benzimidazol-1-yl)alanine will likely inhibit tryptophan synthase at a concentration which is congruent with the  $K_i$  of L-tryptophan. Further studies will need to be conducted on β-(benzimidazol-1-yl)alanine to determine its tryptophan synthase  $K_i$ .

***2-amino-4-(benzimidazol-1-yl)butyric acid***. Initial kinetic studies revealed that 2-amino-4-(benzimidazol-1-yl)butyric acid was tryptophan synthase active at a concentration of 0.250 mM. The significance of this result is that these initial kinetic studies suggest that aromatic homologues of amino acids may serve as potent inhibitors of tryptophan synthase. As was shown in our previous study, homologues of aromatic amino acids function as inhibitors of tryptophan indole-lyase the same conclusion may be applied to inhibitors of tryptophan synthase.

## CONCLUSION

This study revealed that β-(benzimidazol-1-yl)alanine and 2-amino-4-(benzimidazol-1-yl)butyric acid show activity with tryptophan synthase. Although the  $K_i$  for each of the compounds has not been calculated, these initial studies suggest that 2-amino-4-(benzimidazole-1-yl)butyric acid, and homophenylalanine may also function as inhibitors of tryptophan synthase.

Further steady-state kinetics will need to be conducted in order to determine the inhibition constants for  $\beta$ -(benzimidazol-1-yl)alanine and 2-amino-4-(benzimidazol-1-yl)butyric acid as well as whether the hypothesis that homologues of aromatic amino acids will function as inhibitors of tryptophan synthase can be confirmed.

## CHAPTER 5: THE SYNTHESIS OF S-METHYL-D-CYSTEINE

### INTRODUCTION

Nitric oxide is an intercellular signal in animals effecting vasodilatation, smooth muscle relaxation and many neurological functions. Many actions of nitric oxide are caused by S-nitrosothiols or thionitrites. A pathological condition caused by the overproduction of nitric oxide is septic shock. One method for treating septic shock has been to create inhibitors of the enzyme which catalyzes the production of nitric oxide, nitric oxide synthase; however, results from these experiments have not been promising. Lewis et al. recently discovered that S-methyl-L-cysteines serves as a vasoconstrictor, preventing hypotension which is one of the causes of septic shock. Following this discovery, Lewis et al. hypothesized that the pathway through which S-methyl-L-cysteine caused vasoconstriction was a stereospecific process. In order to prove that the action of S-methyl-L-cysteine was stereospecific, Lewis et al. sought to show that vasoconstriction would not occur in rats, when the rats were administered S-methyl-D-cysteine. Due to the high price market price carried by S-methyl-D-cysteine we synthesized S-methyl-D-cysteine and provided Lewis et al. to conduct this study. This work embodies the synthesis of S-methyl-D-cysteine and its use in a vasoconstriction assay to determine whether the vasoconstriction observed when laboratory rats are administered S-methyl-L-cysteine is a stereospecific process. We chose to synthesize and resolve S-methyl-D-cysteine pursuant to the scheme shown in Figure 21.

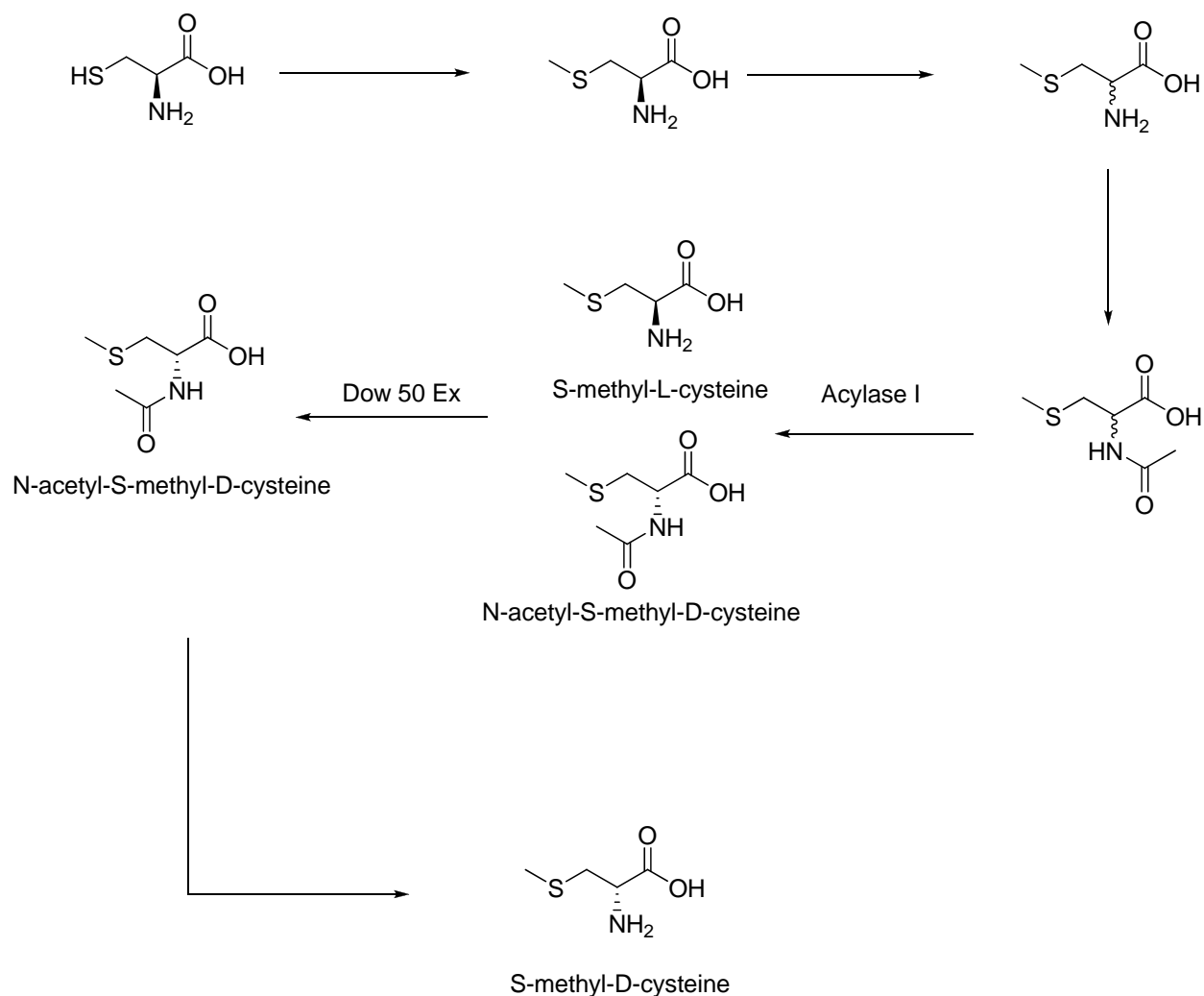


**Figure 21: Synthetic scheme for the S-methyl-D-cysteine.**

## SYNTHESIS AND RESOLUTION OF S-METHYL-D-CYSTEINE

**S-methyl-L-cysteine.** S-Methyl-L-cysteine was synthesized pursuant to Hwang et al. and as seen in Figure 21, above. (Hwang, Helquist, & Shekhani, 1984) L-cysteine hydrochloride hydrate (sigma) (5 g, 10.54 mol) and sodium , 5.5 g, was combined with absolute ethanol, 200

ml, and stirred. When the sodium was completely dissolved, methyl iodide (4.1 ml, 0.065 mol) was added to the reaction mixture. The reaction was allowed to stir for 15 minutes. Water and aqueous hydroiodic acid was then added to the reaction mixture until the white solid which had accumulated in the reaction mixture had dissolved. Diethyl ether, 60 ml, was next added to the reaction mixture and the reaction mixture was refrigerated overnight. The resulting crystals were next collected using suction filtration yielding S-methyl-L-cysteine (7.02 g, 0.0467 mol 88%). S-methyl-L-cysteine was characterized by optical rotation; calculated as  $[\alpha]_D^{25} = -32.5$  which is the same as the literature value. The structure of S-methyl-L-cysteine was further confirmed via proton NMR. (Hwang, Helquist, & Shekhani, 1984)

***Spectral analysis of S-methyl-L-cysteine.*** The  $^1\text{H-NMR}$  shown in Appendix 20 was collected on a 400 Mhz Varian Mercury Plus instrument, in  $\text{D}_2\text{O}$ . The spectrum in Appendix 20 depicts three peaks which are significant to the structure of S-methyl-L-cysteine. The singlet at  $\delta$  1.958 which integrates to 2.61 corresponds to protons ( $\text{H}_c$ ). The complex peak at  $\delta$  2.781 corresponds to the two diastereotopic protons ( $\text{H}_b$ ) and ( $\text{H}_b'$ ). Finally, complex peak at  $\delta$  3.684 which integrates to 1.00 corresponds to ( $\text{H}_a$ ). Based on the foregoing analysis the structure of S-methyl-L-cysteine can be confirmed.

***S-methyl-DL-cysteine.*** S-methyl-L-cysteine (7 g, 0.0467 mol) was combined with acetic acid, 100 ml. The mixture was heated to reflux under nitrogen for a period of 3 hrs. The acetic acid was next removed under reduced pressure at  $70^\circ\text{C}$ . The resulting brown solid was refluxed in 6N HCl for 6 hours under nitrogen. The solvent was then removed at  $70^\circ\text{C}$  under reduced pressure. The resulting solid was purified by DOW-50 EX cation exchange column yielding S-methyl-DL-cysteine (6.5 g, 0.0436 mol 92.8%). The optical activity of the crystals,  $[\alpha]_D^{25} = 0$ ,

revealed that S-methyl-L-cysteine had been successfully racemized. (Hwang, Helquist, & Shekhani, 1984)

***N-acetyl-S-methyl-DL-cysteine.*** N-acetyl-S-methyl-DL-cysteine (6.5 g, 0.0436 mol) was combined with acetic anhydride (4.45 g, 0.436 mol) and acetic acid 100 ml. The reaction was allowed to reflux for 3 hours. The acetic acid was removed at 70 °C under reduced pressure yielding N-acetyl-S-methyl-DL-cysteine (7.41 g, 0.0388 mol 89%). N-acetyl-S-methyl-DL-cysteine was characterized using <sup>1</sup>H-NMR, as seen in Appendix 21.

***Spectral analysis of S-methyl-DL-cysteine.*** The <sup>1</sup>H-NMR shown in Appendix 21 was collected on a 400 Mhz Varian Mercury Plus instrument, in D<sub>2</sub>O. The spectrum in Appendix 21 depicts four peaks which are significant to the structure of N-acetyl-S-methyl-L-cysteine. The singlet at δ 1.882 which integrates to 3.26 corresponds to protons (**H<sub>c</sub>**). The singlet at δ 1.963 which integrates to 2.93 corresponds to protons (**H<sub>d</sub>**). The two complex peaks at δ 2.758 and δ 2.885 correspond to the two diastereotopic protons (**H<sub>b</sub>**) and (**H<sub>b'</sub>**). Finally, complex peak at δ 4.408 which integrates to 1.00 corresponds to (**H<sub>a</sub>**). Based on the foregoing analysis the structure of N-acetyl-S-methyl-L-cysteine can be confirmed.

***N-acetyl-S-methyl-D-cysteine.*** N-acetyl-S-methyl-DL-cysteine (7.41 g, 0.0388 mol) was dissolved in 100 ml of 50 mM potassium phosphate buffer. Acylase I (Sigma), 100 mg, was added to the reaction mixture. The mixture was stirred at room temperature for 3 days. The solvent was next removed at 80 °C under reduced pressure. The resulting crystalline solid was next run through a Dowex-50 cation exchange column. S-Methyl-L-cysteine was absorbed onto the column, while N-acetyl-S-methyl-D-cysteine flowed through the column. N-acetyl-S-methyl-D-cysteine (1.91 g, 0.0101 mol 51%) was isolated from the column. (Uttamsingh, Keller, & Anders, 1998)

*S-methyl-D-cysteine*. N-acetyl-S-methyl-D-cysteine (1.91 g, 0.0101 mol) was dissolved in 6 N HCl and refluxed for 12 hrs. Following reflux, the solvent was removed at 80 °C under reduced pressure. The compound was next characterized by <sup>1</sup>H-NMR, the spectrum of which was identical to that shown in Appendix 20. The presence of S-methyl-D-cysteine was further confirmed by optical rotation which was determined to be  $[\alpha]_D^{25} = +32.5$ , agreeing with the literature value. (Hwang, Helquist, & Shekhani, 1984)

## RESULTS

We are still awaiting results of the effects of using S-methyl-D-cysteine in the vasodilatation assay from our collaborators.

## REFERENCES

- Anyanful, A., Dolan-Livengood, J. M., Lewis, T., Sheth, S., DeZalia, M., Sherman, M. A., et al. (2005). Paralysis and Killing of *Caenorhabditis elegans* by Enteropathogenic *Escherichia coli* Requires the Bacterial Tryptophanase Gene. *Molecular Microbiology*, *57* (4).
- Berger, E. A. (1973). Different Mechanisms of Energy Coupling for the Active Transport of Proline. *Proceedings of the National Academy of Sciences of the United States of America*, *70* (5), 1514-1518.
- Beveridge, T. J. (1999). Structures of Gram-Negative Cell Walls and Their Derived Membrane Vesicles. *Journal of Bacteriology*, *181* (16), 4725-4773.
- Caldwell, H. D., Wood, H., D. Crane, R. B., Jones, R. B., Mabey, D., Maclean, I., et al. (2003). Polymorphism in *Chlamydia trachomatis* tryptophan synthase genes differentiate between genital and ocular isolates. *The Journal of Clinical Investigation*, *111* (11), 1757-1768.
- Costerton, J. W., Stewart, P. S., & Greenberg, E. P. (1994). Bacterial Biofilms: A Common Cause of Persistent Infections. *Science*, *284*, 1318-1322.
- Davis, L., & Metzler, D. E. (1972). *The Enzymes* (3rd Edition ed., Vol. 7). New York: Academic Press.
- Deeley, M. D., & Yanofsky, C. (1981). Nucleotide Sequence of the Structural Gene for Tryptophanase of *Escherichia coli* K-12. *The Journal of Bacteriology*, *147* (3), 787-796.
- Dekker, C., & Fruton, J. (1947). Preparation of D- and L-Methionine by Enzymatic Resolution. *The Journal of Biological Chemistry*, 471-477.
- DiMartino, P., Fursy, R., Bret, L., Sundararaju, B., & Phillips, R. (2003). Indole Can Act as an Extracellular Signal to Regulate Biofilm Formation of *Escherichia coli* and Other Indole-Producing Bacteria. *Canadian Journal of Microbiology*, *49*, 443-449.
- DiMartino, P., Merieau, A., Phillips, R., Orange, N., & Hulen, C. (2002). Isolation of an *Escherichia coli* Strain Mutant Unable to Form Biofilm on Polystyrene and to Adhere to Human Pneumocyte Cells: Involvement of Tryptophanase. *Canadian Journal of Microbiology*, *48*, 132-137.
- Flournoy, D., Reinert, R. L., Bell-Dixon, C., & Gentry, C. A. (2000). Increasing Antimicrobial Resistance in Gram-Negative Bacilli Isolated from Patients in Intensive Care Units. *American Journal of Infection Control*, *28* (3), 244-250.
- Higgins, W., Fairwell, T., & Miles, E. W. (1979). *Biochemistry*, *18*, 4827-4835.
- Hwang, D., Helquist, P., & Shekhani, M. S. (1984). Total Synthesis of (+)-Sparsomycin. Approaches Using Cysteine and Serine Inversion. *Journal of Organic Chemistry*, *50*, 1264-1271.

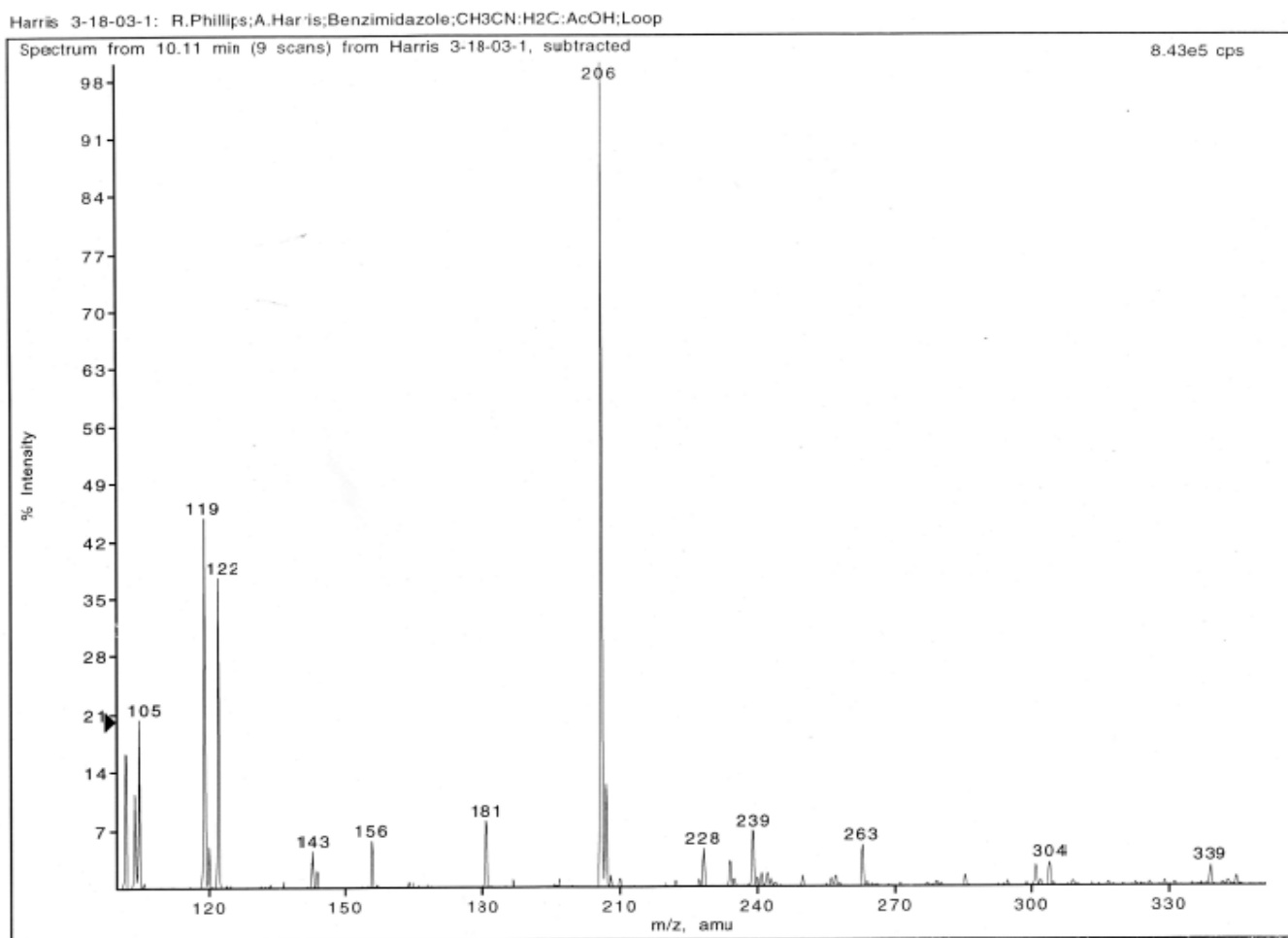
- Kallen, R. G., Korpela, T., Martell, A. E., Y. Matsushima, Metzler, C. M., Metzler, D. E., et al. (1985). *Transaminases* (Vol. 2). New York: John Wiley and Sons.
- Kiick, D. M., & Phillips, R. S. (1988). Mechanistic Deductions from Multiple Kinetic and Solvent Deuterium Isotope Effects and pH Studies of Pyridoxal Phosphate Dependent Carbon-Carbon Lyases: *Escherichia coli* Tryptophan Indole-Lyase. *Biochemistry*, 27 (19), 7339-7344.
- Morino, Y., & Snell, E. E. (1970). *Methods in Enzymology*, 17A, 439-446.
- Phillips, R. S. (1989). Mechanism of Tryptophan Indole-Lyase: Insights from Pre-Steady-State Kinetics. *Journal of the American Chemical Society*, 111 (2), 727-730.
- Phillips, R. S., & Gollnick, P. (1989). Evidence That Cysteine 298 Is in the Active Site of Tryptophan. *The Journal of Biological Chemistry*, 264 (18), 10627-10632.
- Phillips, R. S., Bender, S. L., Brzovic, P., & Dunn, M. F. (1990). Mechanism of Binding of Substrate Analogues to Tryptophan Indole-Lyase: Studies Using Rapid-Scanning and Single Wavelength Stopped-Flow Spectrophotometry. *Biochemistry*, 29 (37), 8608-8614.
- Phillips, R. S., Miles, E. W., & Cohen, L. A. (1984). *Biochemistry*, 23, 6228-6234.
- Phillips, R. S., Miles, E. W., & Cohen, L. A. (1985). Differential Inhibition of Tryptophan Synthase and of Tryptophanase by the Two Diastereomers of 2,3-Dihydro-L-tryptophan. *The Journal of Biological Chemistry*, 260 (27), 14665-14670.
- Phillips, R. S., Miles, E., & Cohen, L. A. (1984). Interactions of Tryptophan Synthase, Tryptophanase and Pyridoxal Phosphate with Oxindolyl-L-Alanine and 2,3 Dihydro-L-Tryptophan: Support for an Indolenine Intermediate in Tryptophan Metabolism. *Biochemistry*, 23, 6228-6234.
- Porter, J. R. (1976). Antony van Leeuwenhoek: Tercentenary of His Discovery of Bacteria. *Bacteriological Reviews*, 40 (2), 260-269.
- Pratt, L. A., & Kolter, R. (1998). Genetic Analysis of *Escherichia coli* Biofilm Formation: Roles of Flagella, Motility, Chemotaxis and Type I Pili. *Molecular Microbiology*, 30, 285-293.
- Rodinov, I. L., Rodionova, L. N., Baidakova, L. K., Romashko, A. M., Balashova, T. A., & Federation, V. (2002). Cyclic Dipeptides as Building Blocks for Combinatorial Libraries. Part 2: Synthesis of Bifunctional Diketopiperazines. *Tetrahedron*, 58 (42), 8515-8523.
- Suelter, C. H., Wang, J., & Snell, E. E. (1976). Direct Spectrophotometric Assay of Tryptophanase. *FEBS Letters*, 66 (2), 230-232.
- Uttamsingh, V., Keller, D. A., & Anders, M. W. (1998). Acylase I-Catalyzed Deacetylation of N-Acetyl-L-cysteine and S-Alkyl-N-acetyl-L-cysteines. *Chemical Research in Toxicology*, 11, 800-809.
- Walsh, C. T., & Wright, G. (2005). Introduction: Antibiotic Resistance. *Chemical Reviews*, 105 (2), 391-394.

Wang, D., Ding, X., & Rather, P. N. (2001). Indole Can Act as an Extracellular Signal in *Escherichia coli*. *Journal of Bacteriology*, *183* (14), 4210-4216.

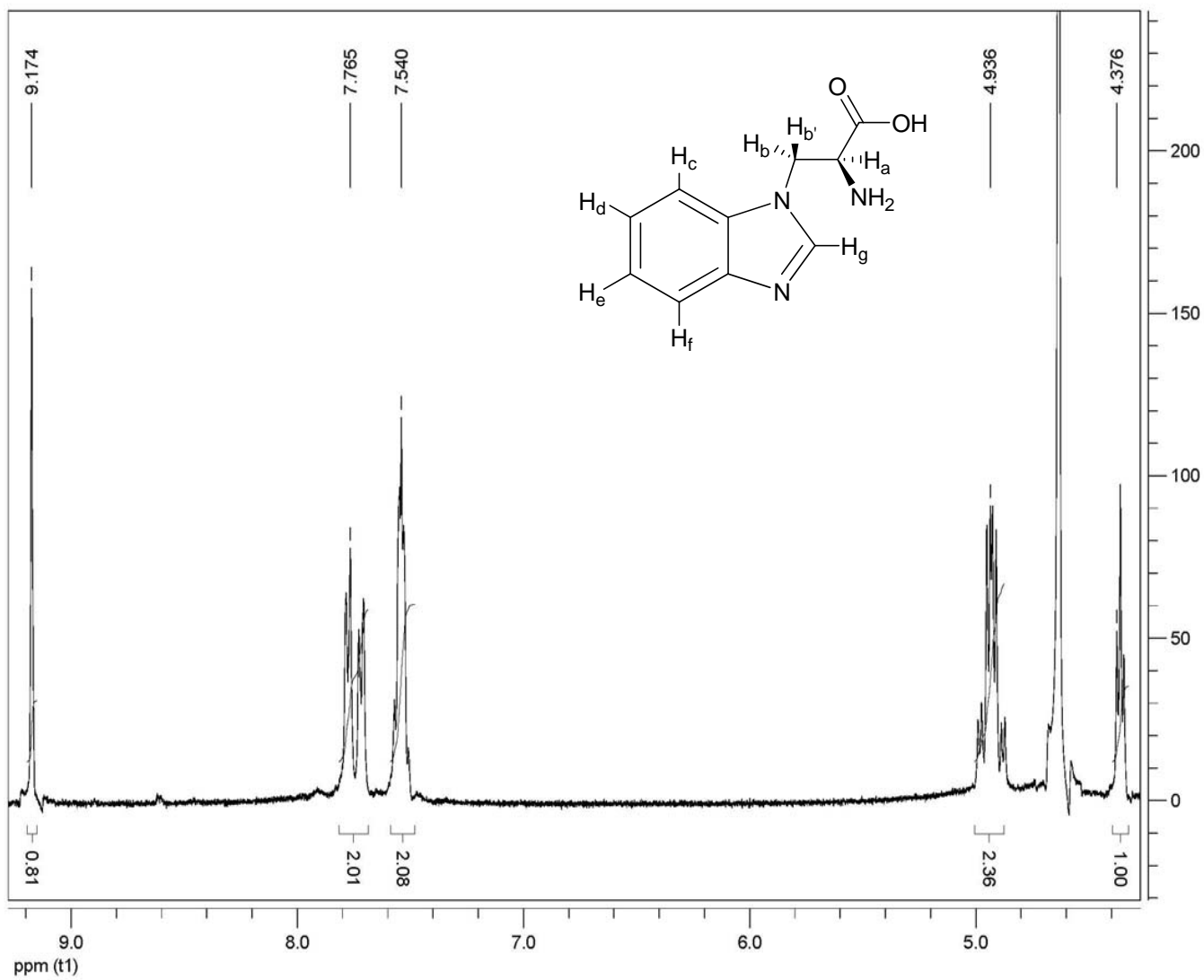
Wiejak, S., Masiukiewicz, E., & Rzeszotarska, B. (2001). Improved Scalable Synthesis of Mono- and Bis-Urethane Derivatives of Ornithine. *Chemical & Pharmaceutical Bulletin*, *49* (9), 1189-1191.

Zhang, L.-h., Kauffman, G. S., Pesti, J. A., & Yin, J. (1997). Rearrangement of N-alpha-Protected L-Asparagines with Iodosobenzene Diacetate. A Practical Route to Beta-Amino-L-Alanine Derivatives. *Journal of Organic Chemistry*, *62* (20), 6918-6920.

## APPENDICES

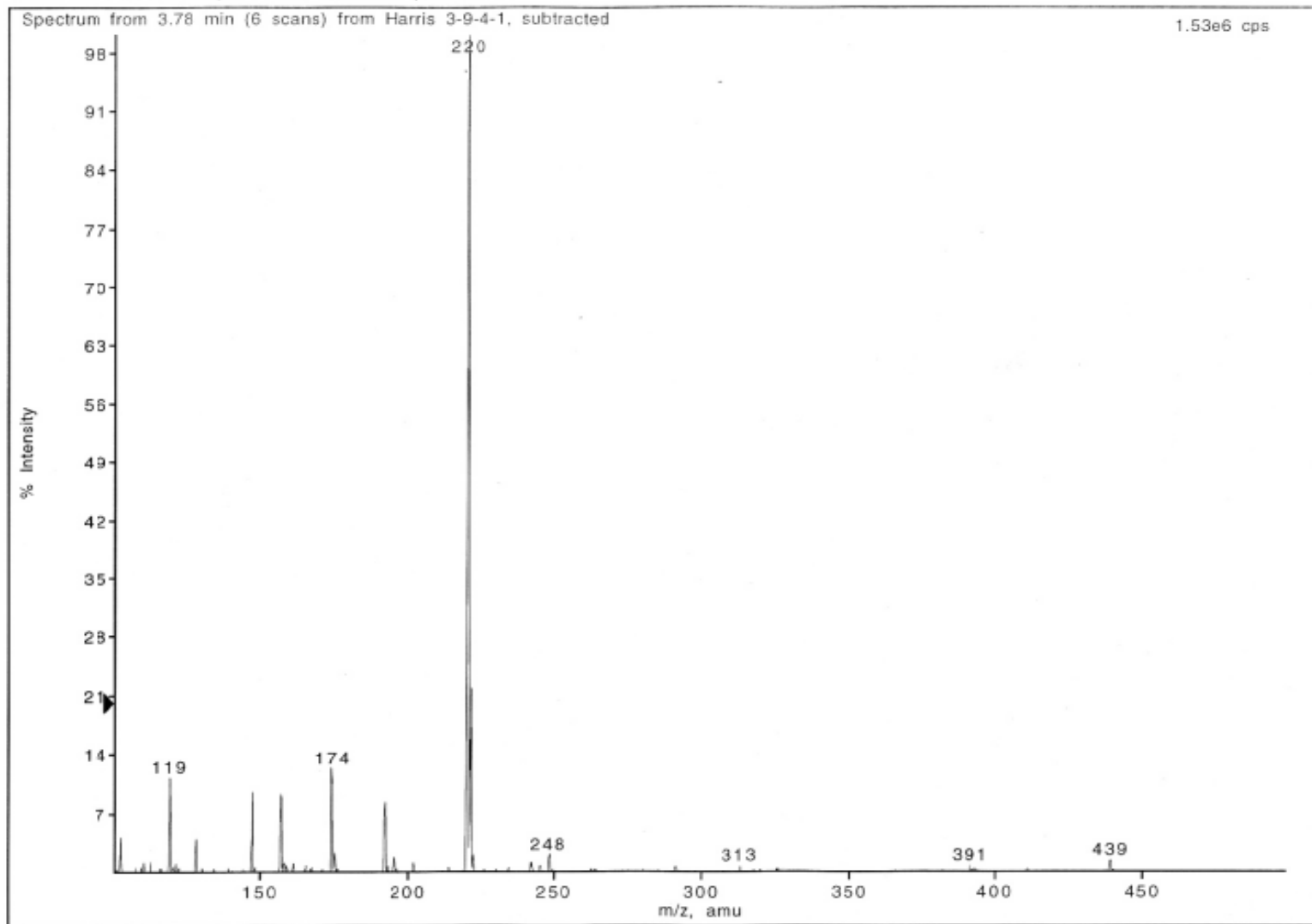


Appendix 1: Electrospray Mass Spectrum of Benzimidazoly-L-Alanine

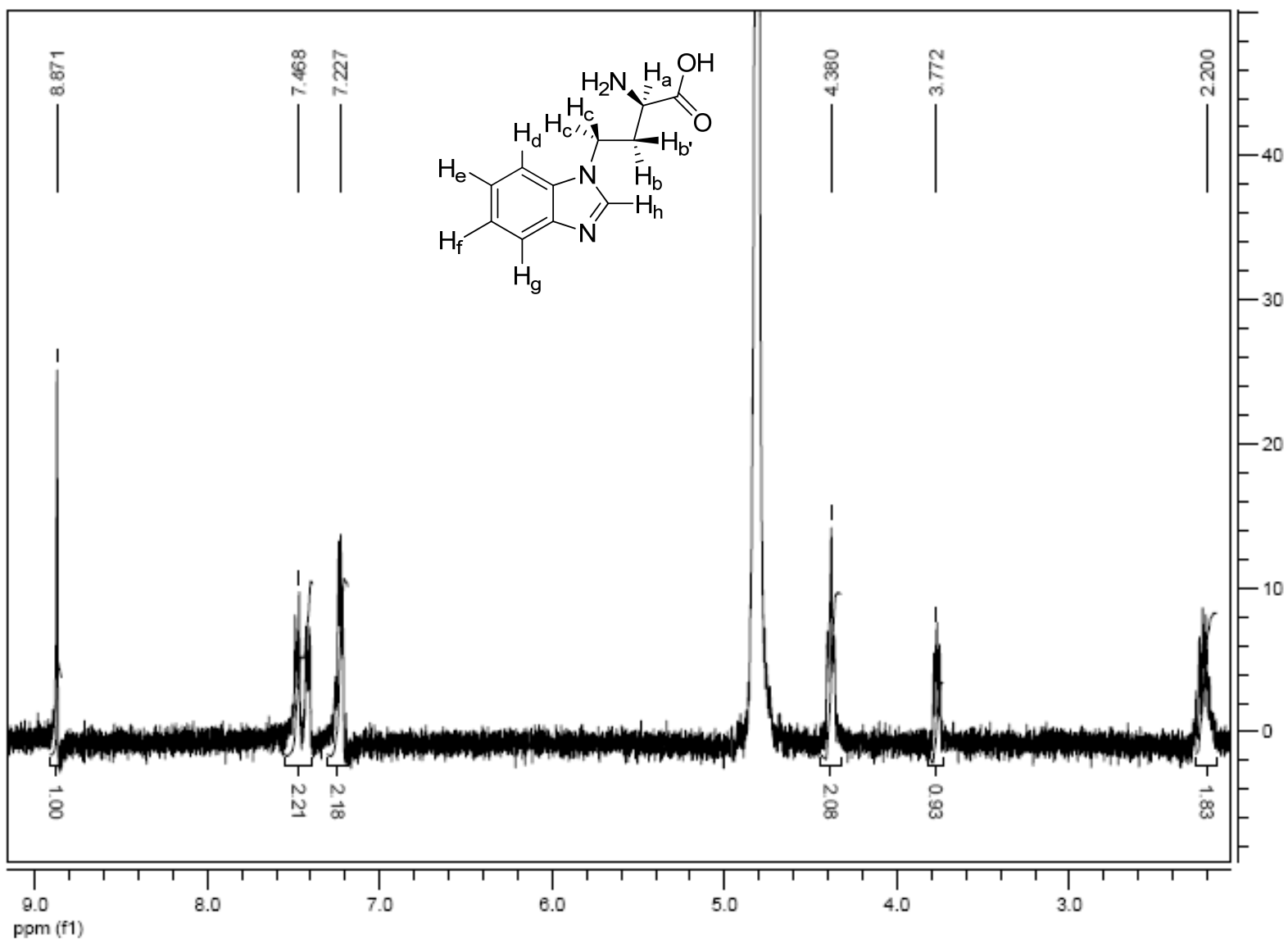


Appendix 2: Benzimidazol-L-Alanine  $^1\text{H-NMR}$ .

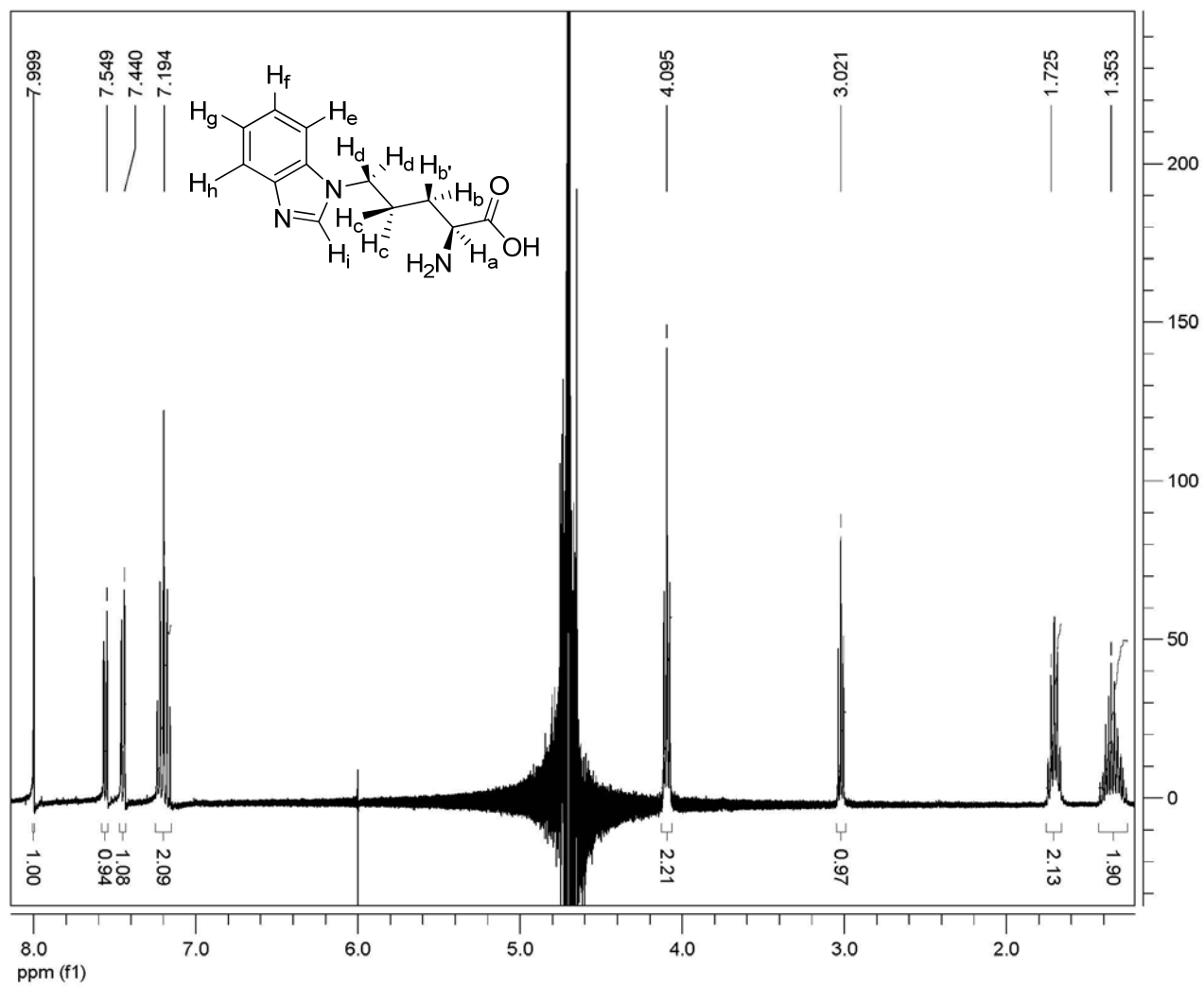
Harris 3-9-4-1: R. Phillips, Harris, Glutamine product 1



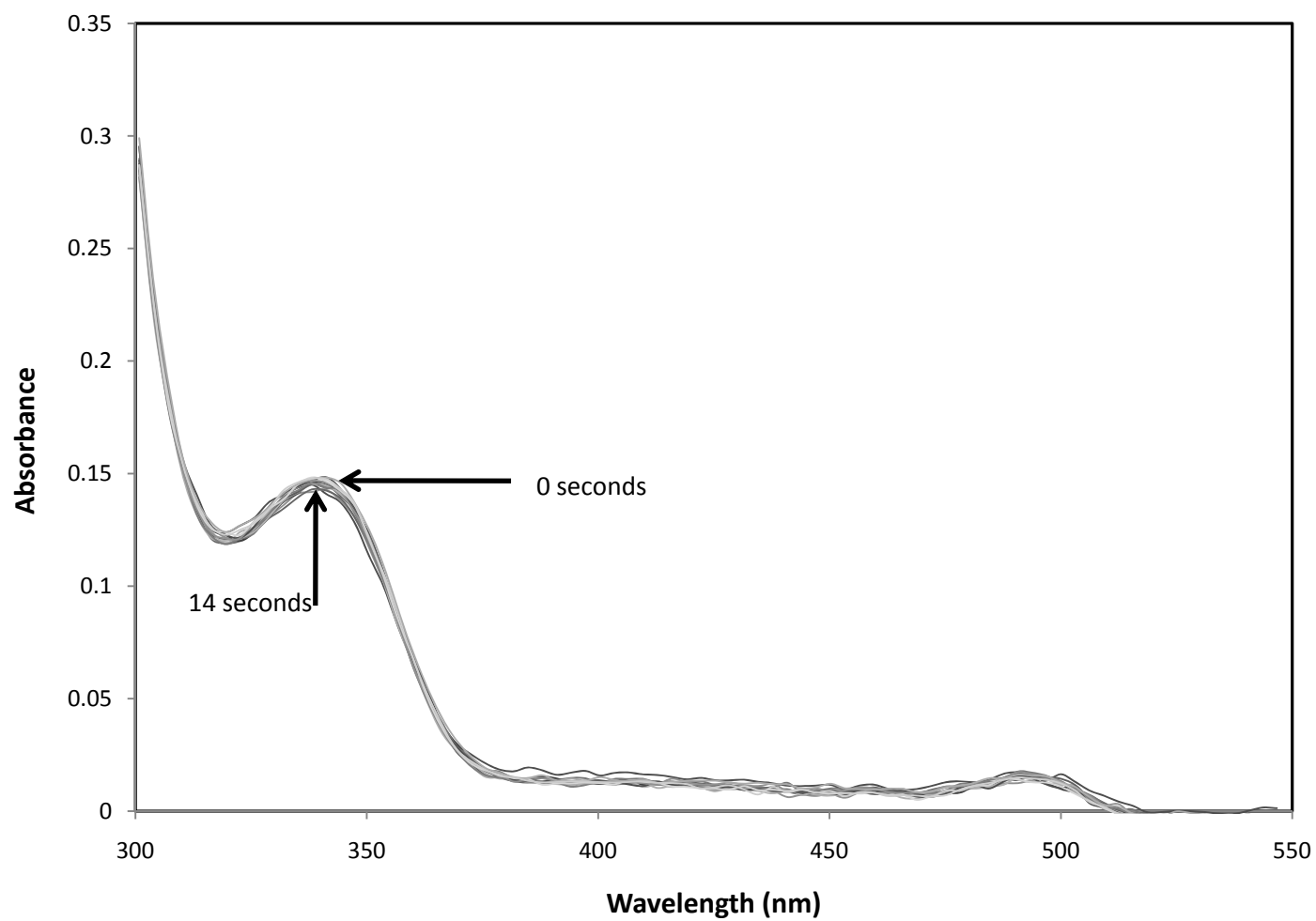
**Appendix 3: Electrospray Mass Spectrum, 2-amino-4-(benzimidazol-1-yl)butanoic acid.**



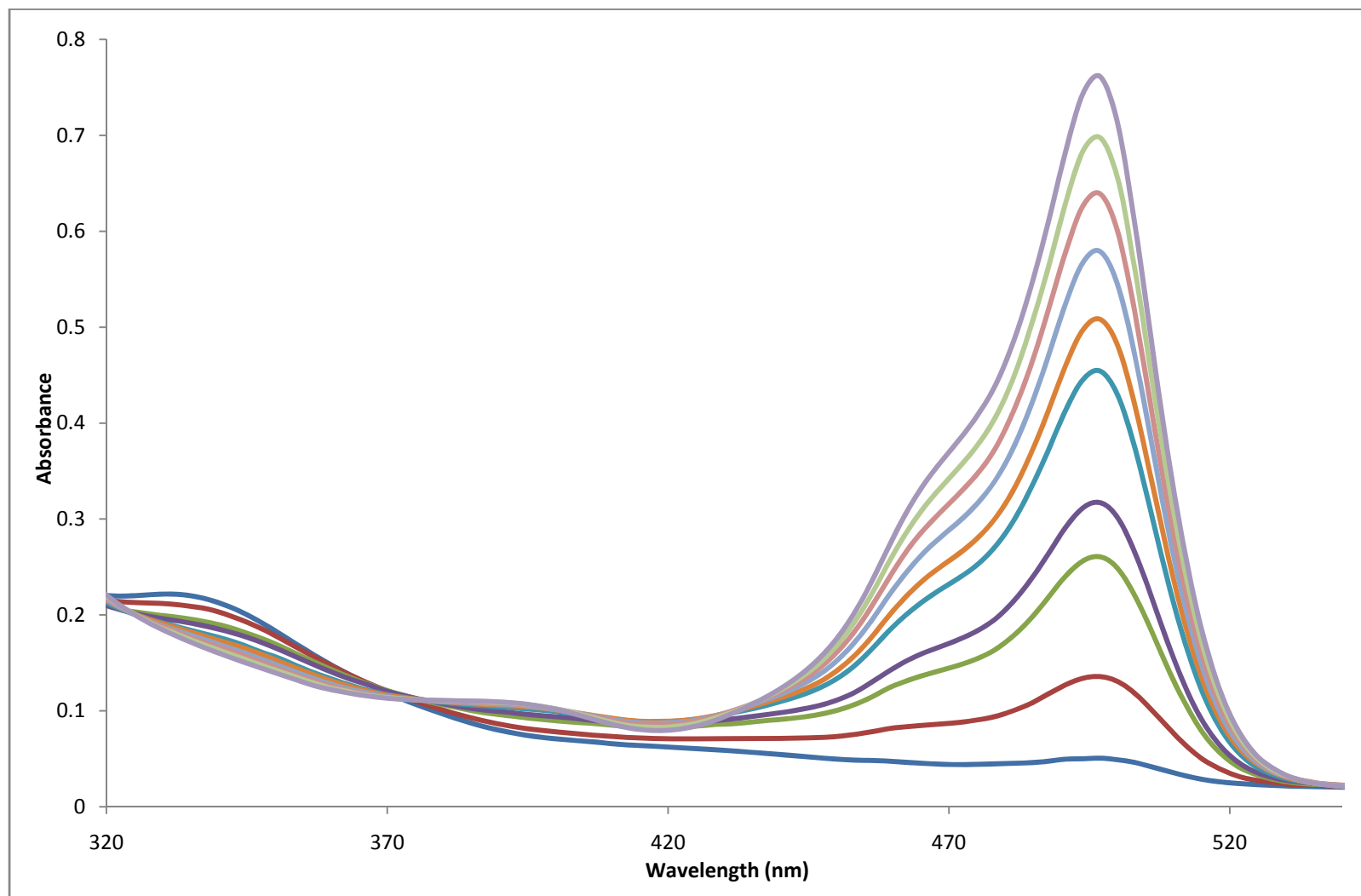
Appendix 4: 2-amino-4-(benzimidazol-1-yl)butanoic acid  $^1\text{H-NMR}$ .



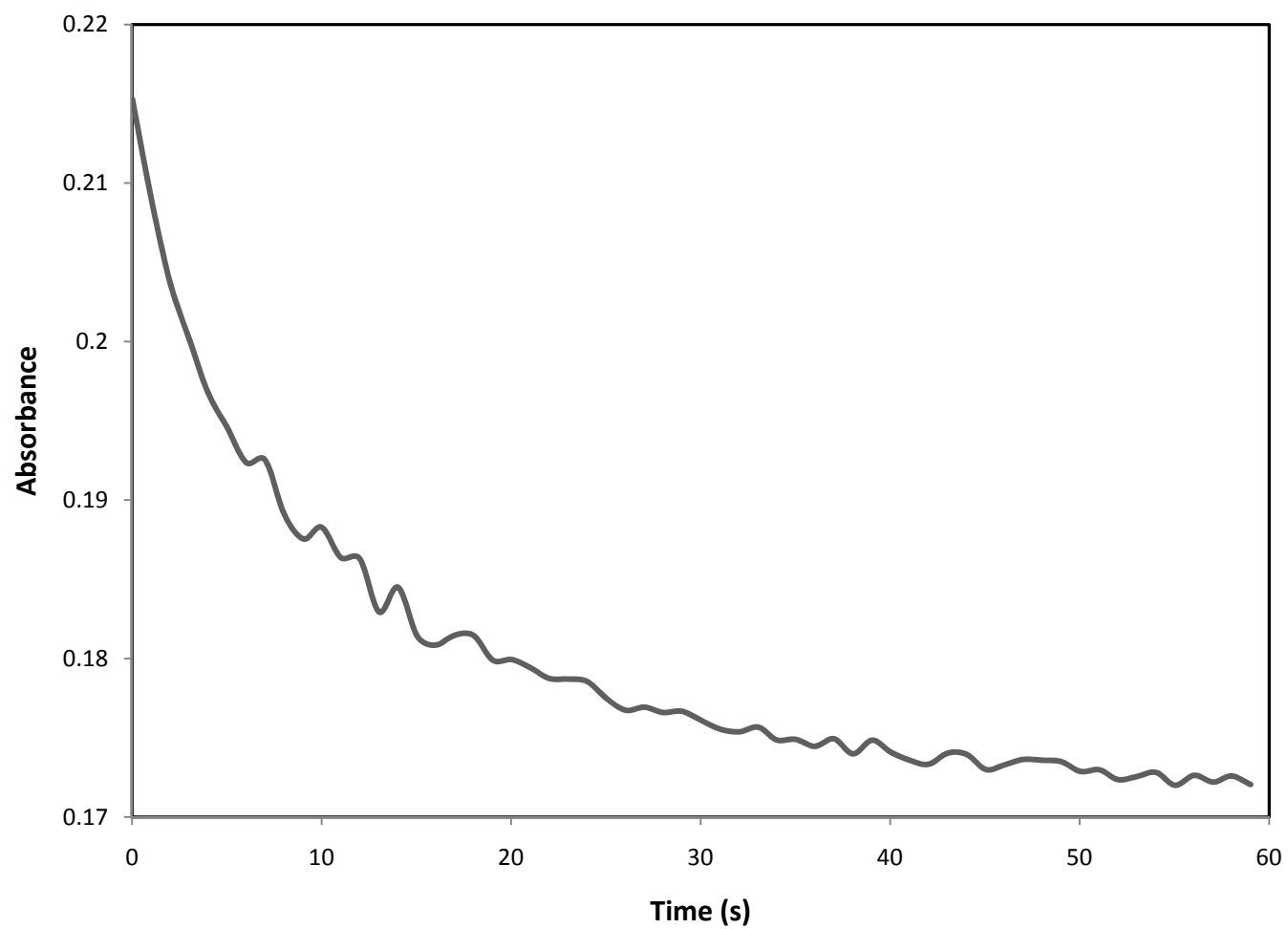
Appendix 5: 2-amino-5-(benzimidazol-1-yl)pentanoic acid  $^1\text{H-NMR}$ .



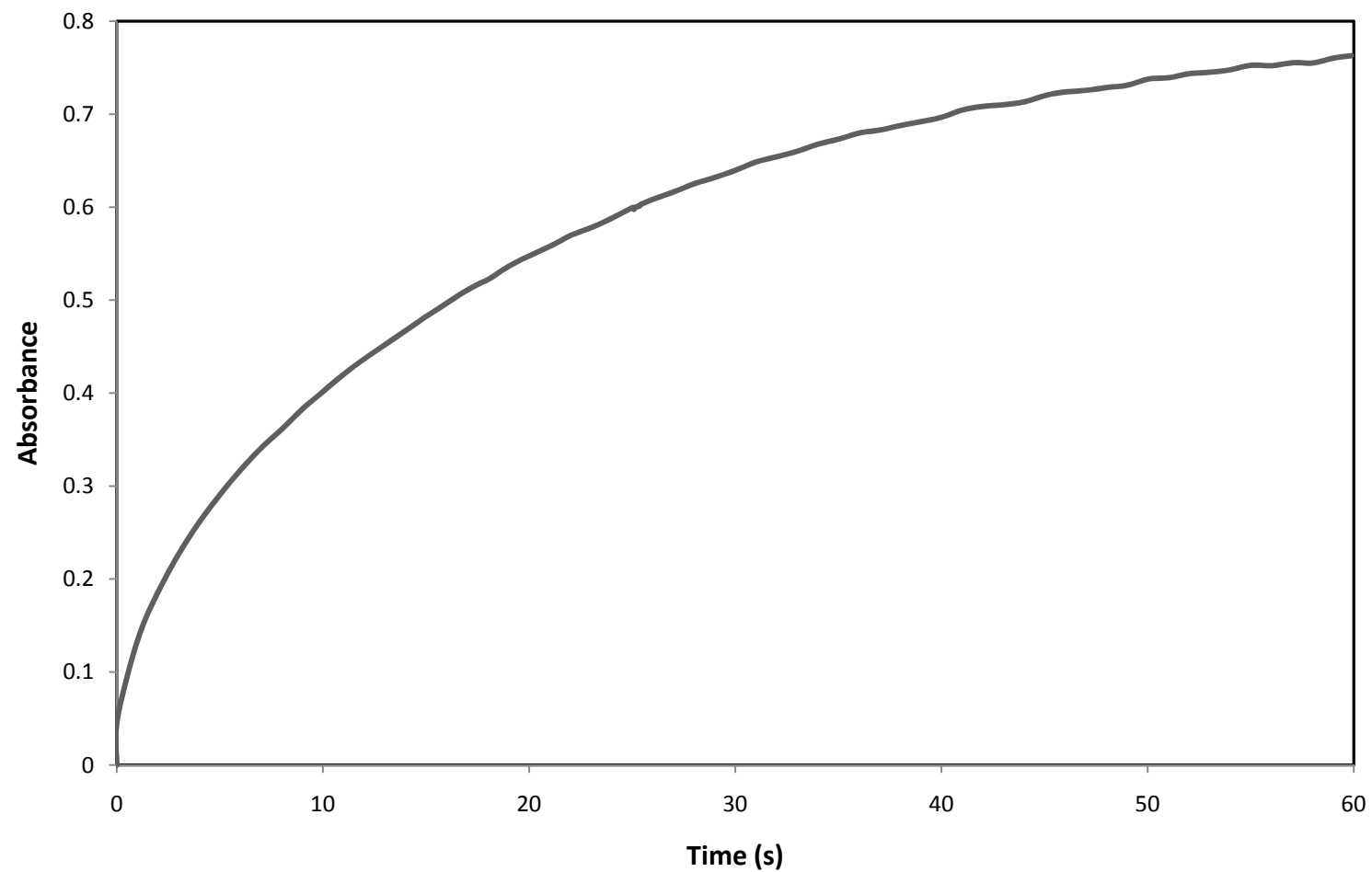
**Appendix 6: Benzimidazol-1-yl-L-alanine 16 mM stopped-flow spectrum.**



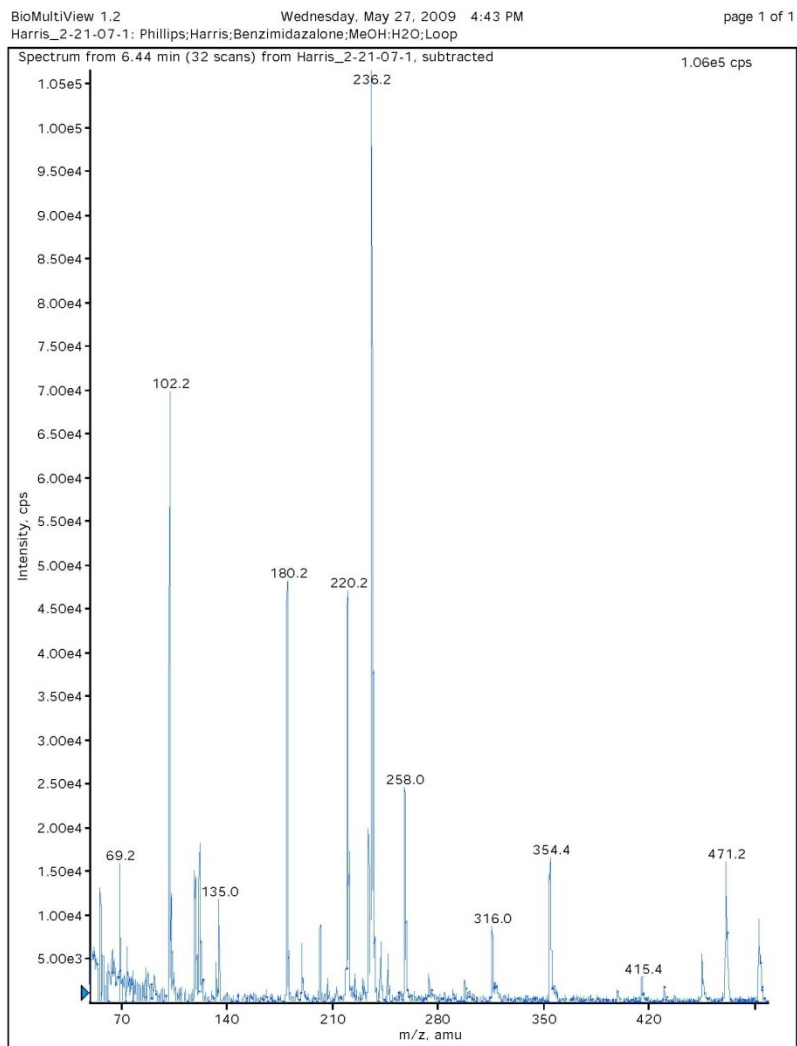
**Appendix 7: 2-amino-4-(benzimidazol-1-yl)butyric acid 2 mM stopped-flow spectrum.**



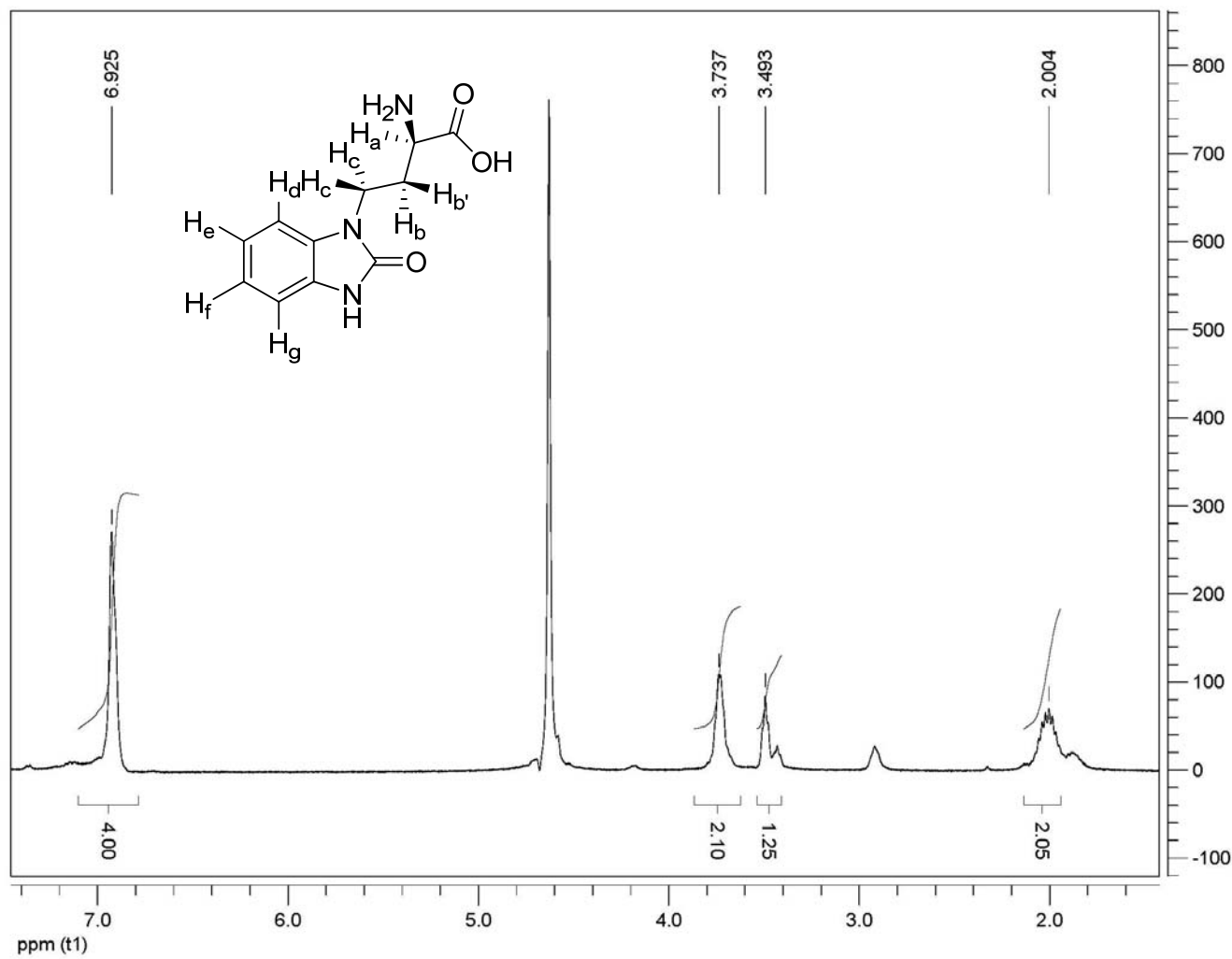
**Appendix 8: Absorbance versus time decay of the 2-amino-4-(benzimidazol-1-yl)butyric acid *gem*-diamine at 340 nm.**



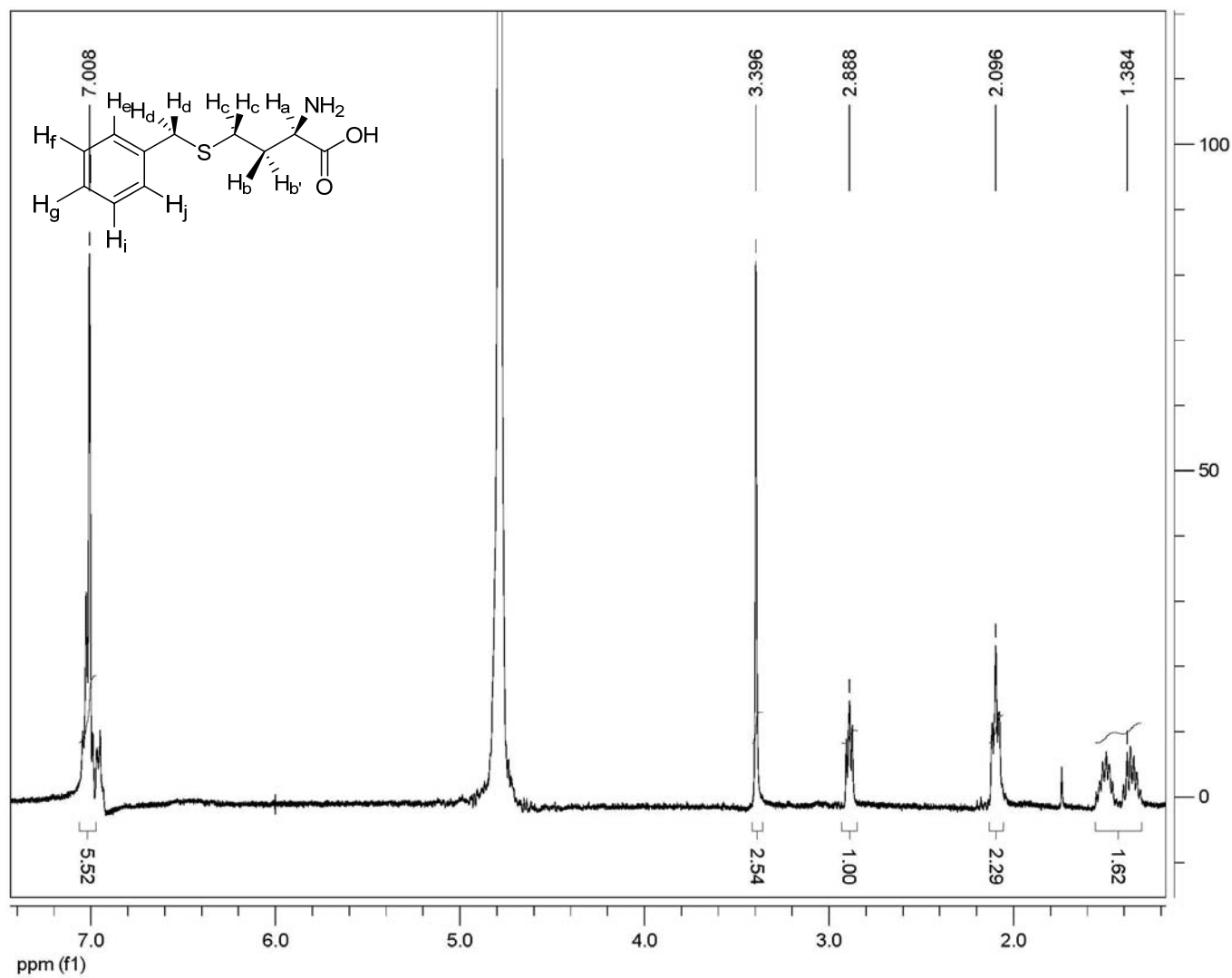
**Appendix 9: Absorbance versus time plot for the formation of the 2-amino-4-(benzimidazol-1-yl)butyric acid quinonoid at 340 nm.**

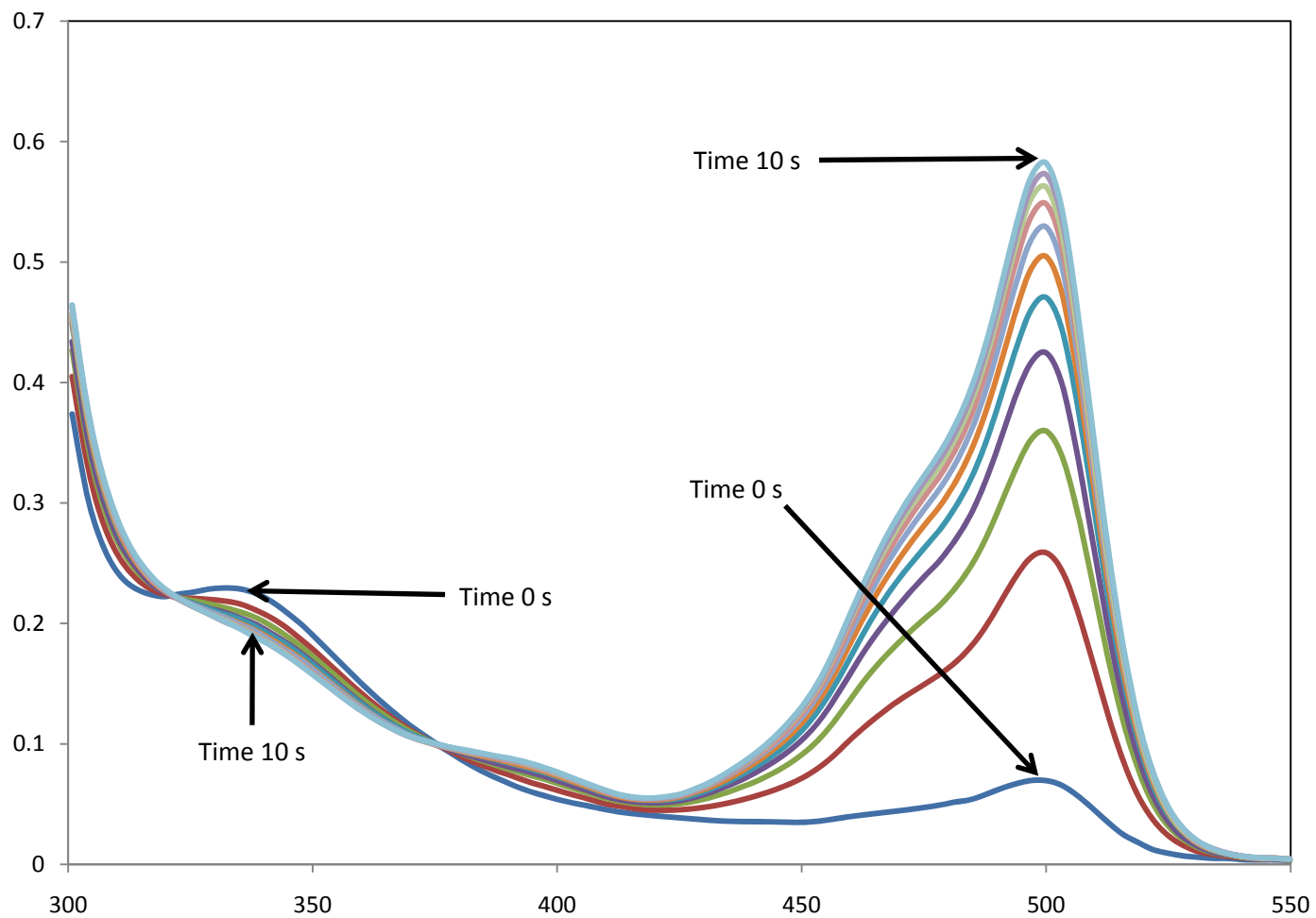


**Appendix 10: Mass Spectrum for 2-amino-4-(benzimidazol-1-yl)butyric acid.**

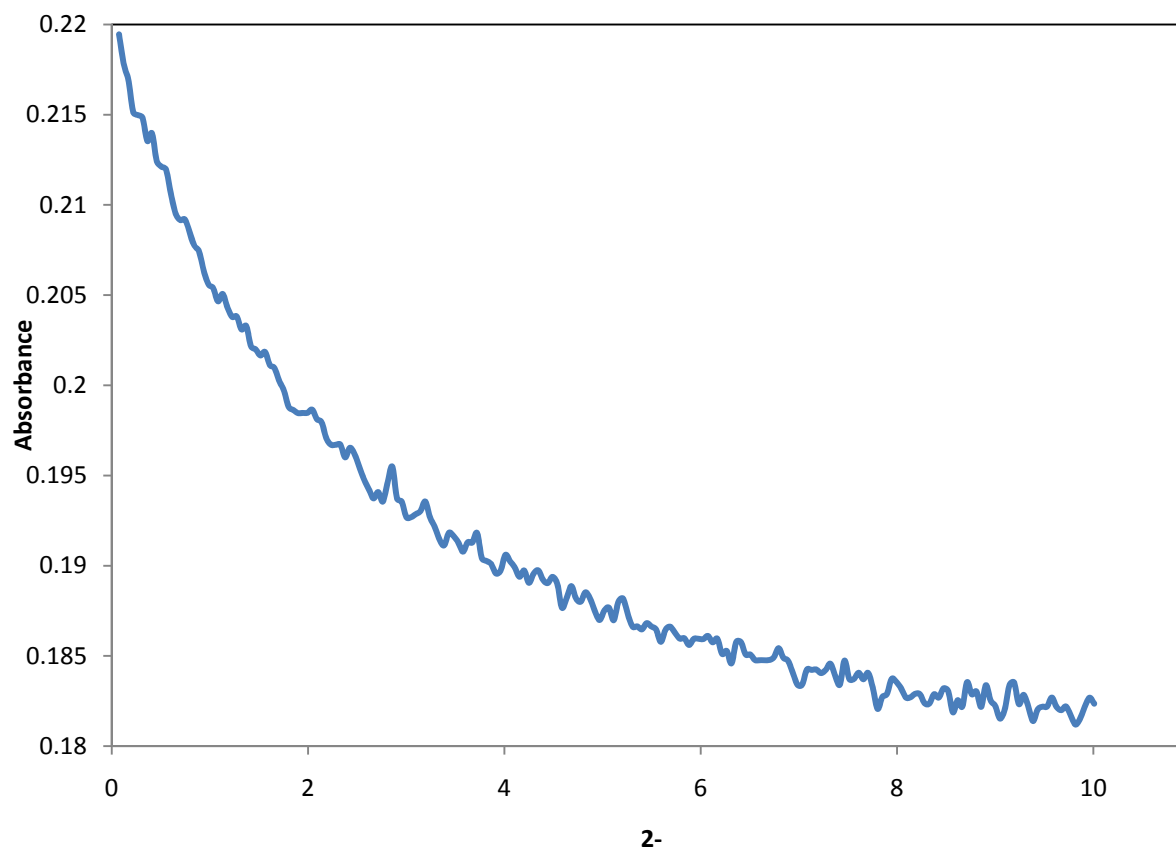


Appendix 11: 2-amino-4-(benzimidazol-1-yl)butyric acid  $^1\text{H-NMR}$ .

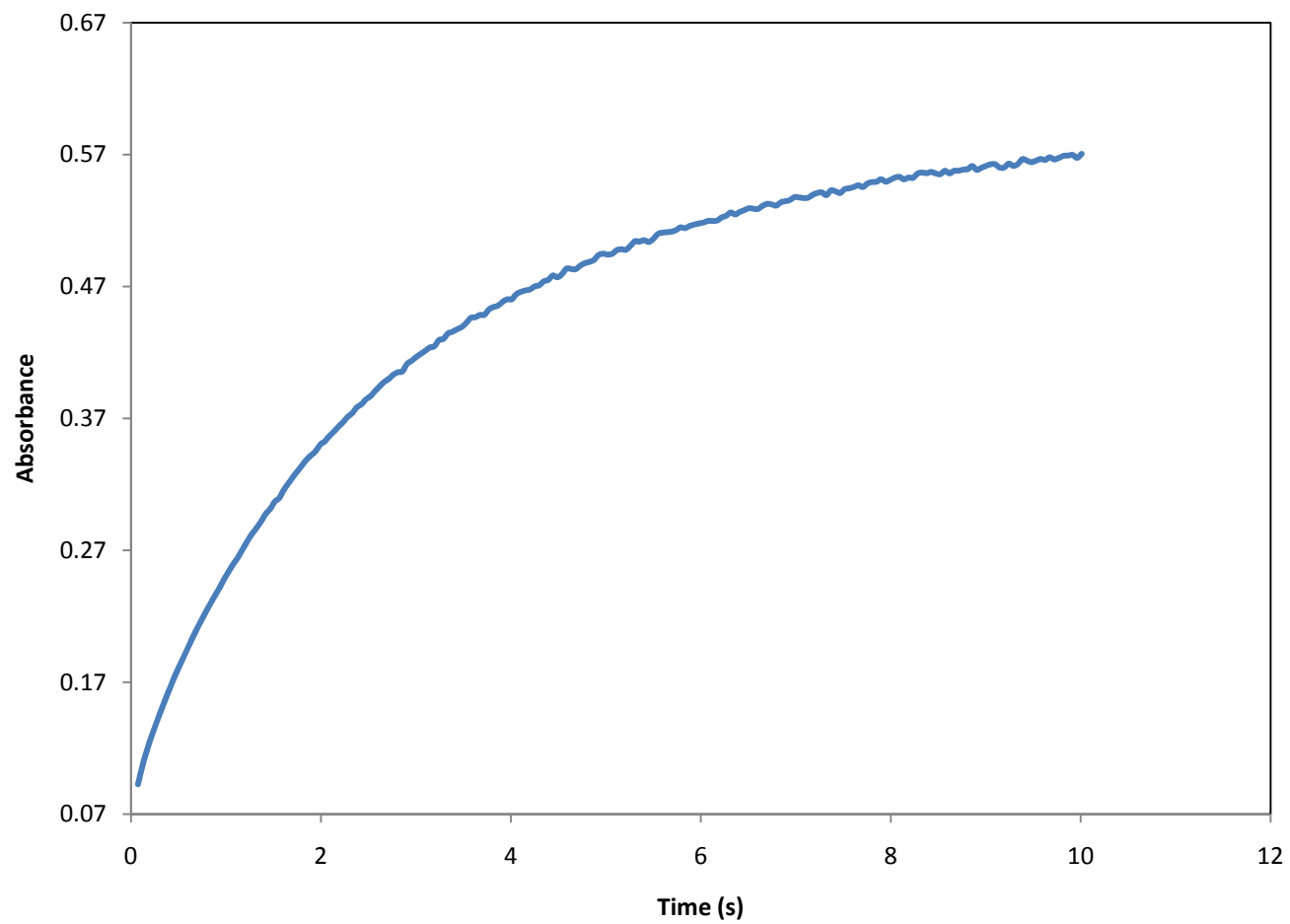
Appendix 12  $^1\text{H-NMR}$  S-benzyl-L-homocysteine



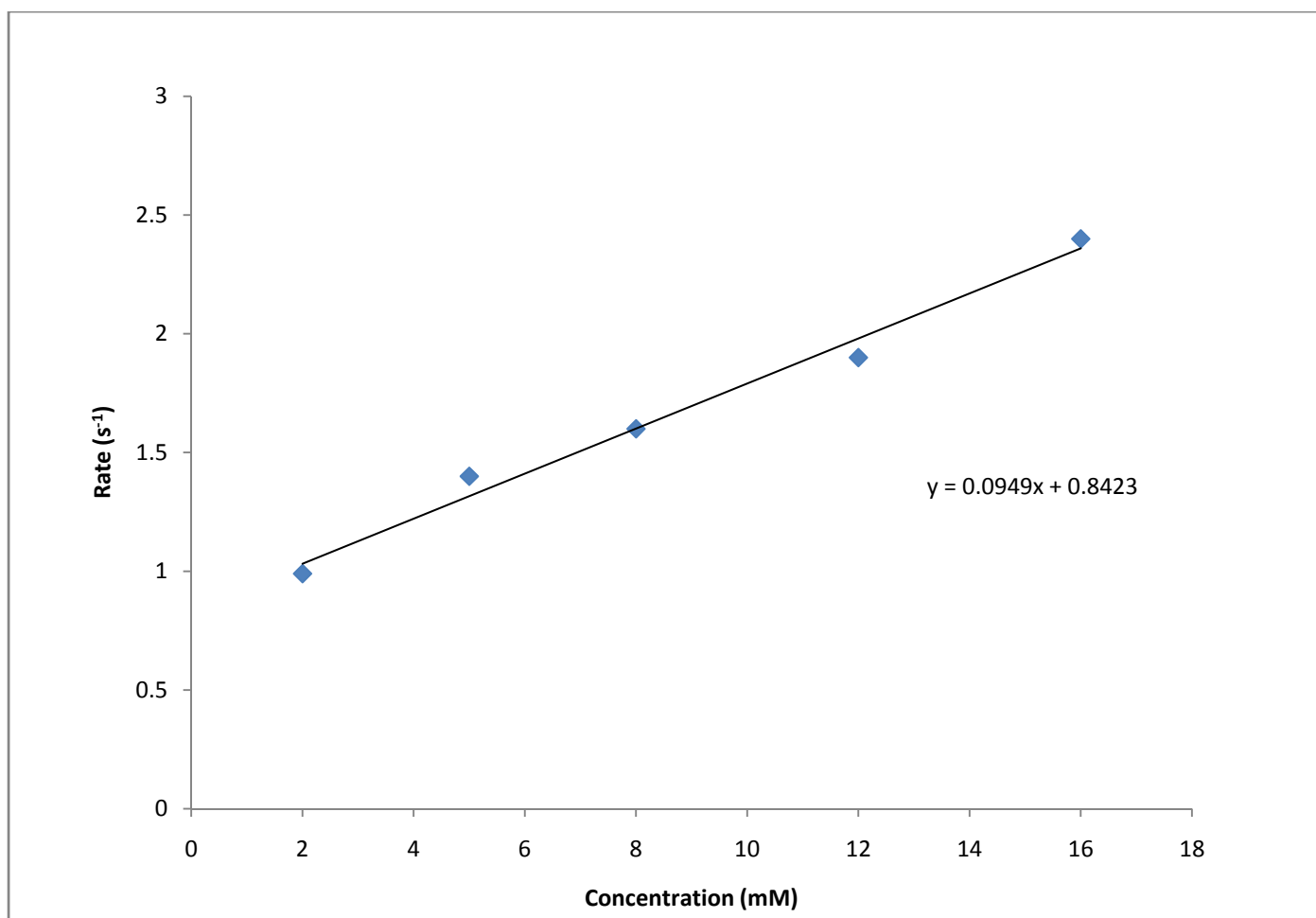
**Appendix 13: 2-amino-4-(benzamidazolone-1-yl)butyric acid stopped flow spectrum.**



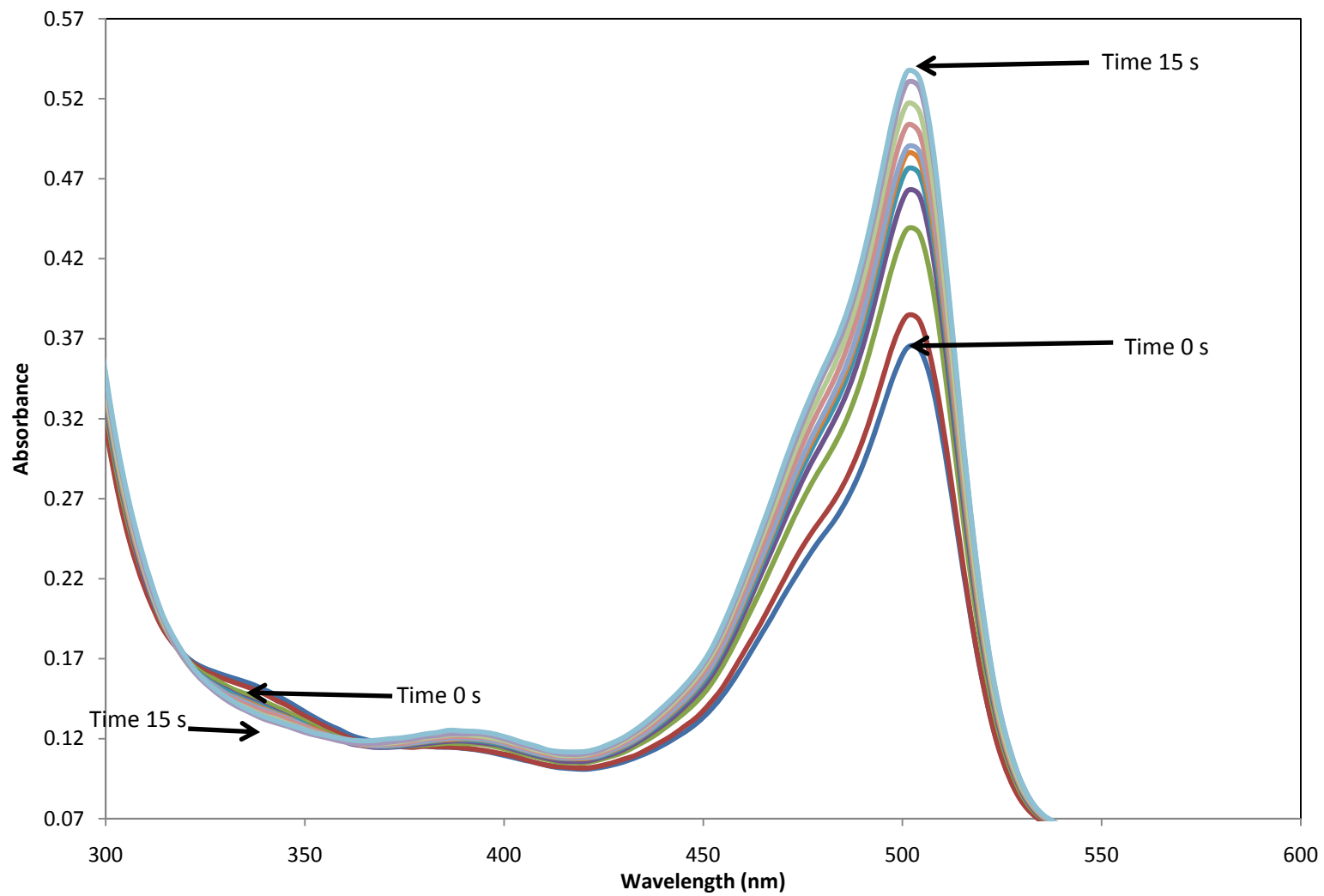
**Appendix 14: Absorbance versus time plot for the decay of the 2-amino-4-(benzimidazol-1-yl)butyric acid *gem*-diamine at 340 nm.**



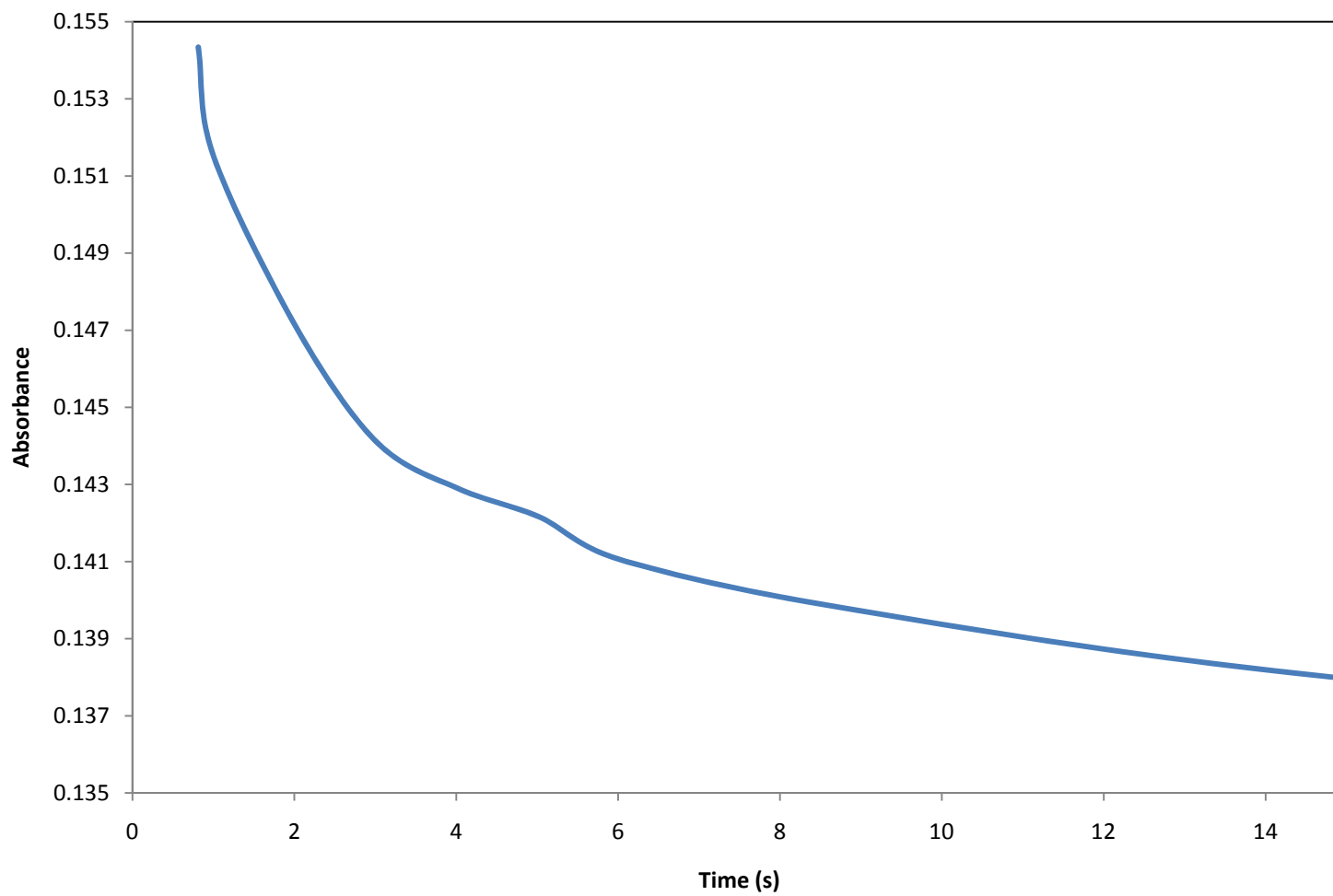
**Appendix 15: Absorbance versus time plot for the formation of the 2-amino-4-(benzimidazol-1-yl)butyric acid quinonoid at 340 nm.**



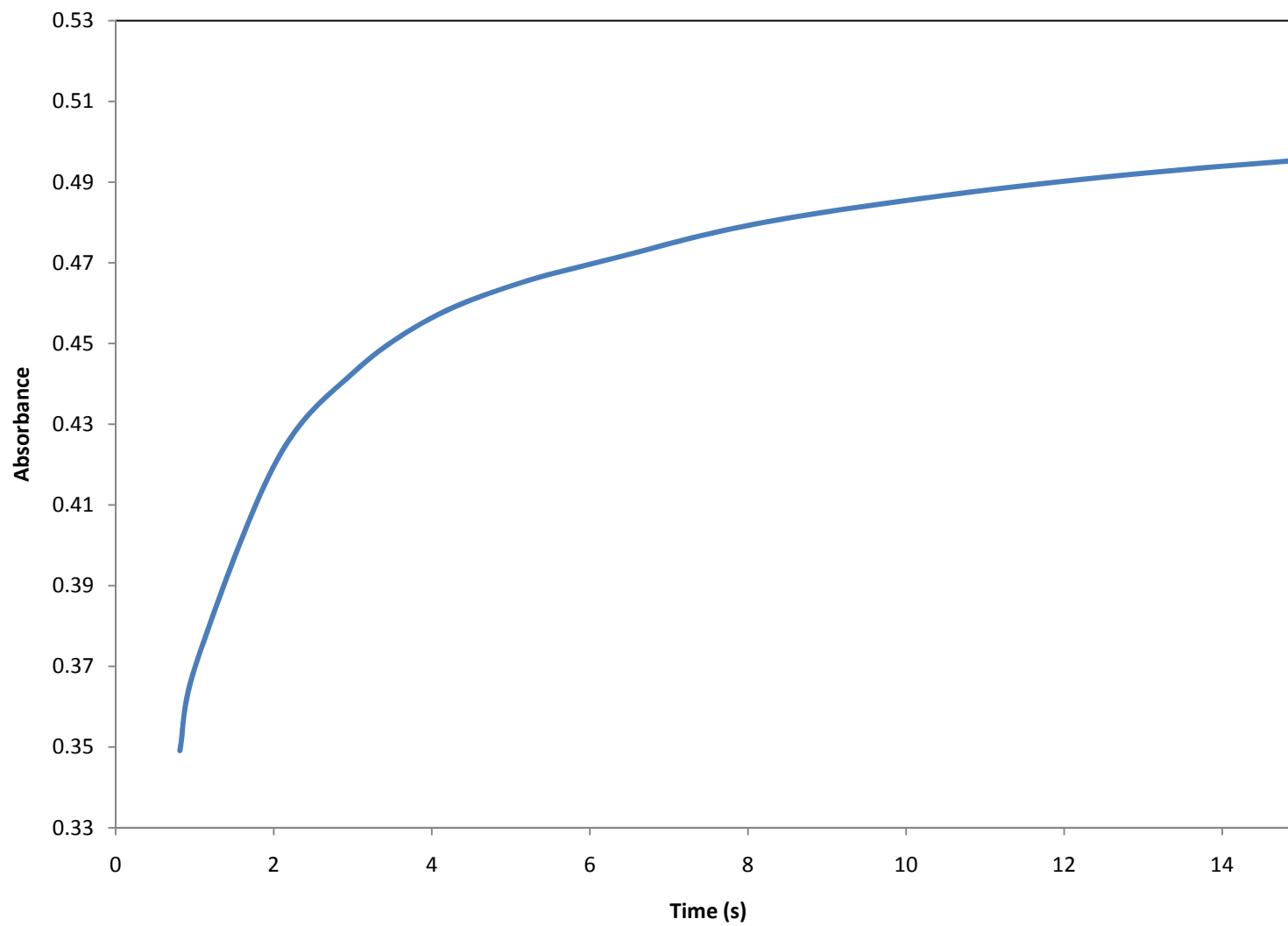
**Appendix 16: Rate versus concentration of 2-amino-(benzimidazol-1-yl)-butyric acid**



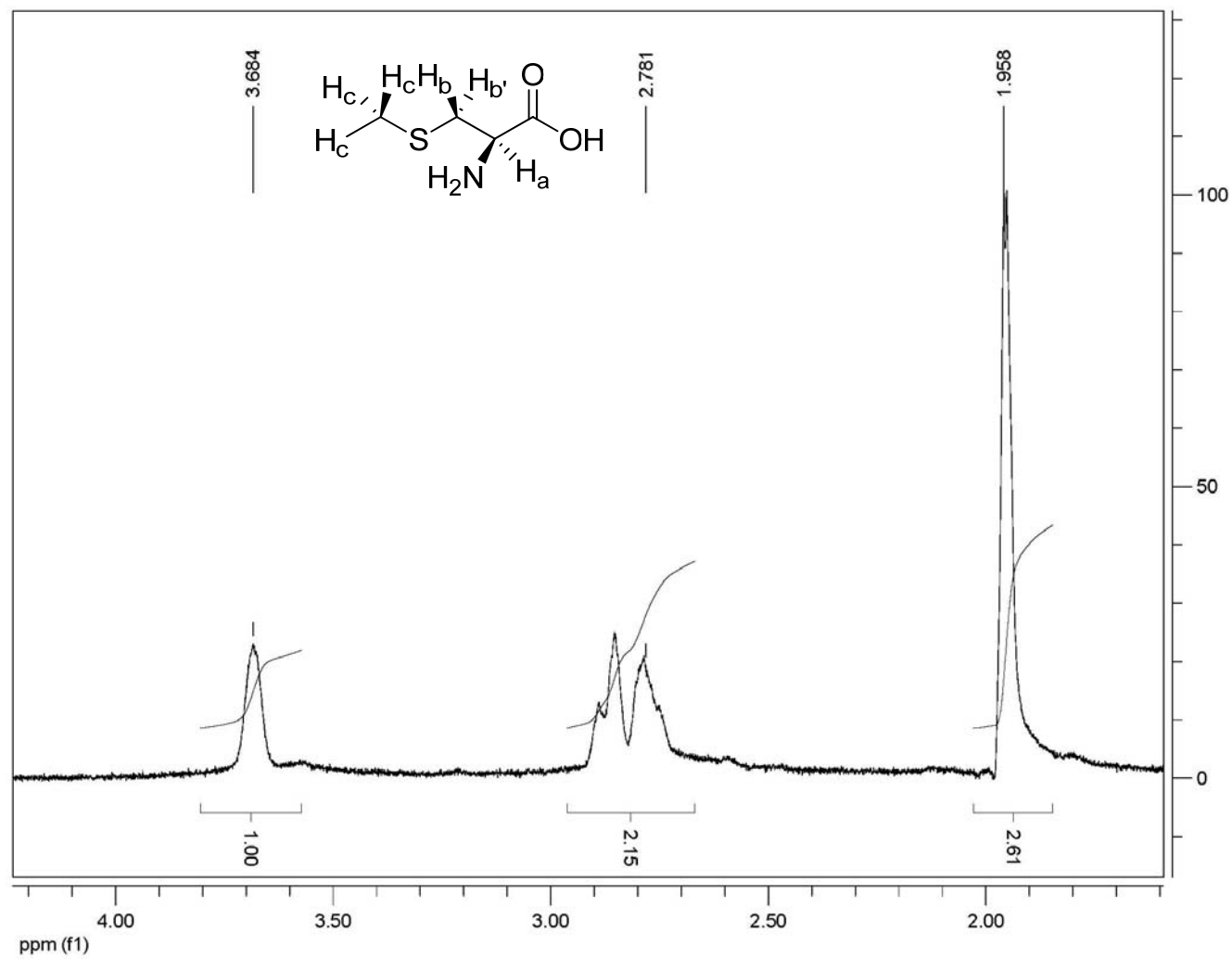
**Appendix 17: S-Benzyl-L-homocysteine stopped-flow spectrum.**



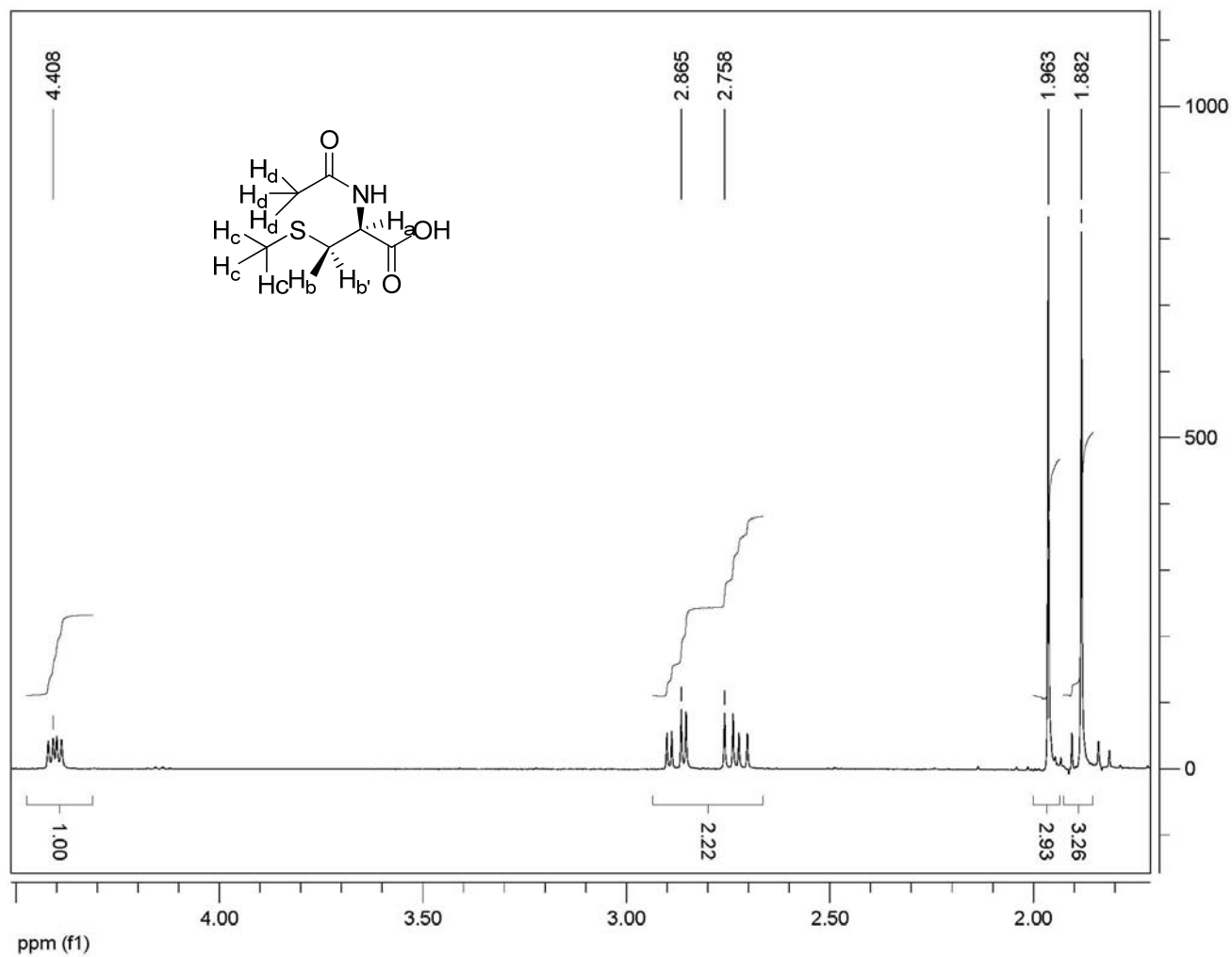
**Appendix 18: Absorbance versus time plot for the decay of the S-benzyl-L-homocysteine acid *gem*-diamine at 340 nm.**



**Appendix 19: Absorbance versus time plot for the formation of the S-benzyl-L-homocysteine quinonoid at 340 nm.**



Appendix 20:  $^1\text{H-NMR}$  spectrum for S-methyl-L-cysteine.



Appendix 21:  $^1\text{H}$ -NMR spectrum of N-acetyl-S-methyl-DL-cysteine.

Concentration of SOPC ( $\mu\text{M}$ )	Concentration of Inhibitor ( $\mu\text{M}$ )	Reaction Rate (s <sup>-1</sup> )	Concentration of SOPC ( $\mu\text{M}$ )	Concentration of Inhibitor ( $\mu\text{M}$ )	Reaction Rate (s <sup>-1</sup> )
35.5600	0.0000	96.9896	35.5600	480.0000	43.3442
71.1100	0.0000	157.7780	71.1100	480.0000	78.6207
106.6700	0.0000	199.4652	106.6700	480.0000	107.9053
142.2200	0.0000	229.8173	142.2200	480.0000	132.5923
177.7800	0.0000	252.9154	177.7800	480.0000	153.6965
35.5600	0.0000	96.9896	35.5600	480.0000	43.3442
71.1100	0.0000	157.7780	71.1100	480.0000	78.6207
106.0000	0.0000	198.8013	106.6700	480.0000	107.9053
142.2200	0.0000	229.8173	142.2200	480.0000	132.5923
177.7800	0.0000	252.9154	177.7800	480.0000	153.6965
35.5600	0.0000	96.9896	35.5600	480.0000	43.3442
71.1100	0.0000	157.7780	71.1100	480.0000	78.6207
106.6700	0.0000	199.4652	106.6700	480.0000	107.9053
142.2200	0.0000	229.8173	142.2200	480.0000	132.5923
177.7800	0.0000	252.9154	177.7800	480.0000	153.6965
35.5600	240.0000	59.9134	35.5600	720.0000	33.9541
71.1100	240.0000	104.9466	71.1100	720.0000	62.8538
106.6700	240.0000	140.0483	106.6700	720.0000	87.7626
142.2200	240.0000	168.1633	142.2200	720.0000	109.4423
177.7800	240.0000	191.2006	177.7800	720.0000	128.4927
35.5600	240.0000	59.9134	35.5600	720.0000	33.9541
71.1100	240.0000	104.9466	71.1100	720.0000	62.8538
106.6700	240.0000	140.0483	106.6700	720.0000	87.7626
142.2200	240.0000	168.1633	142.2200	720.0000	109.4423
177.7800	240.0000	191.2006	177.7800	720.0000	128.4927
35.5600	240.0000	59.9134	35.5600	720.0000	33.9541
71.1100	240.0000	104.9466	71.1100	720.0000	62.8538
106.6700	240.0000	140.0483	106.6700	720.0000	87.7626
142.2200	240.0000	168.1633	142.2200	720.0000	109.4423
177.7800	240.0000	191.2006	177.7800	720.0000	128.4927

**Appendix 22: Steady-state inhibition kinetics data for  $\beta$ -(benzimidazol-1-yl)alanine.**

Concentration of SOPC ( $\mu\text{M}$ )	Concentration of Inhibitor ( $\mu\text{M}$ )	Reaction Rate ( $\text{s}^{-1}$ )	Concentration of SOPC ( $\mu\text{M}$ )	Concentration of Inhibitor ( $\mu\text{M}$ )	Reaction Rate ( $\text{s}^{-1}$ )
36.00000	0.00000	0.00880	180.0000	7.5000	0.0192
72.00000	0.00000	0.01640	36.0000	15.0000	0.0045
108.00000	0.00000	0.02360	144.0000	7.5000	0.0157
144.00000	0.00000	0.02410	180.0000	7.5000	0.0192
180.00000	0.00000	0.02720	36.0000	15.0000	0.0045
36.00000	0.00000	0.00830	72.0000	15.0000	0.0101
72.00000	0.00000	0.01340	108.0000	15.0000	0.0143
108.00000	0.00000	0.02050	144.0000	15.0000	0.0154
144.00000	0.00000	0.02050	180.0000	15.0000	0.0185
180.00000	0.00000	0.02630	36.0000	15.0000	0.0071
36.00000	0.00000	0.00830	72.0000	15.0000	0.0100
72.00000	0.00000	0.01580	108.0000	15.0000	0.0132
108.00000	0.00000	0.01870	144.0000	15.0000	0.0154
144.00000	0.00000	0.02360	180.0000	15.0000	0.0215
180.00000	0.00000	0.02740	36.0000	22.5000	0.0043
36.00000	7.50000	0.00640	72.0000	22.5000	0.0082
72.00000	7.50000	0.01130	108.0000	22.5000	0.0116
108.00000	7.50000	0.01710	144.0000	22.5000	0.0134
144.00000	7.50000	0.01900	180.0000	22.5000	0.0161
180.00000	7.50000	0.02060	36.0000	22.5000	0.0043
36.00000	7.50000	0.00690	72.0000	22.5000	0.0081
72.00000	7.50000	0.01080	108.0000	22.5000	0.0127
108.00000	7.50000	0.01380	180.0000	22.5000	0.0146
144.00000	7.50000	0.01250	36.0000	22.5000	0.0040
36.00000	7.50000	0.00530	72.0000	22.5000	0.0066
72.00000	7.50000	0.01060	108.0000	22.5000	0.0112
108.00000	7.50000	0.01380	144.0000	22.5000	0.0106
144.00000	7.50000	0.01570	180.0000	22.5000	0.0152

**Appendix 23: Steady-state inhibition kinetics data for 2-amino-4-(benzimidazol-1-yl)butyric acid.**

Concentration of SOPC ( $\mu\text{M}$ )	Concentration of Inhibitor ( $\mu\text{M}$ )	Reaction Rate (s <sup>-1</sup> )	Concentration of SOPC ( $\mu\text{M}$ )	Concentration of Inhibitor ( $\mu\text{M}$ )	Reaction Rate (s <sup>-1</sup> )
36.0000	0.0000	0.0216	36.0000	33.2000	0.0143
72.0000	0.0000	0.0330	72.0000	32.2000	0.0225
108.0000	0.0000	0.0587	108.0000	32.2000	0.0395
144.0000	0.0000	0.0781	144.0000	32.2000	0.0392
36.0000	0.0000	0.0237	36.0000	32.2000	0.0133
72.0000	0.0000	0.0363	72.0000	32.2000	0.0223
108.0000	0.0000	0.0541	108.0000	32.2000	0.0333
144.0000	0.0000	0.0647	144.0000	32.2000	0.0561
36.0000	16.6000	0.0170	36.0000	49.8000	0.0149
72.0000	16.6000	0.0257	72.0000	49.8000	0.0185
108.0000	16.6000	0.0388	108.0000	49.8000	0.0284
144.0000	16.6000	0.0587	144.0000	49.8000	0.0428
36.0000	16.6000	0.0157	36.0000	49.8000	0.0109
72.0000	16.6000	0.0261	72.0000	49.8000	0.0170
108.0000	16.6000	0.0403	108.0000	49.8000	0.0319
144.0000	16.6000	0.0502	144.0000	49.8000	0.0441

**Appendix 24: Steady-state inhibition kinetics data for 2-amino-4-(benzimidazol-1-yl)butyric acid.**

Concentration of SOPC ( $\mu\text{M}$ )	Concentration of Inhibitor ( $\mu\text{M}$ )	Reaction Rate ( $\text{s}^{-1}$ )	Concentration of SOPC ( $\mu\text{M}$ )	Concentration of Inhibitor ( $\mu\text{M}$ )	Reaction Rate ( $\text{s}^{-1}$ )
50.0000	0.0000	0.0186	50.0000	40.0000	0.0028
100.0000	0.0000	0.0313	100.0000	40.0000	0.0047
200.0000	0.0000	0.0578	200.0000	40.0000	0.0147
400.0000	0.0000	0.0625	400.0000	40.0000	0.0295
500.0000	0.0000	0.0679	500.0000	40.0000	0.0416
600.0000	0.0000	0.0712	600.0000	40.0000	0.0426
50.0000	0.0000	0.0170	50.0000	40.0000	0.0019
100.0000	0.0000	0.0331	100.0000	40.0000	0.0046
200.0000	0.0000	0.0548	200.0000	40.0000	0.0144
400.0000	0.0000	0.0629	400.0000	40.0000	0.0315
500.0000	0.0000	0.0635	500.0000	40.0000	0.0351
600.0000	0.0000	0.0672	600.0000	40.0000	0.0397
50.0000	20.0000	0.0115	50.0000	60.0000	0.0006
100.0000	20.0000	0.0181	100.0000	60.0000	0.0011
200.0000	20.0000	0.0386	200.0000	60.0000	0.0033
400.0000	20.0000	0.0509	400.0000	60.0000	0.0111
500.0000	20.0000	0.0539	500.0000	60.0000	0.0196
600.0000	20.0000	0.0541	600.0000	60.0000	0.0237
50.0000	20.0000	0.0099	50.0000	60.0000	0.0005
100.0000	20.0000	0.0180	100.0000	60.0000	0.0012
200.0000	20.0000	0.0375	200.0000	60.0000	0.0034
400.0000	20.0000	0.0514	400.0000	60.0000	0.0126
500.0000	20.0000	0.0513	500.0000	60.0000	0.0181
600.0000	20.0000	0.0502	600.0000	60.0000	0.0241

**Appendix 25: Steady-state inhibition kinetics data for S-benzyl-L-homocysteine.**

Concentration $\beta$ -(benzimidazol-1-yl)alanine ( $\mu\text{M}$ )	Reaction Rate ( $\text{s}^{-1}$ )
48	0.0052
96	0.0102
192	0.0162
288	0.0226
384	0.0221
48	0.0042
96	0.008
192	0.0117
288	0.0164
384	0.0184

**Appendix 26:  $\beta$ -(benzimidazol-1-yl)alanine substrate data.**